Investigation of Factors Affecting the Performance of Roadside Noise Barriers

by

Shira Daltrop

B.Sc., The University of British Columbia, 2009

A THESIS SUBMITTED IN PARTIAL FULFILLMENT OF
THE REQUIREMENTS FOR THE DEGREE OF

MASTER OF APPLIED SCIENCE

in

The Faculty of Graduate Studies

(Mechanical Engineering)

THE UNIVERSITY OF BRITISH COLUMBIA

(Vancouver)

September 2011

Abstract

Roadside noise barriers are used to prevent traffic noise from reaching nearby residences. Two factors that may affect the acoustical performance of highway noise barriers — surface absorption and nearby vegetation — were investigated. Three experimental techniques were used: full-scale laboratory tests, field tests, and scale-model tests. Tests with a 1.2 m high barrier on a hard surface were performed in an anechoic chamber, using source and receiver positions corresponding to different diffraction angles. Absorption was added to the wall in various configurations and the change in insertion loss (IL) was measured. IL's of 12-18 dBA behind and -1 dBA in front of the reflective wall were found. Surface absorption increased IL by up to 2 dBA behind the barrier and 1 dBA in front. For the field tests, traffic noise was measured behind reflective noise walls without and with nearby foliage. Effects were small, less than 5 dB, but suggest that vegetation can either attenuate sound, increasing the IL, or scatter sound into the barrier shadow zone, decreasing the IL. A 1:31.5 scale-model highway configuration was created and tested in an anechoic chamber. Scale-model materials were chosen by performing excess attenuation measurements and doing a best fit using flow resistivity. Absorption was tested on single and parallel noise barriers of varying heights, allowing for a comparison between adding absorption and increasing the height. Foliage tests were performed on single and parallel barriers with various configurations of model trees. Barrier absorption prevented the amplification of sound between parallel barriers and adding absorption was equivalent to increasing the height by 0.33 m. The foliage test results were similar to the field tests; the effects were small and dependent on frequency and the size of the foliage. Predicting these results was attempted using ray tracing, the method of images (MOI), and finite element methods (FEM). An existing ray tracing model, PRAY, was modified and used; however the predicted ILs were 10-30 dB greater than those measured. FEM gave IL's 2-8 dB lower and MOI gave IL's 5-20 dB lower than measurements.

Table of Contents

Appendices

List of Tables

List of Figures

Acknowledgements

I would like to thank my supervisor Dr. Murray Hodgson for his constant guidance and support. I would also like to thank Chris Bibby, Benjamin Collin, Maureen Connelly and Behrooz Yousefzadeh for their help with field tests and for sharing their knowledge. Additionally, I would like to thank Clair Wakefield for contributing his experience and knowledge of traffic noise to this project. I'd also like to thank Armtec and Retaining Walls Northwest for supplying the commercial absorbent noise barriers for testing. Finally I would like to thank the British Columbia Ministry of Transportation and Infrastructure for funding this research.

Chapter 1

Introduction

Traffic noise is a big problem for residents living near main roads and highways. Excessive noise can drastically impair residents' ability to communicate, concentrate and sleep, and therefore effective noise control in these situations is crucial. Much work goes into the mitigation of such noise; governments or consultants responsible for this mitigation look for ways to increase the effectiveness without greatly increasing the cost.

One common method of noise control is the use of roadside noise barriers; they block the direct sound path between the source — the traffic — and the receiver — the person or household subject to the noise. These barriers can be walls, earth berms, or walls on top of earth berms. The topic of study here is noise walls, which are typically made of concrete to ensure little to no sound is transmitted, as well as ensuring durability. While one way to increase the effectiveness of a noise wall is to increase the height, there is a maximum acceptable height in most places; in British Columbia this limit is currently 3 m [1]. This is in place to limit the visual impact for both the drivers and the residents as well as to control costs. While earth berms avoid this visual impact and therefore do not have a height limit, there are many cases where berms are not feasible, either because of geographical topography or a lack of adequate space. Therefore, means of obtaining greater noise reductions from noise walls is a topic of much investigation. Acoustical consultant Clair Wakefield and the British Columbia Ministry of Transportation and Infrastructure wish to gain more knowledge on several factors which affect the performance of these noise walls, and therefore the ministry has funded this research project.

Concrete noise barriers are typically sound reflective; therefore sound can reflect back from them and increase noise levels on the source side of a barrier. In the case of parallel barriers, when barriers are on either side of a road or highway, reflected sound will amplify the noise between the barriers. The sound level at each barrier will therefore increase and more sound will reach the opposite sides of the barriers. Therefore, the barriers become less effective. One way to avoid this degradation is to make the barriers out of sound absorbing materials. That way, very little sound is reflected back from the barriers and little sound amplification occurs. A single absorptive barrier may also be more effective than a single reflective one; sound which contacts the top of the barrier before reaching the other side would be absorbed, causing noise levels behind the barrier to decrease. Constructing barriers out of sound absorbing materials is more expensive, and so researching the effectiveness and the optimal placement of absorption is important. The increase in barrier height equivalent to adding sound absorbing material is a convenient way to quantify the benefit of these barriers. The use of sound absorptive barriers is one factor affecting barrier performance that was investigated here.

Many barriers are located near trees or other foliage, and the effect this has on the performance of barriers is unclear. One effect could be that the foliage back-scatters sound which would normally reach the shadow zone — the area shielded from sound by the barrier — back towards the road, decreasing noise levels behind the barrier. Another possible effect is that sound is absorbed by the foliage, causing energy to be converted from sound into vibrations of the leaves and branches. This would also lead to a decreased sound level behind the barrier, effectively improving the performance of the barrier. The third possible effect is that the foliage scatters sound into the shadow zone which would normally pass above the barrier, increasing the sound level behind the barrier and effectively decreasing the barrier's performance. Studying the effects of foliage on the performance of noise barriers is the second factor which was investigated here.

There are several investigative techniques available to test the effectiveness of noise barriers: full-scale laboratory testing, scale-model testing, field-testing and prediction work. These will now be discussed in regards to the detailed objectives of this work. The objectives of this work were:

- To determine the optimal amount and placement of absorption on a barrier and the effects it has on barrier performance
- To investigate the effects of absorption on the performance of parallel barriers
- To investigate the frequency-dependent effects of different types of foliage on the performance of barriers
- To determine the practical implications of this research

The first objective was to determine the optimal amount and placement of absorption on a barrier and the effects it has on barrier performance. To achieve this objective, a reflective wall was to be built on a hard floor in an anechoic chamber. By absorbing all sound incident on the walls and ceiling by the use of fiberglass wedges, the anechoic chamber creates ideal outdoor conditions. Absorptive materials were to be added to the wall in different configurations to determine the optimal amount and placement with regard to the barrier's effectiveness.

Another method to be used to achieve this objective was to use computer modelling. Three different prediction models implemented in MATLAB were to be used to predict the results of the full scale anechoic chamber measurements: ray tracing, finite elements and the method of images. This was to be done to validate the models, in hopes of using them to predict conditions similar to those found in the field.

The second objective was to investigate the effects of absorption on parallel barriers. It was desired to know if adding absorption reduced or removed the amplification which was seen for parallel reflective barriers. A scale model was to be created in the anechoic chamber

to achieve this objective. Scale-model materials were to first be selected, as material properties are not constant with frequency and play a crucial role in the effectiveness of a noise barrier. A four-lane highway configuration was to be created, where one or two barriers, either reflective or absorptive, could be set up and tested.

If the prediction methods stated above proved to be valid, predictions of reflective and absorptive parallel barriers were to be performed.

The third objective was to investigate the frequency-dependent effects of foliage on the performance of noise barriers. One method used to achieve this objective was to perform field tests along highways. Each site was required to have foliage in some configuration near a barrier and to be located near a stretch of barrier with no foliage. Frequency-dependent sound levels from the passing traffic were to be measured simultaneously behind the foliage and no-foliage sections of the barrier, and the results compared. This way, the effects of the foliage could be isolated from other factors, such as barrier configuration and traffic noise variability.

The scale-model created for the testing of absorption was to be used here to test the effects of foliage growing near a barrier. Scale-model foliage was to be chosen which accurately modelled full-scale foliage. This foliage was then to be placed in different configurations around barriers similar to those seen in the field. Sound levels were to be measured with and without the foliage.

Computer modelling was also to be used to achieve this objective. Ray tracing was to be used to predict measurements performed on tree foliage to determine how the foliage should be modelled. Once this was accomplished, this program was to be used to further predict the effects of foliage on the performance of barriers.

The final objective of this research was to determine how the findings could be applied in the field. Once the above testing was completed, the practical implications were to be stated and recommendations given.

This work is organized as follows. Chapter 2 discusses acoustic theory which is relevant to this work: the wave equation, surface acoustical properties, outdoor sound propagation and noise barriers. Chapter 3 reviews the literature on absorptive noise barriers, sound propagation through foliage and the effect of foliage on noise barriers. The detailed objectives of this work are then discussed. Chapter 4 describes the full-scale experiment performed in the anechoic chamber and discusses the results. Chapter 5 discusses the field tests performed at several test sites with different foliage configurations near barriers. Chapter 6 describes the theory behind scale modelling, as well as previous work done with scale models to study noise barriers. It then describes the scale-model experiment, model material selection and scale-model results. Chapter 7 discusses the three prediction methods and two diffraction algorithms used to predict the results of several measurements done previously in the thesis. The predictions done here are discussed and the results are compared with measurements. Chapter 8 presents the conclusions of the completed work as well as discusses possible future work.

Chapter 2

Theoretical Considerations

2.1 The Wave Equation

Sound propagates as waves, and therefore the governing equation in acoustics is the wave equation:

$$\nabla^2 p - \frac{1}{c^2}\frac{\partial^2 p}{\partial t^2} = 0, \tag{2.1}$$

where $\nabla^2 = \frac{\partial^2}{\partial x^2} + \frac{\partial^2}{\partial y^2} + \frac{\partial^2}{\partial z^2}$ is the three-dimensional Laplacian operator using Cartesian coordinates, p is the acoustical pressure in Pa, and c is the temperature-dependent speed of sound in m/s:

$$c = 20\sqrt{T + 273.15}, \tag{2.2}$$

where T is the temperature in $^{\circ}$C. The speed of sound is also related to the frequency f in s^{-1} and wavelength λ in m of the wave, by $c = \lambda f$. Using separation of variables and assuming a harmonic time dependence $e^{i\omega t}$, where ω is the angular frequency equal to $2\pi f$, Equation 2.1 can be rewritten as the Helmholtz Equation:

$$\nabla^2 p + k^2 p = 0, \tag{2.3}$$

where p is the time-independent pressure and $k = \frac{\omega}{c} = \frac{2\pi}{\lambda}$ is the wavenumber in m^{-1}.

In free-field conditions, the radiative boundary condition is implemented, which enforces

the sound pressure to go to zero as it travels an infinite distance from the source:

$$\lim_{r\to\infty} p(r) = 0, \tag{2.4}$$

where r is the distance from a point source, using spherical coordinates. A solution to the Helmholtz equation using this boundary condition is:

$$p = p_s \frac{e^{-ikr}}{r}, \tag{2.5}$$

where p_s is the source amplitude.

2.2 The Decibel

When discussing sound levels in Pascals, the range of values is very large. Therefore, noise levels are typically converted from Pascals (Pa) to a logarithmic scale called decibels (dB). There are several definitions of the decibel. One relates to the sound pressure level, which is defined to be zero at a reference level $p_0 = 2\text{x}10^{-5}$ Pa. This is considered to be the minimum audible sound pressure for the average person. The sound pressure level L_p in dB is defined in terms of the pressure p in Pa as:

$$L_p = 20 \log_{10} \left(\frac{p}{p_0} \right). \tag{2.6}$$

The sound power level is another decibel which is commonly used, defined with reference to $W_0 = 10^{-12}$ W. Because sound power is proportional to p^2, it can be calculated in a similar way to L_p, however with a factor of 10 in front instead of 20:

$$L_w = 10 \log_{10} \left(\frac{W}{W_0} \right). \tag{2.7}$$

2.3 Surface Properties

There are three ways a sound wave can react when it hits a surface; it can be reflected, absorbed and transmitted. The amount of each that occurs is dependent on the material, the frequency and the angle of incidence. The amount of sound energy reflected from a surface is determined by the complex reflection coefficient β, which is defined as the ratio of the reflected energy to the total incident energy. Sound can be reflected in two ways: specularly or diffusely. In specular reflection, the angle of incidence equals the angle of reflection. When diffuse reflections occur, sound is reflected in all directions.

Sound can also be transmitted through the material. The transmission coefficient τ is defined as the ratio of the energy transmitted to the incident energy. Energy that is neither reflected nor transmitted is absorbed by the material, with an absorption coefficient α. Conservation of energy states that:

$$\alpha + \beta + \tau = 1. \tag{2.8}$$

In many cases, a complex pressure reflection coefficient R is of interest, as a surface can change the phase of a wave, which is not accounted for when using an energy-based coefficient. One can derive the energy coefficient β from R by:

$$\beta = |R|^2, \tag{2.9}$$

as energy is proportional to the pressure squared.

Assuming that transmission through a material is negligible ($\tau \approx 0$), as assumed here for many surfaces such as noise barriers, and for infinitely thick materials such as grounds, the absorption coefficient α can be derived from R as:

$$\alpha = 1 - |R|^2. \tag{2.10}$$

Surfaces can be quantified either by their reflection and absorption coefficients or their acoustical impedance Z, measured in Rayls (Pa·s/m). The specific acoustic impedance of a material is defined as:

$$Z = \frac{p}{u}, \tag{2.11}$$

where p is the acoustical pressure and u is the particle velocity. The characteristic impedance of a medium is given as:

$$Z = \rho c, \tag{2.12}$$

where ρ is the density of the medium in kg/m^3 and c is the speed of sound in that medium.

Ground surfaces can be characterized as either locally or extended reacting. They are locally reacting when the speed of sound in the ground is much lower than the speed of sound in air. This causes the sound in the ground to propagate normal to the ground surface, regardless of the sound's angle of incidence on the ground. Therefore the ground impedance is independent of the angle of incidence. When this is not the case, extended reaction occurs and the impedance is dependent on the angle of incidence.

2.4 Outdoor Sound Propagation

Outdoor sound propagation in the simplest case involves a source and a receiver above a specularly-reflecting plane. There are two sound paths between the source and receiver, as shown in Figure 2.1: the direct path and the reflected path. The sound pressure at the receiver is therefore given by:

$$p = p_s \left(\frac{e^{-ikr_d}}{r_d} + R\frac{e^{-ikr_r}}{r_r} \right), \tag{2.13}$$

where p_s is the source amplitude, R is the reflection coefficient of the ground, and r_d and r_r are the direct and reflection sound path distances, respectively.

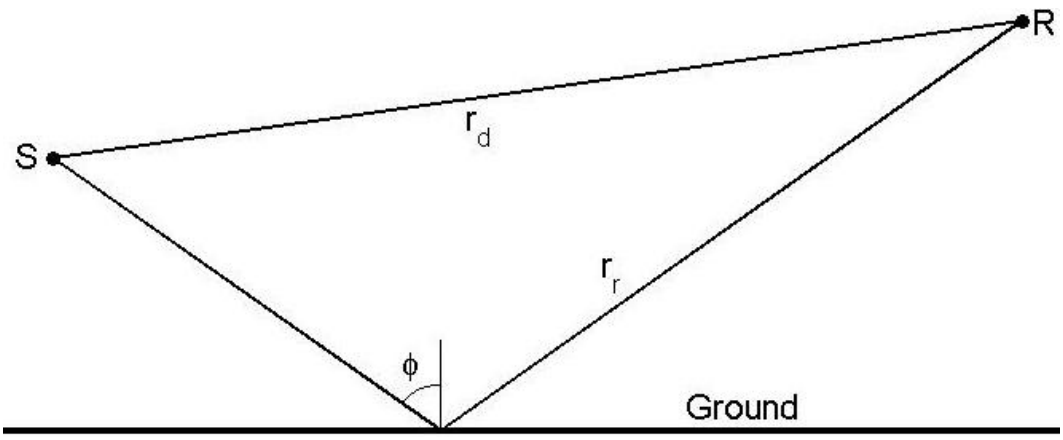

Figure 2.1: Idealized sound propagation between a source S and receiver R over a ground surface.

Sound propagating in a free field is attenuated due to geometrical spreading: 3 dB per doubling of distance for cylindrical waves and 6 dB for spherical waves. The reflected sound path is longer, and therefore is subject to more attenuation due to geometrical spreading. The sound is also attenuated due to the reflection from the ground if the magnitude of the reflection coefficient is less than one. A phase change during reflection can also occur.

Because of this path length difference, constructive and destructive interference occurs between the direct and reflected waves. Because of this interference, dips in the sound level will occur at several frequencies. In the case of acoustically hard ground, these frequencies correspond to when the path length difference is an odd multiple of $\pi/2$, where the waves are 180^o out of phase.

Several atmospherical effects occur which impact the propagation of sound outdoors. Absorption by air occurs, causing the sound pressure of a wave to decrease as it propagates through air. Energy is converted into modes of vibration of oxygen and nitrogen molecules, and is dependent on frequency, relative humidity and temperature. These effects only become significant at high frequencies or large distances.

Other atmospherical effects include wind and temperature gradients [2] and turbulence [3]. Wind and temperature gradients affect the speed of sound, causing it to vary

with height; therefore sound waves refract in the atmosphere. As these phenomena affect the performance of noise barriers only for large propagation distances, they are not relevant in this work.

Turbulence consists of random eddies in the air, which can change the local direction or amplitude of sound waves at random and may affect the performance of a noise barrier in an unpredictable way. Because of this, prediction models which do not take turbulence into account may vary from measurements.

2.5 Noise Barriers

The effectiveness of a noise barrier is quantified by the insertion loss (IL), the change in sound level at a certain receiver position due to the barrier, given as:

$$IL = L_{p,nobarrier} - L_{p,barrier} \tag{2.14}$$

where $L_{p,nobarrier}$ and $L_{p,barrier}$ are the sound pressure levels taken without and with the barrier, respectively. A positive IL indicates a reduction in noise levels, while a negative IL indicates an increase (amplification).

Sound reaches the opposite side of a noise barrier by means of diffraction, the bending of sound waves around an edge. The amount of sound that is diffracted depends on the thickness and absorption of the edge, as well as the source and receiver positions and frequency. There are several models used to predict diffraction, which are discussed in Section 7.1. Typically, the IL of a barrier increases with frequency, meaning that less sound is diffracted as the wavelength decreases.

Maekawa [4] developed a simple method of predicting the IL of a semi-infinite plane

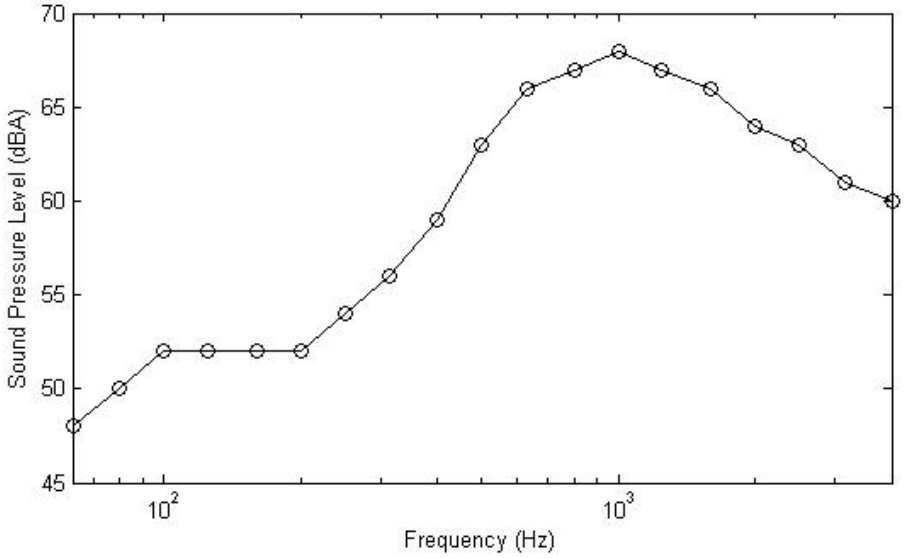

Figure 2.2: Typical A-weighted traffic-noise spectrum used to determine total A-weighted IL's. [5]

screen in a free-field. He defined a Fresnel number N to be:

$$N = \pm\frac{2\delta}{\lambda} \tag{2.15}$$

where δ is the path length difference between a direct source-receiver path and a source-edge-receiver path. The negative sign is used when there is a direct line of sight between the source and receiver. From N, one can determine the IL from a graph, which shows the IL increasing monotonically with N and therefore frequency. When studying roadside noise barriers, the sound source of interest is traffic, which has a characteristic frequency spectrum. Figure 2.2 shows a typical A-weighted traffic spectrum, measured by Wakefield Acoustics [5]. A-weighting takes human hearing into account, as people do not perceive every frequency to be of equal loudness.

As well as considering the frequency-dependent IL, it is of interest to consider the total IL, where $L_{p,nobarrier}$ and $L_{p,barrier}$ are the total levels which encompass all frequencies.

When discussing the total IL, it can be given in A-weighted decibels (dBA) so as to relate to what people would hear. The results in this work that are presented as A-weighted IL's have been calculated using the A-weighted traffic noise spectrum in Figure 2.2 as a reference. When a sound source was used, its power output was subtracted from the noise levels and then the A-weighted traffic spectrum was added, before summing the levels up over all frequencies to get a total value. These totals in dBA were then subtracted as in Equation 2.14 to determine the total A-weighted IL. As a reference of acceptable IL values, the B.C. Ministry of Transportation and Infrastructure Noise Policy [1] states that a mitigating noise wall must provide an IL of at least 5 dBA.

Chapter 3

Literature Review and Objectives

This chapter reviews existing literature on the effects of using absorptive noise barriers. It then discusses the literature on sound propagation through foliage, followed by the effects of combining foliage with noise barriers. Once this literature is reviewed, the detailed objectives of this work are presented.

3.1 Absorptive Noise Barriers

Rawlins [6] conducted theoretical studies on the diffraction of sound by an absorbent edge of a screen. He solved the boundary value problem of a rigid barrier with an absorbent edge, which he then studied asymptotically. He showed that a strip, one wavelength wide, of absorbent material at the top of a half plane led to the same diffracted sound field as a fully covered screen.

Fujiwara et al. [7] derived approximate theory for diffraction around an absorptive barrier. They then developed charts which had the effects of absorption in dB as a function of the reflection coefficient of the absorptive surface. Different charts were made for various angles of diffraction. They found large absorption effects of up to 7 dB.

Isei [8] developed a prediction method which used the specific flow resistance to define the acoustical properties of a barrier and ground. He saw that the field behind a barrier showed interference between the direct and reflected sound paths. He found that the type of ground influenced the IL more than the absorption of the barrier.

May and Osman [9] used a 1:16 scale model to study different shapes of noise barriers.

They tested both absorptive and reflective noise barriers and found that making the source side absorptive resulted in a measurable reduction in the amplification due to parallel barriers. They found that the higher the NRC value of the absorptive material, the greater the improvement of the IL. For a single barrier, using a point source, covering the source side of a thin barrier with absorptive material gave an IL increase of 0.8 dBA. Covering the top of a 2.44 m wide barrier with absorptive material gave an IL increase of 2 dBA over a wide reflective barrier. They studied the 500 and 1000 Hz third-octave bands, but did not perform a more detailed frequency analysis.

Bowlby et al. [10] used geometrical acoustics to study reflections from a reflective noise barrier and the effects it had on the performance of parallel noise barriers. They found that using sound absorptive material on parallel barriers minimized the increase in noise caused by these reflections.

Tobutt and Nelson [11] used a computer model to test the effectiveness of absorptive treatment on 3 m high parallel noise barriers set 45 m apart. The receivers were set 20 to 70 m behind the barrier and up to a height of 4.5 m. The difference in noise levels with and without absorptive treatment ranged from 1.5 to 3 dBA.

Fujiwara, Hothersall and Kim [12] used a boundary element model to study the insertion loss of noise barriers with rectangular, T-shaped and cylindrical edges and rigid, absorbing or soft surfaces. They found the mean IL for the rectangular, absorbing barrier to be 3.9 dB higher than for the rectangular and rigid barrier. They found that cylindrical edges and soft surfaces made for the most effective barrier.

Morgan, Hothersall and Chandler-Wilde [13] also used a numerical boundary element model, this time examining track-side railway noise barriers. They studied different shapes of barriers, both with reflective and absorbing surfaces. The results from the two models were compared. Two source distances were considered, corresponding to both the near and far sides of the tracks — approximately 3 and 8 m away, respectively. They found

that adding an absorbing surface to the track-facing side of a barrier significantly improved the performance. When the source was on the near side of the track the IL increased by approximately 10 dB when an absorptive surface was added. When the source was on the far side of the track the IL increased by approximately 4 dB. Increasing the height of the absorbing barrier also improved the performance.

Watts and Godfrey [14] studied the effects on roadside noise levels of applying sound-absorptive materials to the traffic face of noise barriers. They chose two sites. The first site had a single 3 m high barrier erected next to an eight-lane highway. The other site had 3.7 m high barriers on both sides of the road which ran in a shallow cutting, with a separation distance of 34 m. Both sites had the same absorbent panels on the traffic side and were reflective on the reverse side. They measured both sites as they were, and then reversed the panels such that the reflective side faced the traffic.

For the 3 m high barrier, which was placed 5.6 m from the edge of the road, receivers were placed 9.5 m behind the barrier, at heights of 1.7, 2.7 and 4.7 m. For the other site, where the barrier was 7.5 m from the road, receivers were placed both 15 and 30 m behind the barrier; they were at heights of 1.5, 4.5 and 7.5 m. In both cases they placed a reference microphone further down the road where there were no barriers set up. They found, in both cases, that there was a decrease in noise due to absorption of generally less than 1 dB when the absorptive side faced the traffic. The one exception was in the second case, where the receiver was 15 m behind the barrier and at a height of 7.5 m. Here there was a decrease in noise of around 2 dB. In general, the results were lower than predicted.

Previous studies have been done in anechoic chambers at full scale to study absorption. L'Esperance, Nicolas and Daigle [15] built a barrier in a semi-anechoic chamber. The barrier had a height of 0.577 m and was 5 m in length. The barrier was made of 2.5 cm thick plywood, with the upper 1.0 cm tapered to a sharp edge. A source was placed 0.6 m from the barrier, at a height of 1.1 cm. The receiver was placed at 1.2, 0.6, 0.3 and 0.15

m from the barrier on the receiver side in four different tests, all at a height of 6 mm.

They measured the insertion loss for three barrier conditions: both sides of the barrier reflective, the source side of the barrier covered with a 4 cm thick fiberglass layer, and both sides covered with the fiberglass. They compared these results to theory, which combined an approximate diffraction solution with a classical theory for propagation over ground.

The experiment examined the effect of the angle of diffraction on the insertion loss. The results showed that the effect of the absorptive layer can increase the IL by up to 10 dB when the diffraction angles are large. They examined two previous studies on barrier absorption which gave contradicting results. They pointed out that when the results in Isei's work [8] showed little increase in IL due to absorption, the angle of diffraction was quite low (source and receiver 2 m away from a barrier 0.26 m high). They found that when a greater increase in IL was seen in Fujiwara's work [7], the diffraction angles were greater.

They found that covering both sides with an absorbent barrier increased the IL, especially when both the receiver and the source were located near the barrier. The results also showed that covering the receiver side was just as effective as having the source side covered. They saw an IL increase of 2 dB when the absorptive layer was added to the source side, and a greater increase (ranging from 1-7 dB, depending on the angle) when both sides were covered.

Ilgurel and Sozen [16] built a wall in a semi-anechoic chamber with dimensions 11 m x 6 m x 4.5 m. The barrier was 2.6 m high, made from two-sided 12 mm gypsum panels with a 10 cm air gap and a 5 cm Rock-wool filling. Measurements were taken with and without a 5 cm thick Rock-wool layer on one entire side of the barrier (the side facing the source) as an absorptive layer.

The noise source was placed 1 m high and 1 m away from the barrier. Receivers were placed on seven different axes, 15 degrees apart, ranging from 0 degrees (directly above

the barrier) to 90 degrees (perpendicular to the barrier). Six receivers were placed on each axis, 1 m apart. The lowest receiver was placed at a height of 1.6 m.

Results were obtained for overall and 125-8000 Hz octave-band levels. They found noise reduction levels between 13.3 and 15.4 dBA without the absorptive layer and between 16.3 and 20.0 dBA with the absorptive layer. Specifically, they found possible noise reductions due to the absorptive layer of 1.5-3.5 dBA. This was not found for the receivers set up at 0-30 degrees, where there was still a direct line of sight from the source to the receiver. The absorptive layer provided extra noise reduction at frequencies over 1000 Hz.

3.2 Tree Foliage

3.2.1 Sound Propagation Through Foliage

The first study of the effects of foliage on sound was in 1946, performed by Eyring [17]. He investigated the sound propagation through a jungle during the wet season in Panama. He measured sound produced by loudspeakers over several hundred feet. He concluded that within a jungle, temperature and wind gradient effects are negligible. Terrain loss coefficients, ignoring spherical divergence, were found to increase with frequency and have total values of 0.05-0.13 dB/m. Typical loss coefficients over open terrain were found to be 0.003-0.03 dB/m, depending on the thickness of the grass. Wiener and Keast [18] measured the excess attenuation of sound through a dense evergreen forest, where trees were 6-12 m tall. They also found that attenuation increased with frequency, with approximately attenuation coefficients of 0.03 dB/m at 500 Hz and 0.20 dB/m at 4000 Hz.

Another trend reported in literature was higher foliage attenuation at low and high frequencies with a decrease at middle frequencies [19] [20] [21]. Attenuation coefficients of 0.2 to 0.6 dB/m were seen. Morton [21] noted that as he measured further from the ground, the low frequency attenuation decreased and the trend became similar to that

seen by Eyring, an increase in attenuation with frequency; he found values going from 0.10 dB/m at 100 Hz up to 0.30 dB/m at 10 kHz. Therefore, the low frequency attenuation was attributed to ground effects; grounds beneath trees contain roots, which affect the porosity and impedance.

Cook and Van Haverbeke [22] looked into using trees and shrubs for noise abatement in great detail. They studied many different types and configurations of trees with three different noise sources: a diesel truck, an urban bus and arterial cars. For a 6 m thick tree belt with shrubs to increase density, they found an attenuation of 8 dBA when taken 6 m behind the foliage. They also found that putting the trees closer to the source rather than the receiver increased the attenuation provided by the foliage. They recommended, for moderate-speed cars in urban areas, to use 6 to 15 m wide belts of trees and shrubs, with the trees placed as close to the road as possible.

Measuring the attenuation provided by tree belts was done by Kragh [23], who measured sound levels from passing trains, both over a grass terrain and through tree belts. The author stated that the attenuation found by taking the difference of the two measurements was both due to the foliage and variations in terrain, whose effects were impossible to separate. It was found that a dense, 50 m wide tree belt which contained beeches, birches, elms and various conifers provided 8 or 9 dB of attenuation. A dense, 25 m wide belt which consisted of oaks, hornbeams, poplars, silver firs and various bushes was found to give 6 or 7 dB of attenuation.

Several studies were done on both foliated and defoliated trees to determine the effects of the foliage compared to the branches. Aylor [20] examined the same hardwood brush in summer and in autumn. He found a decrease in attenuation of up to 0.16 dB/m in the autumn. He found increasing leaf density reduced sound transmission. Aylor also studied the effect of leaf size and density on the sound transmission of trees [24]. He found that to attenuate noise effectively, vegetation should be dense and broad-leafed.

Price et al. [25] measured sound propagation through trees during the winter and the summer to determine the effects of trees with and without foliage. They found significant differences between winter and summer, both in a peak attributed to ground effects and in the high-frequency attenuation, which increased by up to 10 dB in the summer. They then developed prediction models which included contributions from the ground effects and the dimensions and density of both the trunk and other foliage.

Martens [26] set up foliage testing in an anechoic chamber using different plants in earthenware pots. He measured the sound pressure level 6 m from the source for several foliage situations: pots with no foliage, birch trees fully defoliated with stems and branches present, half of the 46 trees foliated, and then all of them foliated. There was little difference found between the first two cases up to 8000 Hz. At 8-10 kHz, where the wavelength corresponded to the dimensions of the birch tree stems, a 3 dB drop in sound pressure level was seen. When looking at the influence of foliage, a general trend was seen. Some noise amplification was measured at mid-frequencies up to a certain frequency, depending on the type of plant, above which a drop in noise was seen.

An empirical formula was developed by Hoover [27], who performed many measurements of sound propagating through a forest. He gave the attenuation due to foliage A_f in dB as:

$$A_f = 0.01 r_f f^{\frac{1}{3}}. \tag{3.1}$$

Here, r_f is the distance in meters and f is the frequency in Hz.

3.2.2 Foliage and Barriers

While much work has been done on studying sound propagation through foliage, there have been only a few studies on the effects of the performance of barriers placed near foliage.

Cook and Van Haverbeke [28] studied the combination of barriers with trees as a method of noise control. They compared the total A-weighted sound levels behind different con-

figurations, including bare walls, trees and walls with trees, with no walls or foliage. They found that trees gave approximately 4-5 dBA of attenuation, while a bare wall gave 10-11 dBA and trees with a wall gave 13-14 dBA of attenuation.

Renterghem et al. [29] studied the effect of using tree foliage as a wind screen to prevent the refraction of sound around a barrier in a downwind direction. Sound refraction occurs when the speed of sound changes with height, as occurs in wind. The bending of sound waves can make a barrier less effective at large distances and therefore preventing this effect is desirable. They created a 1:20 scale model in a wind tunnel and used windscreens to model the scale-model trees. They first confirmed the decrease in IL when wind was present, finding IL decreases of up to 8 dB at a distance of 10 times the barrier height away from the barrier. Once the windscreens were inserted, in the absence of wind they found that the change in IL was very small and sometimes negative. They attributed this to the scattering of the wind screen. For farther distances when wind was present, the windscreen always increased the IL, by up to 4 dB. When closer than five times the height of the barrier, no effect was greater than 1 dB.

Renterghem et al. [30] also performed field tests, where measurements behind a noise barrier with and without trees were compared. They found that for downwind sound propagation, the trees increased the effectiveness of the noise barrier. As wind speed increased, so did the improvement in performance by the barrier; improvements of up to 4 dBA were seen for winds at 12 m/s. For upwind sound propagation, trees only affected the performance slightly, starting with a slightly negative change in IL for low velocity winds and increasing to 0.5 dB for faster-moving winds. They did a frequency dependent study on noise levels behind a barrier with and without a single row of 8 m tall trees behind it in the absence of wind. They found that at low frequencies, noise levels in the no-trees case were higher; above 1000 Hz they found that noise levels in the treed case were higher, with all effects under 5 dB.

Chapter 4

Full-Scale Laboratory Testing

In the research described in this chapter, a full-scale reflective barrier was built in an anechoic chamber to better understand the effects of absorption placement on a single barrier's performance. This was achieved by placing three different absorptive materials on the reflective wall in different configurations. These materials had their absorption coefficients measured by two techniques: the spherical decoupling method and the impedance tube method. Insertion loss measurements were first made using a porous absorber as the surface absorption. Then measurements were made using two commercially available absorbent barrier treatments. The insertion loss was measured in third-octave bands for various configurations of the reflective and absorptive barriers; from these, total A-weighted values relevant to a typical traffic-noise spectrum were calculated. Soft ground effects, occurring when the barrier is placed on an acoustically soft surface, were also examined. The size of the anechoic chamber limited the source and receiver distances and the height of the wall, and therefore realistic dimensions could not be achieved.

4.1 Absorption Measurements

Two methods were used to determine the normal-incidence absorption coefficients of the absorptive surfaces: the spherical decoupling method [31] and the impedance tube method [32].

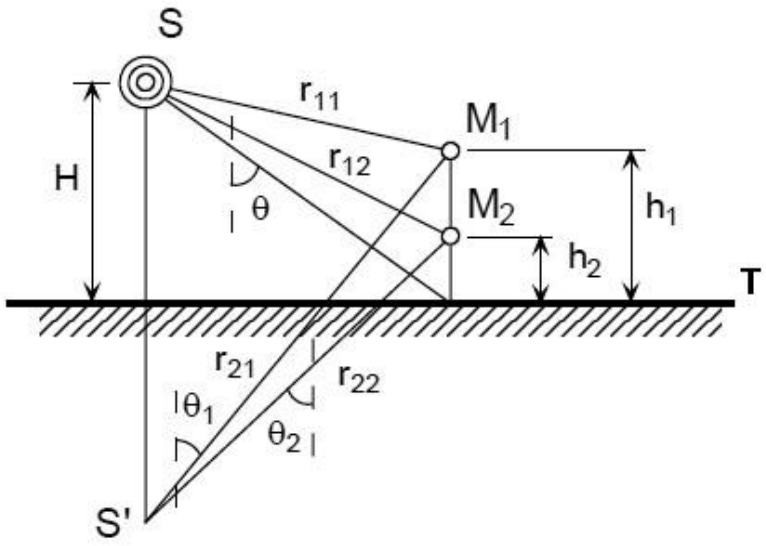

Figure 4.1: The spherical decoupling method geometry [31].

4.1.1 Spherical Decoupling Method

The spherical decoupling method uses two microphones located perpendicular to a material at some spacing to determine its acoustical properties. The transfer function between the microphones is measured and from this the complex sound reflection coefficient, energy absorption coefficient and acoustical impedance can be calculated. Figure 4.1 shows the set up of a typical measurement. Two microphones, M_1 and M_2 are placed at heights h_1 and h_2 above a surface. A source S is placed at height H above the surface, creating an angle of incidence θ with the surface beneath the microphones.

Assuming specular reflection and a time dependence of $e^{i\omega t}$, the pressure at each microphone is given as:

$$P_j(f,\theta_j) = P_o(f)\left[\frac{e^{-ikr_{1j}}}{r_{1j}} + R\left(f,\theta_j\right)\frac{e^{-ikr_{2j}}}{r_{2j}}\right], \tag{4.1}$$

for $j = 1, 2$, where $P_o(f)$ is the source amplitude and $R(f,\theta)$ is the reflection coefficient [31]. The frequency response function between microphones, defined as $H_{12} = \frac{P_2(f,\theta)}{P_1(f,\theta)}$, can be

simplified to:

$$H_{12}(f,\theta_1,\theta_2) = \frac{\frac{e^{-ikr_{12}}}{r_{12}} + R\left(f,\theta_2\right)\frac{e^{-ikr_{22}}}{r_{22}}}{\frac{e^{-ikr_{11}}}{r_{11}} + R\left(f,\theta_1\right)\frac{e^{-ikr_{21}}}{r_{21}}}. \tag{4.2}$$

For sufficiently large source heights and small receiver heights, $\theta_1 \approx \theta_2 \approx \theta$. By using this approximation and rearranging Equation 4.2, the complex reflection coefficient is given by:

$$R(f,\theta) = \frac{\frac{e^{-ikr_{12}}}{r_{12}} - H_{12}(f,\theta)\frac{e^{-ikr_{11}}}{r_{11}}}{\frac{e^{-ikr_{21}}}{r_{21}}H_{12}(f,\theta) - \frac{e^{-ikr_{22}}}{r_{22}}}. \tag{4.3}$$

The energy absorption coefficient α can be derived from the reflection coefficient by the following equation:

$$\alpha = 1 - |R|^2, \tag{4.4}$$

which assumes that no sound is transmitted through the material.

The impedance, as a function of the reflection coefficient, is given as:

$$Z = \frac{1+R(f,\theta)}{1-R(f,\theta)}\frac{1}{\cos\theta\left(1+\frac{1}{ikr_o}\right)}, \tag{4.5}$$

where r_o is the distance from the source to the ground directly beneath the microphones.

This method is not valid at all frequencies. Boden and Abom [33] examined ways to minimize the error in the reflection coefficient when using the two-microphone method. They suggested the following frequency limits:

$$0.1 * \frac{c}{2(h_1-h_2)\cos\theta} < f < 0.8 * \frac{c}{2(h_1-h_2)\cos\theta}. \tag{4.6}$$

4.1.2 Impedance Tube Method

The impedance tube method is also a two-microphone method, although the measurements only apply to normal incidence. The impedance tube is a hollow tube which has a loudspeaker at one end and the material of interest placed at the other; the size of the tube

varies depending on the frequency range of interest. The sample of the material must be a circle with a diameter matching that of the tube, in this case 10 cm. Two microphones are inserted into the side of the tube so they are set up perpendicular to the sample and the loudspeaker.

The equations from the previous section still hold, although now $\theta = 0$ and therefore $\cos\theta = 1$. The reflection coefficient can therefore be written as:

$$R = \frac{H_{12} - e^{-iks}}{e^{iks} - H_{12}} e^{ikh_1}, \tag{4.7}$$

where s is the spacing between the microphones. The impedance is calculated from the reflection coefficient by:

$$Z = \frac{1+R}{1-R}. \tag{4.8}$$

The impedance tube is limited to frequencies below which only plane waves propagate in the tube and at which wavelengths are greater than twice the microphone spacing, causing the upper limit to be given by the minimum of the following [32]:

$$f_u < 0.58\frac{c}{d} \tag{4.9}$$

$$f_u < 0.45\frac{c}{s}, \tag{4.10}$$

where d is the tube diameter and s is the spacing between the microphones. The lower frequency limit is [32]:

$$f_l > 0.05\frac{c}{s}. \tag{4.11}$$

Figure 4.2: The reflective barrier in the anechoic chamber.

4.2 Experimental Setup

The tests were done in an anechoic chamber with dimensions 4.1 m x 4.7 m x 2.6 m. A 3.66 m x 3.66 m floor was built on top of the existing wire mesh floor, as a strong support and reflective surface for the wall to be placed on. This allowed for outdoor conditions to be modelled, with perfectly absorbing walls and ceiling and a sound reflective ground. The floor was made of seven 3.66 m long 2x4's, evenly spaced on the wire mesh floor, with 19 mm plywood boards screwed on top. The wall, shown in Figure 4.2, was 3.66 m long and 1.22 m high, and was made from 12 mm drywall on either side of a wooden frame, made from 2x4's. An extra layer of 12 mm drywall was screwed onto the source side of the wall to increase the transmission loss. To reduce sound transmission, the cavity was filled with fiberglass batt insulation. Air gaps between the barrier and the floor were filled with putty. The wall was set up in the center of the floor in the chamber. Absorptive materials were hung in different configurations on the faces of the wall, including either half or all of either the source and receiver sides. Due to lack of absorbent materials, all of both sides were not simultaneously covered.

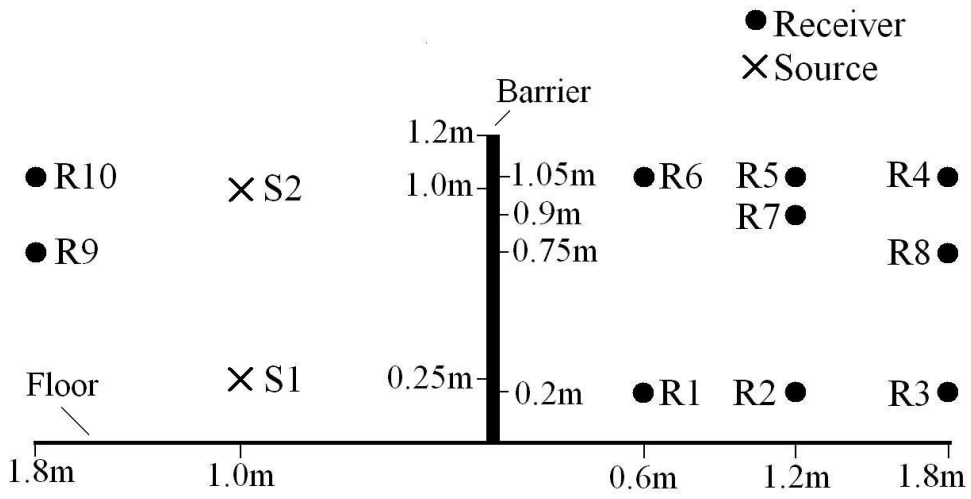

Figure 4.3: The barrier configuration, including source and receiver positions. Note that R6, R7 and R8 correspond to the same diffraction angle.

The sound source was placed 1 m behind the barrier, at heights of 0.25 and 1.0 m. The sound sources used were omni-directional point sources — one for high frequency (above 500 Hz) and the other for low frequency (below 500 Hz) [34].

Figure 4.3 shows the test configuration. The receiver was placed at distances of 0.6, 1.2 and 1.8 m on the non-source side of the barrier, at heights of 0.2 and 1.05 m. The receiver was also placed 1.8 m behind the barrier at a height of 0.75 m, and 1.2 m behind the barrier at a height of 0.9 m. This allowed for examination of both different angles of diffraction as well as varying distances at a constant angle. Receiver positions were also on the source side for the low source height, 1.8 m away, at heights of 0.75 and 1.05 m in order to measure the effects of reflections from the barrier. A Bruel & Kjaer 1/2" type 4190 microphone was used, along with a B&K type 2669 preamp. A SINUS Soundbook was used as the white-noise signal generator and the analyzer, allowing both narrow-band and limited-band analysis.

(a) (b)

Figure 4.4: The commercial absorbent materials on the barrier: a) Durisol; b) WhisperWall.

4.3 Absorptive Materials

The first absorptive material used on the wall was cotton acoustic baffles. Each baffle was 1.22 m x 0.61 m and 25 mm thick. Two layers of these baffles were used, giving a total thickness of 50 mm.

Two different commercial absorbent barrier surfaces were also tested. The first involved Durisol panels which were each 1.22 m x 0.61 m and made of cement and wood fibers. One side of the panels was fluted, with a base of 5.1 cm and a flute depth of 3.2 cm. Figure 4.4(a) shows the Durisol panels covering one side of the barrier.

The other commercial absorbent barrier surface tested was WhisperWall. The tiles were 0.61 m x 0.61 m and were 10.2 cm thick. Figure 4.4(b) shows the WhisperWall tiles covering one side of the barrier.

The normal-incidence absorption coefficients of these materials were measured using the spherical decoupling method and the impedance tube method. The frequency range of validity for the set up used here for the spherical decoupling method was 340 to 2750 Hz and for the impedance tube was 250 to 2000 Hz. The random-incidence absorption coefficients (α_{RI}) of the three absorbent materials were calculated on the assumption of

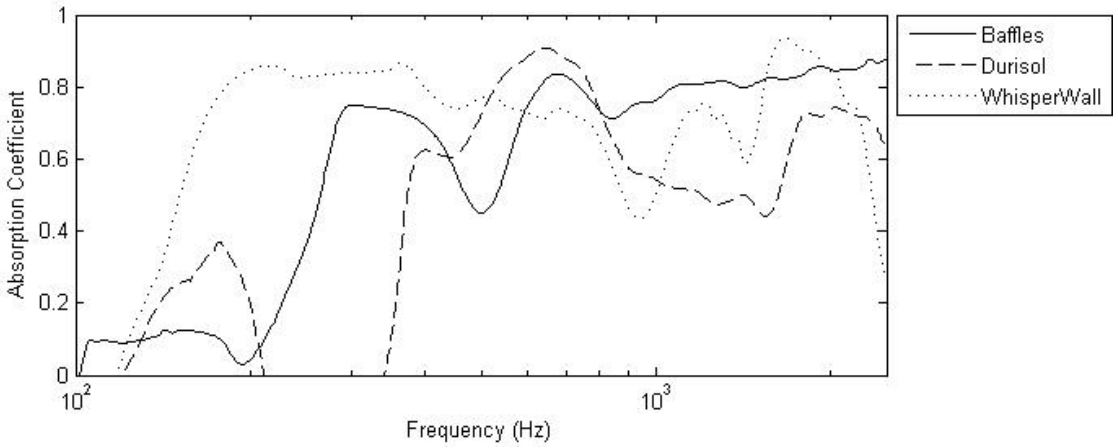

(a)

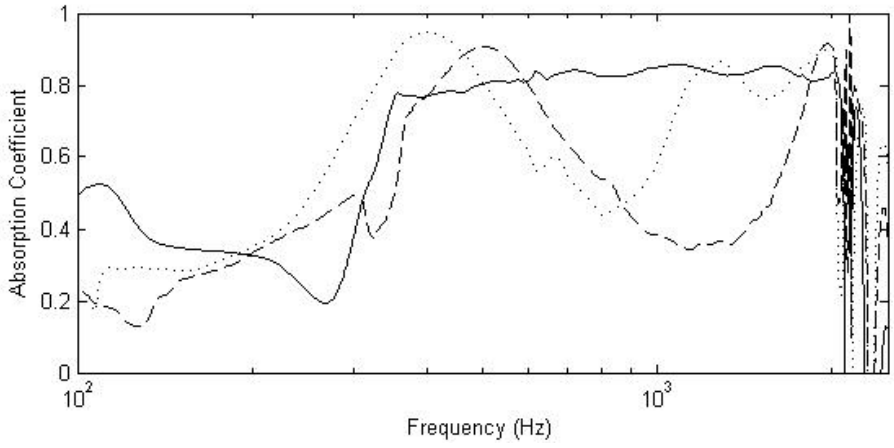

(b)

Figure 4.5: Random-incidence absorption coefficient as measured by: a) the spherical decoupling method; b) the impedance tube method.

local reaction by the following equation:

$$\alpha_{RI} = 8\kappa \left[1 + \left(\frac{\kappa^2 - \gamma^2}{\gamma} \right) \tan^{-1} \left(\frac{\gamma}{\gamma^2 + \kappa(\kappa+1)} \right) - \kappa \ln \left(\frac{(\kappa+1)^2 + \gamma^2}{\kappa^2 + \gamma^2} \right) \right], \qquad (4.12)$$

where

$$\kappa = \mathrm{Re}\left(\frac{1}{Z} \right), \quad \gamma = \mathrm{Im}\left(\frac{1}{Z} \right). \qquad (4.13)$$

These values are shown in Figure 4.5.

Figure 4.6: Half of the reflective wall covered in the acoustic baffles.

Using the impedance tube results, the NRC values — the average octave-band absorption coefficients at 250, 500, 1000 and 2000 Hz — were calculated. The NRC of the baffles was 0.71, of the Durisol panels was 0.56, and of the WhisperWall tiles was 0.64. Note that there is some reason to believe these WhisperWall panels had not been manufactured in a way to optimize their sound absorption.

4.4 Results

4.4.1 Acoustic Baffles

The baffles were attached to the wall using insulation hangers; they were attached in five different configurations, which covered the barrier as follows: the full source side, the top half of the source side, the full receiver side, the top half of the receiver side, and the top half of both the source and receiver sides. Figure 4.6 shows the top half of the source side of the wall covered with baffles. The insertion losses of these configurations and of the reflective wall were measured.

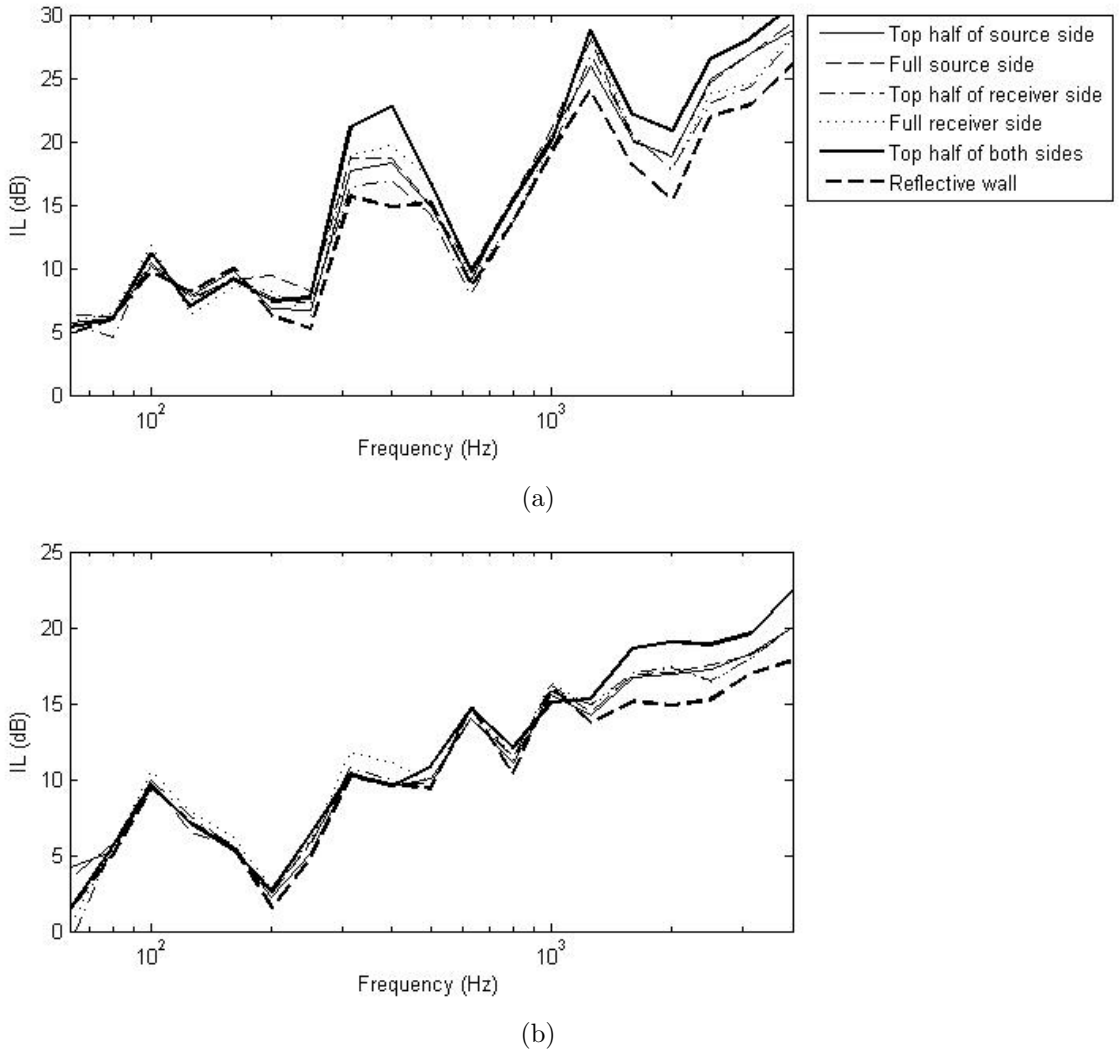

Figure 4.7: Measured third-octave insertion loss at receiver position R6 for different baffle configurations for: a) the low source position; b) the high source position.

The IL in third-octave bands at receiver position R6 is shown in Figure 4.7 for the different baffle configurations. For the low source position, the absorptive material was more effective at increasing the IL in the frequency ranges where the baffles were highly absorptive. Between 300 and 400 Hz, where the absorption coefficient of the baffles was highest, covering the top half of both sides increased the IL by 7-8 dB over that of the reflective wall, a 4 dB increase over any other absorptive configuration. At frequencies above 1000 Hz, where porous absorbers were expected to be highly absorptive, there was

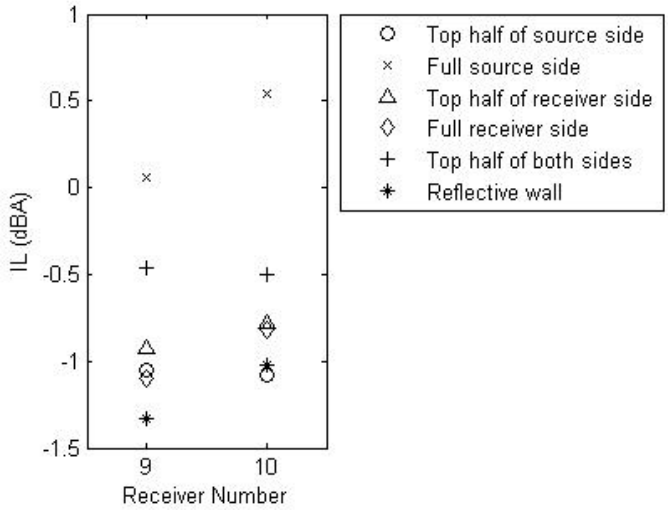

Figure 4.8: The A-weighted insertion loss for the low source position as measured at the source-side receiver positions, for various configurations of reflective and absorptive barriers.

a 3-5 dB increase in IL due to covering the top half of both sides with baffles. For the high source position this high frequency increase in IL was again seen; however below 1000 Hz there was very little increase in IL due to the absorptive treatment, regardless of the configuration. This was due to the smaller diffraction angles that were present for the high source position. These trends were consistent for the other receiver positions.

Figure 4.8 displays the total A-weighted IL at the source-side receiver positions for the low source height. The IL was expected to be negative since sound that, without the wall in place, would be absorbed by the chamber walls was now reflected back to the receiver. As expected, covering the full source side of the wall with absorptive material increased the IL to positive values, which confirmed it was highly effective at preventing reflections.

Figure 4.9 shows the total A-weighted insertion loss at each receiver position for both the low and high source positions for each baffle configuration. The reflective wall provided 12-18 dBA of attenuation, and the overall IL improvement due to absorption was 1-2 dBA. It was seen that, of the configurations tested, placing the absorptive material on the top

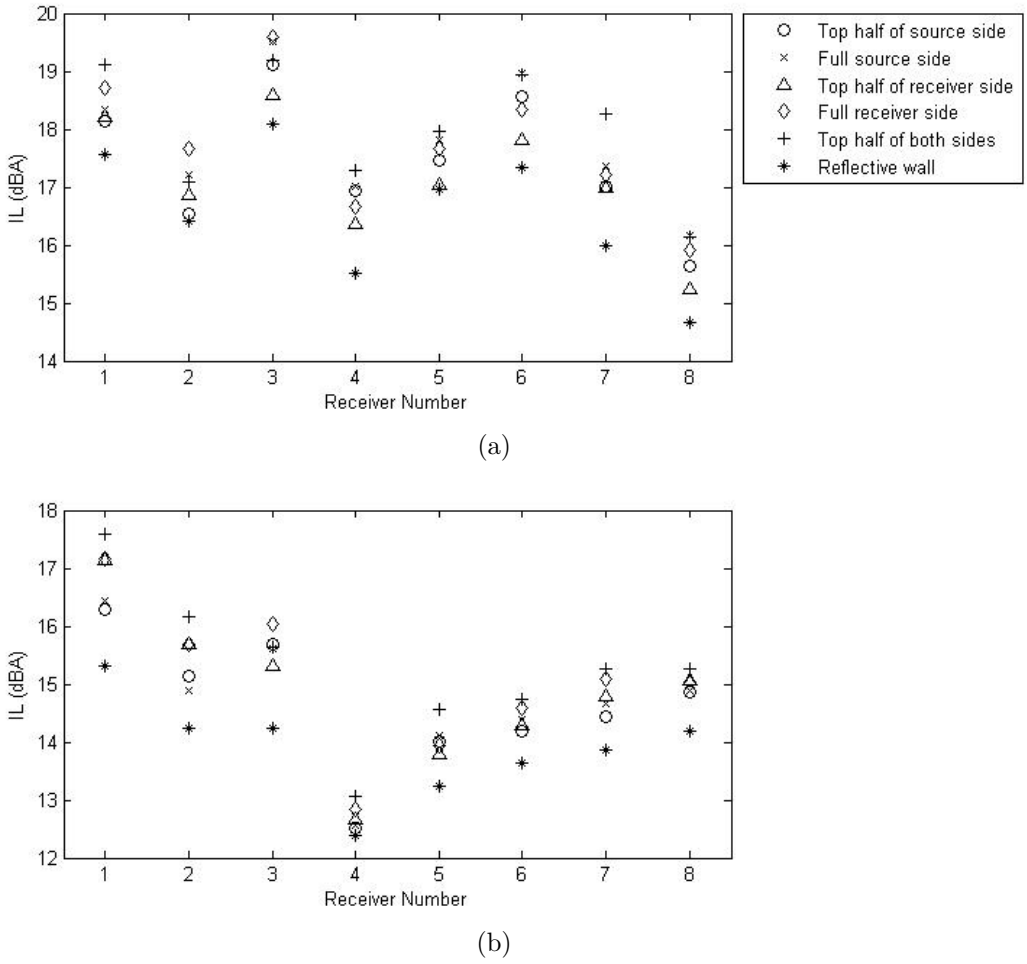

Figure 4.9: Measured A-weighted insertion losses at the eight receiver positions on the non-source side of the barrier for different baffle configurations for: a) the low source position; b) the high source position. The receiver positions are labeled 1 through 8 as shown in Figure 4.3.

half of both sides of the wall produced the highest IL for both source positions, while the reflective wall produced the lowest IL, as expected. Covering the full side of the barrier compared to covering half — either the source or receiver side — showed an IL increase of approximately 0.5 dB. Covering the full side of both sides of the barrier was not tested; however based on the other measurements an improvement in IL of 2-3 dBA over the reflective wall could be expected.

For the higher source position, R1, R2 and R3 showed the highest insertion loss. These

were the lowest receiver positions, corresponding to the greatest diffraction angles and greatest path length differences. Receiver R4 had the lowest IL, as it was the highest and farthest receiver position from the wall, giving it the lowest diffraction angles and the smallest path length difference. Receivers R6, R7 and R8 were positioned such that they had the same angle of diffraction, and therefore the IL was expected to increase with path length difference. Increasing IL's from R6 to R8 was in fact seen in the results.

For the lower source position, the IL at all receiver positions was higher compared to the higher source position, as expected due to the larger diffraction angles. However the results were not as expected at several receiver positions. The IL decreased from R6 to R8, contrary to expectation. The IL at R3 was higher than at both R1 and R2, where it was expected to be lower. There may have been interactions between the direct and reflected waves, either constructive or destructive interference, which affected the sound levels at particular frequencies for different receiver positions.

4.4.2 Commercial Absorbent Barriers

The Durisol panels were screwed onto the reflective wall in three different configurations: covering the full source side, the top half of the source side and the top half of both sides. In the field, the manufacturer constructs barriers with a solid concrete layer in the center and absorptive panels on either side. The WhisperWall tiles were measured in one configuration: covering the full source side of the barrier. This is the configuration that the manufacturer reported using in the field.

The IL differences between the three configurations of the Durisol panels were very similar to those of the baffle configurations. Covering the top half of both sides of the barrier gave the highest IL at receivers on the non-source side, and covering the full source side gave the highest IL on the source side of the barrier.

The three different absorptive materials were compared for one configuration: covering

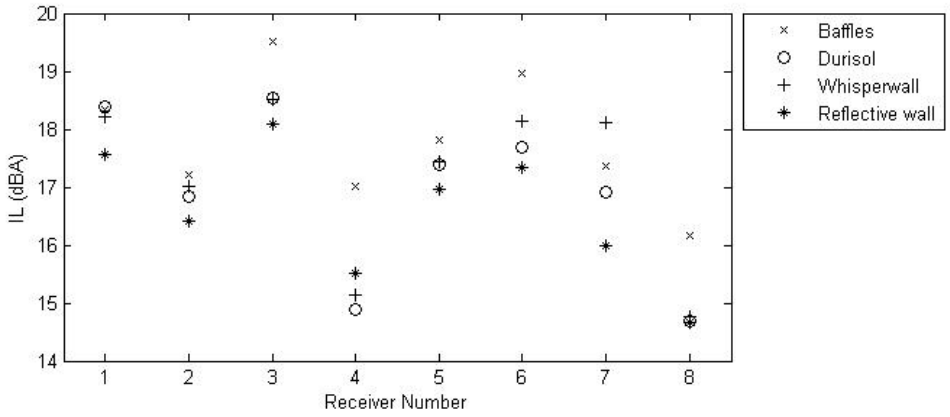

(a)

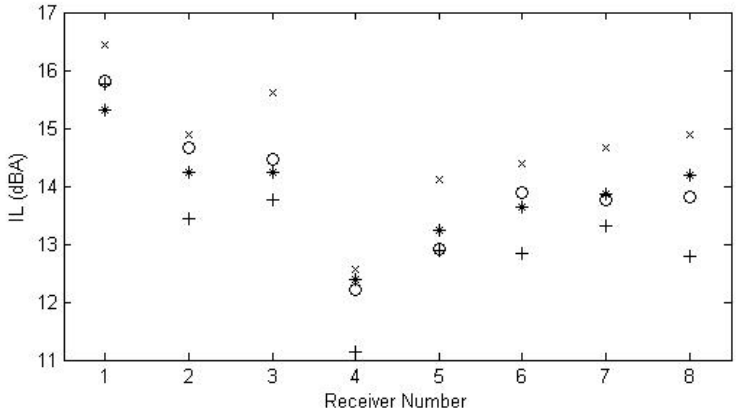

(b)

Figure 4.10: Measured A-weighted insertion losses for the reflective wall and for the full source side covered by the three absorptive materials for: a) the low source position; b) the high source position. The receiver positions are labeled 1 through 8 as seen in Figure 4.3.

the full source side of the barrier. Figure 4.10 shows the total A-weighted IL of the reflective wall as well as of the full source side of the wall covered with the three absorptive surfaces. Based on the absorption coefficients, the baffles were expected to give the greatest IL since their absorption was the highest around 1000 Hz, where the traffic noise spectrum is at a maximum. This is what was seen in the results. Both Durisol and WhisperWall gave IL values 0.5-2 dB lower than the baffles. For the low source position, the Durisol and WhisperWall results were quite similar. For the high source position, the Durisol panels gave IL's 0.5-1 dB higher than the WhisperWall tiles for almost all receiver positions. The

thickness of the WhisperWall tiles could cause this difference. With the lower source position and higher diffraction angles, the effective thickness that sound had to travel through for the WhisperWall tiles was increased more than for the Durisol panels, which allowed for more opportunity for sound to be absorbed. At this effective thickness, WhisperWall and Durisol were very similar. At the higher diffraction angles, where Durisol out-performed WhisperWall, the effective thickness was virtually the same as the actual thickness, and therefore the increase seen with the lower source position did not occur. This suggested that the Durisol panels absorbed more sound per distance than WhisperWall.

4.4.3 Soft Ground Effects

When sound propagates over soft ground, a phase change occurs on reflection. Therefore destructive interference occurs between the direct and reflected waves. Typically in the absence of a barrier, acoustically soft ground creates a decrease in the noise level at low frequency. However when a barrier is inserted, this destructive interference does not occur, possibly resulting in increased noise levels and decreased IL. The acoustic baffles were placed on top of the plywood floor, and the reflective wall and the wall with different configurations of the Durisol panels were tested to see how the acoustically soft ground would affect the IL.

Figure 4.11 shows the results for the low and high source positions at receiver position R6. For the high source position, there was a dip in IL around 200 Hz for all absorptive configurations. The IL became negative, meaning that the barrier did, in fact, increase noise levels. This dip was not seen for the low source position, however the large peak seen in Figure 4.7 was not present. The soft ground appears to have prevented the interference between the direct and reflected waves which occurred with the plywood floor. Plywood can flex and therefore absorb sound at low frequency. This can introduce phase changes and interference, causing the unsmooth nature shown in Figure 4.7 and not seen with the

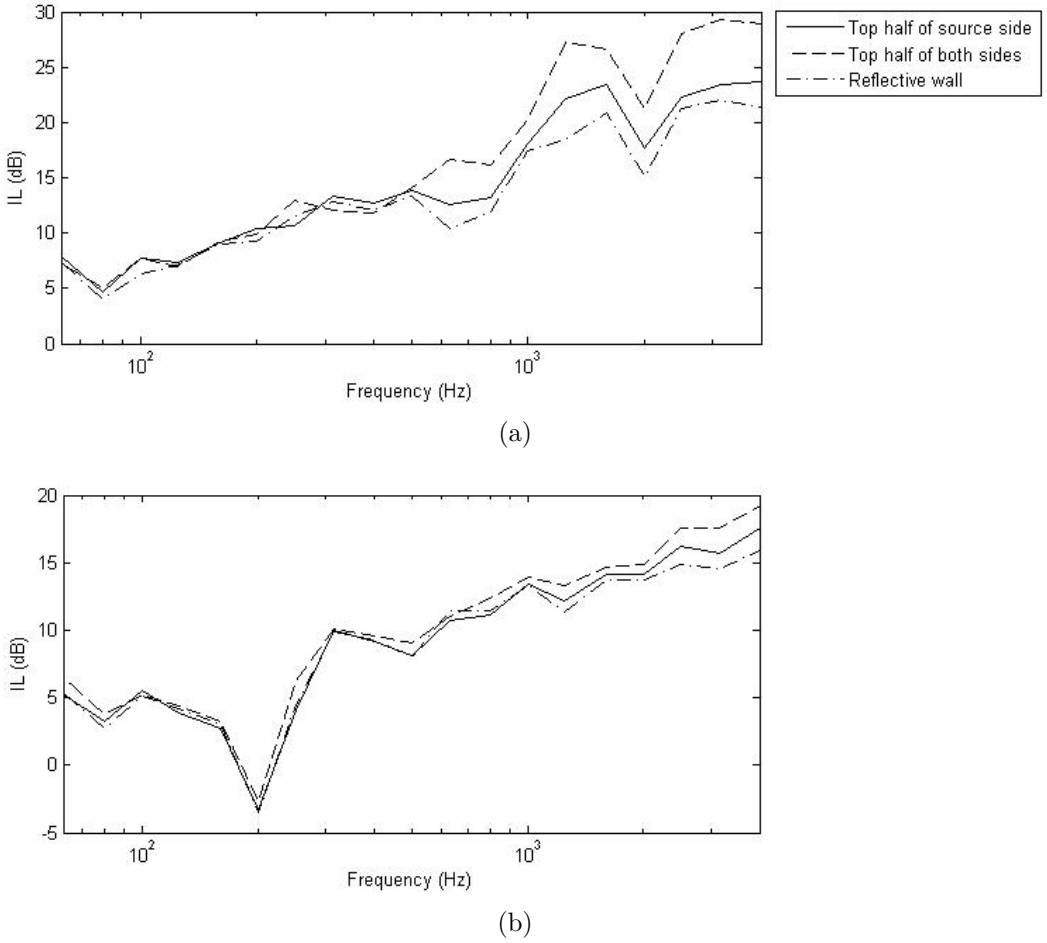

Figure 4.11: Measured third-octave insertion loss at receiver position R6 for different Durisol configurations, with acoustic baffles covering the reflective floor creating a soft ground, for: a) the low source position; b) the high source position.

soft ground. The absorptive material on the wall had similar effects on the IL as for the hard ground case.

4.5 Summary

Different configurations of absorbent material on a 1.2 m high reflective stud wall in an anechoic chamber were examined. Receivers were placed 0.2-1.05 m high and 0.6-1.8 m from the barrier, while the source was placed 1 m from the wall, either 0.25 or 1 m high. It was

found that of the configurations tested the highest IL for non-source side receiver positions came from covering the top half of both sides of the barrier with absorbing material, improving the IL by 1-2 dBA. Covering the full source side with absorbing material gave the highest IL on the source side of the barrier, preventing the sound amplification seen with a reflective wall from occurring. The benefit of this to the non-source side of parallel barriers could not be confirmed with just one wall, but further testing with scale models was done to investigate this. Materials with the highest absorption coefficient — in this case the cotton acoustic baffles — gave the greatest increase in the IL; the performance of two commercial absorbent barrier surfaces was slightly lower. The effects of absorptive surfaces on the IL were similar for both hard and soft ground.

Chapter 5

Field Tests

Field tests were performed at several locations along highways to better understand the effects of nearby foliage on noise barriers. Sites were chosen which had some configuration of foliage near a barrier, as well as a long stretch of bare wall to use as a reference. Noise levels behind both sections of the barrier were simultaneously measured, so that the effects of the foliage could be isolated.

The first site was on 59A St. along Highway 17 in Ladner, British Columbia. Then data were collected on Vancouver Island at three sites: along Nanaimo Parkway near the intersection with Highway 1, on Highway 1 near Helmcken Road, and on Highway 17 near McKenzie Avenue. The equipment used was the Rion NA-28 SLM, the Sinus Soundbook and the Larson-Davis SLM. The microphones were nominally set up 6 m from the barrier, and 1.5 m below the tops of the barriers, which were typically 3 m tall. Each microphone was calibrated before every test to ensure microphone consistency and accuracy. In several cases additional measurements were taken in the same area, either closer to the barrier or higher to determine the effect of position behind the barrier. At each test site, a microphone was also placed 1 m above the noise wall to measure the unshielded traffic noise so that barrier attenuation could be estimated. In all cases there was a fairly continuous flow of vehicles travelling at constant speed. Tests were performed in five minute intervals for 30 minutes. Noise levels were analyzed in third-octave bands from 20 to 20,000 Hz; total un- and A-weighted levels were also calculated. As the noise source was traffic noise, using the A-weighted traffic noise spectrum was not needed to calculate the A-weighted levels.

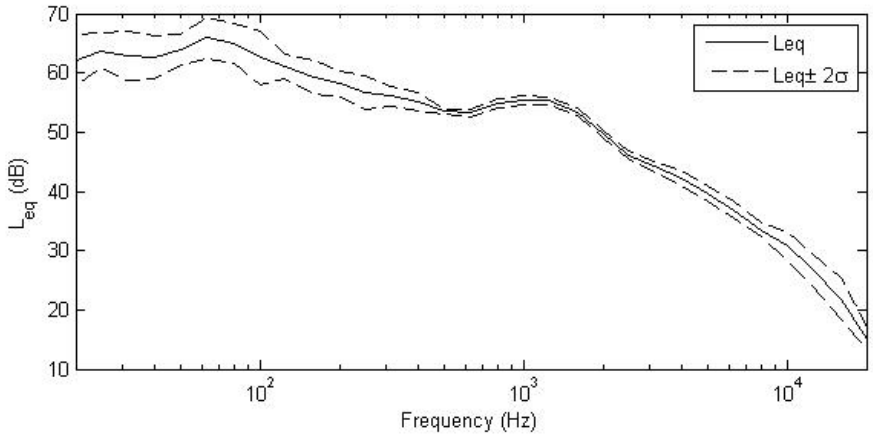

(a)

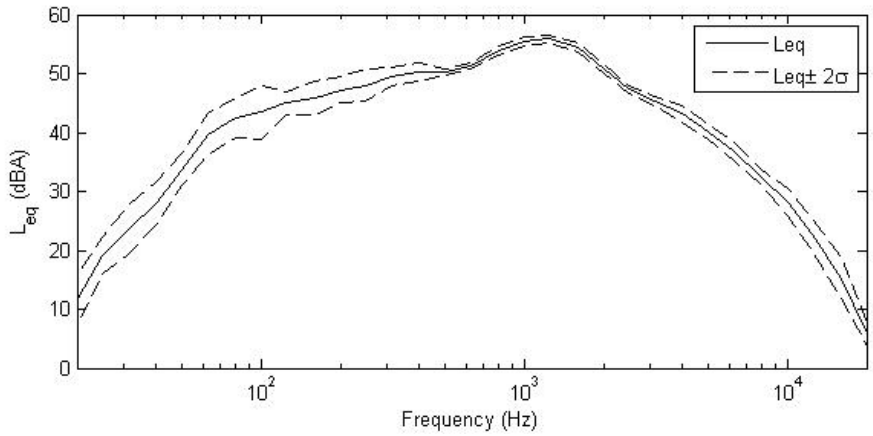

(b)

Figure 5.1: Average third-octave band L_{eq} and variation (2σ) from all 5 min intervals over a 30 min period at a typical site: a) Un-weighted; b) A-weighted.

5.1 Traffic Noise Consistency

Figure 5.1 shows the average un- and A-weighted L_{eq}'s in third-octave bands taken at one site, a result which looked very similar for all other field measurements. The dashed lines are the 95% confidence limits, associated with the standard deviation of the six measurements. Above 600 Hz, the results were quite consistent (variation less than ±2 dB) suggesting that 5 minutes was a sufficient length of time to average variations in traffic noise. Accuracy was the highest (variation of ±1 dB) where the A-weighted-spectrum peaked, which was

where the noise was perceived to be the loudest. At frequencies below 100 Hz there was quite a lot of variation (up to ±5 dB). There was a peak in the spectrum around 1000 Hz, which was typical of traffic noise.

5.2 Ladner

Figure 5.2 shows three of the six sites where measurements were taken in Ladner. The foliage in the backyard of 5052, shown in Figure 5.2(a), was cedar and 8-10 m high. The foliage in the backyard of 5040 59A St. (cedar, ∼10 m high), shown in Figure 5.2(b), was similar to 5052 but was only present above the barrier. The end of 51st St. was the no-foliage case.

The un- and A-weighted L_{eq}'s in dB and dBA from these three sites sites, as well as from the unshielded microphone located above the wall, are presented in Table 5.1. The A-weighted L_{eq} above the wall was 15 dBA higher than in any of the protected backyards, suggesting that the barrier attenuated A-weighted levels by at least 15 dBA.

Figure 5.3 shows the L_{eq} in third-octave bands, averaged from the six five-minute intervals for these locations, which were taken simultaneously. All three spectra were similar with little variation above 100 Hz; below 100 Hz the traffic noise was inconsistent, likely explaining the difference in noise levels occurring there. Above 1100 Hz, noise levels at the two sites with foliage were slightly higher (by up to 2 dB) than at the no-foliage site. Here, some sound was scattered into the shadow zone. The foliages at 5040 and 5052 were quite similar, and therefore the small variation between the two sites was expected. This foliage seemed to have little effect on the total A-weighted sound levels behind the barriers, with all three sites' L_{eq}'s being within 1 dBA of each other.

(a) 5052 59A St. (b) 5040 59A St. (c) The end of 51st St.

Figure 5.2: Three of the test sites in Ladner.

Table 5.1: The un- and A-weighted L_{eq}'s from three sites and above the noise wall along Highway 17 in Ladner.

	Above wall	5052	5040	51^{st}
L_{eq} (dB)	86.3	74.0	74.0	75.7
L_{eq} (dBA)	79.6	63.4	64.2	64.2

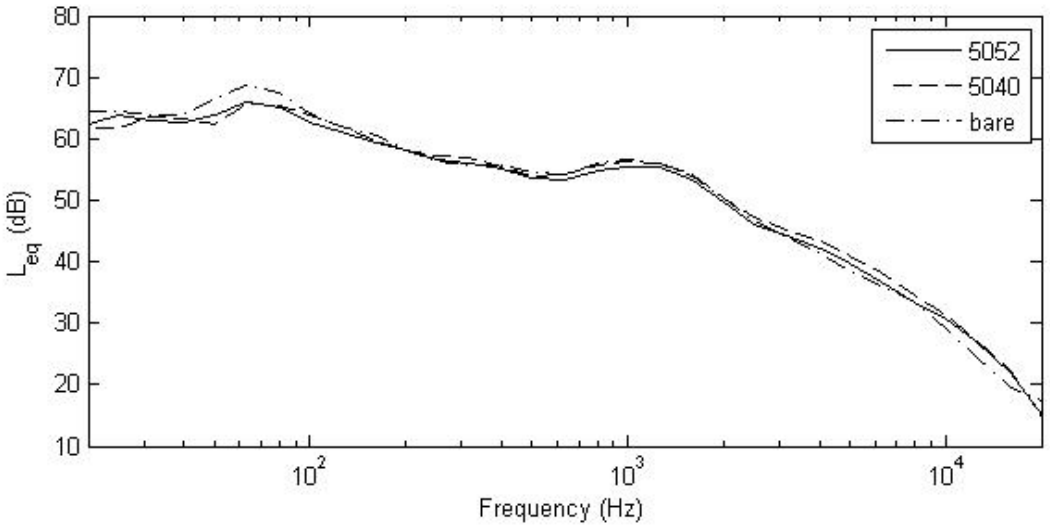

Figure 5.3: The L_{eq} in third-octave bands averaged over 30 minutes in the backyards of 5052 59A St. and 5040 59A St. and the end of 51st St.

Figure 5.4 shows the other three sites where measurements were taken in Ladner. The trees at 5122 59A St., shown in Figure 5.4(a), were deciduous and had broader leaves (∼30 m high, bare trunks to 4 m). The foliage was less dense and less aligned along the wall than in the other yards. The backyard of 5018 59A St., shown in Figure 5.4(b), contained a dense evergreen hedge (cedar, ∼6.5 m high). 5076 59A St. was the no-foliage case.

The un- and A-weighted L_{eq}'s from these sites, as well as from the unshielded microphone located above the wall, are presented in Table 5.2. The A-weighted L_{eq} above the wall was 13 dBA higher than in any of the protected backyards, suggesting that the barrier attenuated A-weighted levels by at least 13 dBA. Figure 5.5 shows the average L_{eq} in third-octave bands for these three sites. The foliages at 5018 and 5122 were quite different and so were the L_{eq} levels above 300 Hz. The L_{eq} at 5018 was several dB lower than for the no-foliage case. Here, the foliage was very dense and appeared to back-scatter and absorb sound. The L_{eq} at 5122 was up to 8 dB greater than for the no-foliage case above 1000 Hz, and here the foliage was very tall, broad-leafed and not very dense. There was wind present during the day, possibly causing the foliage to rustle and produce noise. Therefore the higher L_{eq} could be due to both scattering into the shadow zone and wind. The no-foliage case was very similar (within 0.5 dB above 1000 Hz and 3 dB below) to the no-foliage case in the previous set of measurements, suggesting that the traffic noise was fairly constant between the two sets of measurements.

At one site, the backyard of 5122, receivers were placed at two different distances from the barrier, 3 m and 6 m. The results are shown in Figure 5.6. The L_{eq} in third-octave bands at the position closer to the barrier was approximately 1 dB higher than at the further one. The closer position was deeper into the shadow zone and could therefore be expected to have a lower sound level. However, this result was consistent with treating the diffracting edge of a barrier as a secondary source; the L_{eq} was greater when closer to the diffracting edge.

(a) 5122 59A St. (b) 5018 59A St. (c) 5076 59A St.

Figure 5.4: Three of the test sites in Ladner.

Table 5.2: The un- and A-weighted L_{eq}'s from three sites and above the noise wall along Highway 17 in Ladner.

	Above wall	5122	5018	5076
L_{eq} (dB)	86.3	76.7	75.7	77.6
L_{eq} (dBA)	79.6	66.7	62.2	65.3

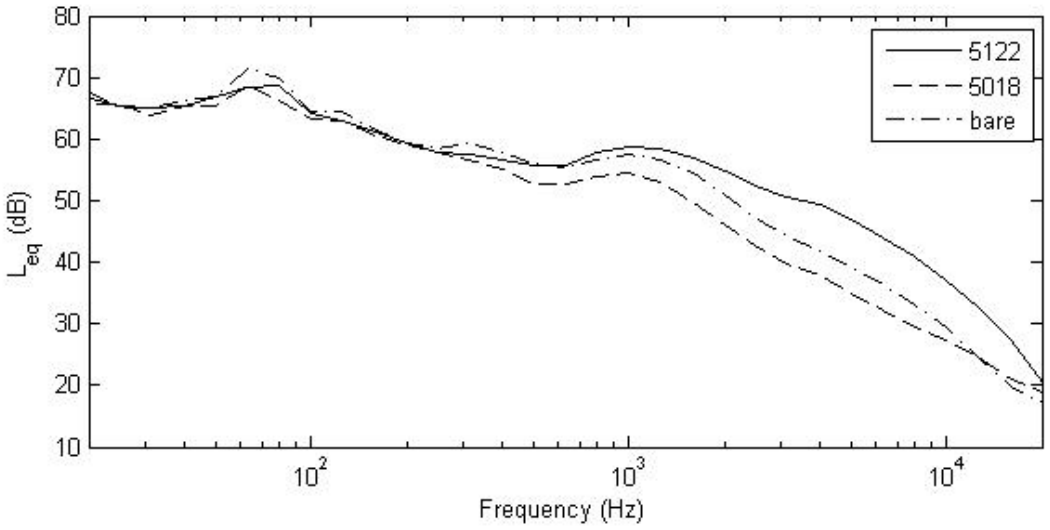

Figure 5.5: The L_{eq} in third-octave bands averaged over 30 minutes in the backyards of 5018 59A St., 5122 59A St. and 5076 59A St.

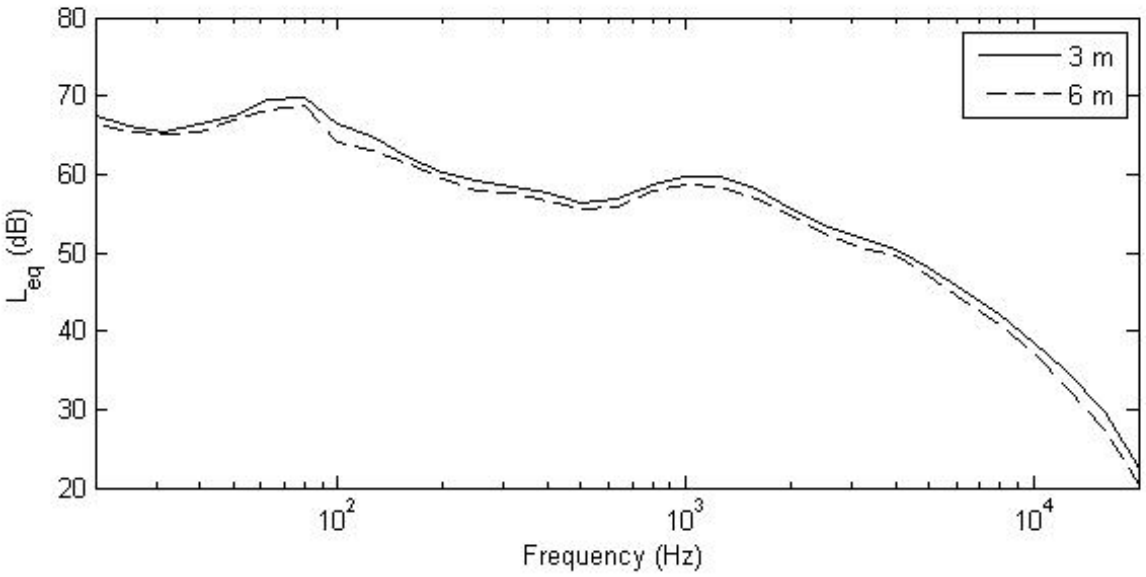

Figure 5.6: The L_{eq} in third-octave bands averaged over 30 minutes for two barrier-receiver distances in the backyard of 5122 59A St.

5.3 Nanaimo Parkway

Figures 5.7(a)-5.7(c) show the three foliage cases studied at the Nanaimo site on Vancouver Island. At the first location (N1), a small amount of evergreen foliage, approximately 4 m high, was on the road side of the noise barrier. At the second (N2), there were evergreen trees, approximately 6 m high, behind the microphone on the opposite side than the wall. The third location (N3) was the no-foliage case. The ground was not completely even; therefore the microphone height was measured from the top of the barrier and was kept constant. For all three locations, the microphone was placed 2 m away from the wall and 1.5 m below the top of the wall. At site N1, a second height of 2.3 m from the top was also measured. At site N3, another microphone was placed 1 m above the barrier to approximate the unshielded traffic noise.

Table 5.3 shows the un- and A-weighted L_{eq}'s for all three foliage cases at Nanaimo

Parkway. The equipment used to calculate levels above the wall only recorded total A-weighted levels, and therefore no unweighted L_{eq} value was obtained. This was the case for all measurements taken above the noise walls on Vancouver Island. Again, the L_{eq} from above the wall was 13 dBA higher than from behind the barrier, suggesting the barrier attenuated levels by at least 13 dBA.

Figure 5.8 shows the L_{eq} in third-octave bands averaged from the six five-minute intervals for the three different foliage cases, measured simultaneously. The three levels were quite similar, within 3 dB, up to 1000 Hz. From 1000 to 5000 Hz, site N1, where the foliage was in front of the barrier, had the highest L_{eq}. Location N2, which had the foliage behind the microphone, had the lowest L_{eq} up to 9000 Hz. The no-foliage case was in the middle. The stretch of barrier where these tests took place was on a bend at an intersection, and therefore the three cases were not the same distance to the traffic-noise source, namely Nanaimo Parkway. N1 was the closest to Nanaimo Parkway, then N3 then N2. This could explain the results, which were not expected and did not lead to any significance in determining the behaviour of foliage.

At site N1 receivers were placed at two different heights, 2.3 m and 1.5 m from the top of the barrier. The results are shown in Figure 5.9. The two L_{eq}'s were very similar except around 1000 Hz, where the level at the higher position was approximately 3 dB greater than at the lower position. The lower microphone position was more into the shadow zone and further from the diffracting edge, and therefore it was expected that the L_{eq} would be lower there. There was some frequency variation, which suggested possible ground effects.

(a) N1 (b) N2 (c) N3

Figure 5.7: Three test sites along Nanaimo Parkway.

Table 5.3: The un- and A-weighted L_{eq}'s from the three foliage cases and from above the wall at the Nanaimo site.

	Above wall	N1	N2	N3
L_{eq} (dB)	-	71.7	69.8	71.0
L_{eq} (dBA)	73.2	60.3	57.0	59.5

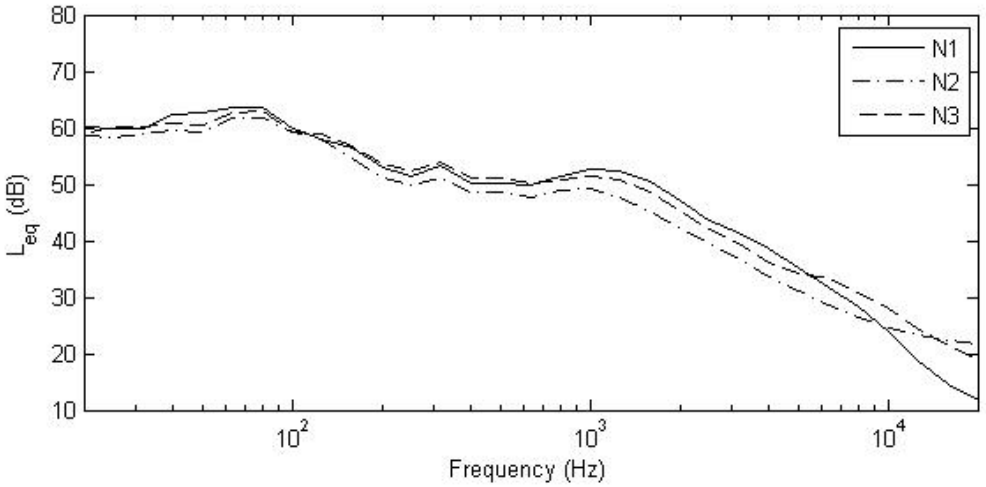

Figure 5.8: The third-octave band L_{eq} averaged over 30 minutes from three locations along Nanaimo Parkway, measured simultaneously. N1 has foliage in front of the barrier, N2 has foliage behind the microphone and N3 is the no-foliage case.

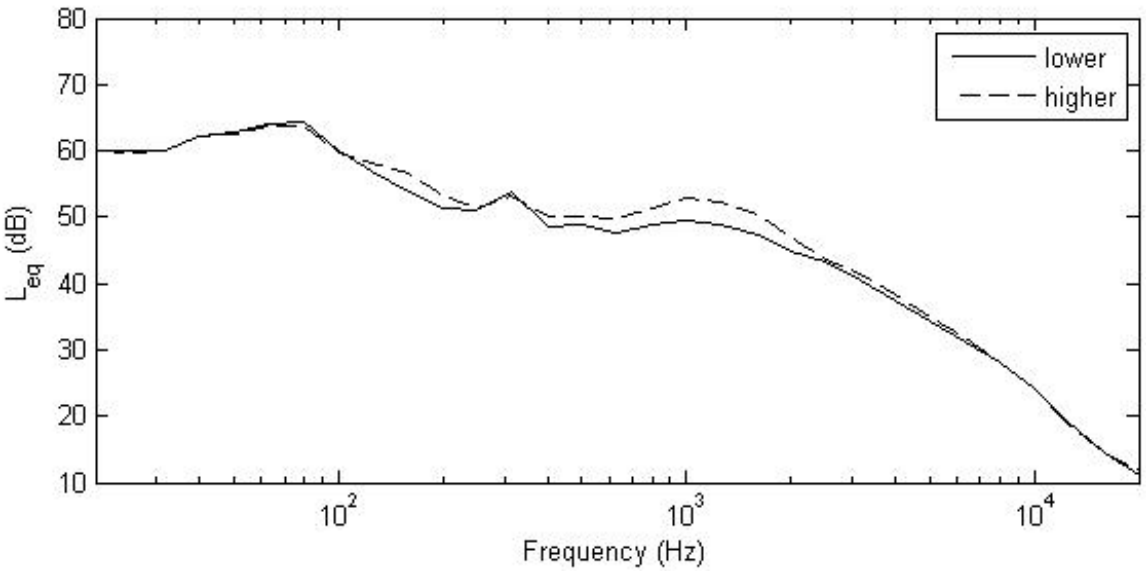

Figure 5.9: The L_{eq} in third-octave bands averaged over 30 minutes for two receiver heights at site N1: 2.3 m and 1.5 m from the top of the barrier.

5.4 Highway 1 and Helmcken Road

Three different foliage cases were measured along Highway 1 near Helmcken Road on Vancouver Island, shown in Figures 5.10(a)-5.10(c). At the first location (V1), several large broad-leafed trees, approximately 10 m high, were between the barrier and the microphone. Very close by, there was a stretch of approximately 10 m of bare wall with foliage at either end, which was case V2. The third case (V3) was farther down the highway and again had no foliage. However this stretch of bare wall was much longer than in case V2. Here again the ground was quite uneven and therefore the microphone height was measured from the top of the barrier. The microphones were placed 3 m from the barrier and 1.5 m from the top. The microphone was also placed 2.55 m from the top at V1. Again at the no-foliage site, V3, a microphone was placed 1 m above the barrier.

Table 5.4 shows the un- and A-weighted L_{eq}'s from all three cases. Here, the A-weighted

L_{eq} from above the wall was 12 dBA higher than from behind the barrier, suggesting the barrier attenuated levels by at least 12 dBA.

Figure 5.11 shows the L_{eq} in third-octave bands averaged from the six five-minute intervals for the three different sites, which were measured simultaneously. As shown in the figure and in Table 5.4, V3 (the longer no-foliage case) had the highest L_{eq} of the three locations. Above 200 Hz, the L_{eq} of V3 was 5 dB higher than that of V2, the shorter no-foliage case. V1 and V2 were along an on-ramp on the way to the highway, whereas V3 was along the actual highway; therefore the speed of the cars and the volume of traffic along the road could have affected the noise levels. Above 1000 Hz, the L_{eq} at V1 (the foliage case) was greater than that at V2 by up to 3 dB. This higher frequency noise could have resulted from sound scattering from the broad-leafed foliage into the shadow zone. Below 1000 Hz, back-scattering and absorption of up to 4 dB was seen. The results of V1 and V2 very closely resembled Renterghem et al.'s frequency-dependent results [30].

At site V1 receivers were placed at two different heights, 2.55 m and 1.5 m from the top of the barrier. The results are shown in Figure 5.12. Above 1000 Hz, the higher microphone position had levels 1 dB higher than at the lower microphone position. This was to be expected, as the higher microphone position was further out of the shadow zone and closer to the diffracting edge.

(a) V1 (b) V2 (c) V3

Figure 5.10: Three test sites along Helmcken Road.

Table 5.4: The un- and A-weighted L_{eq}'s from the three foliage cases and from above the noise wall at the Helmcken Road site.

	Above wall	V1	V2	V3
L_{eq} (dB)	-	70.7	73.5	74.8
L_{eq} (dBA)	79.6	62.6	61.9	67.3

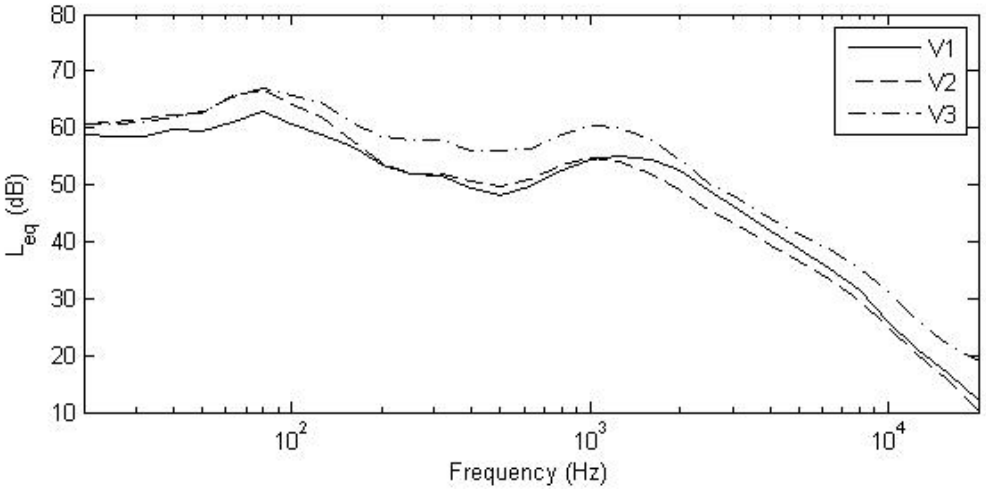

Figure 5.11: The L_{eq} in third-octave bands averaged over 30 minutes from three locations near Helmcken Road, measured simultaneously. V1 is the broad-leafed foliage case, V2 is the shorter no-foliage case and V3 is the longer no-foliage case.

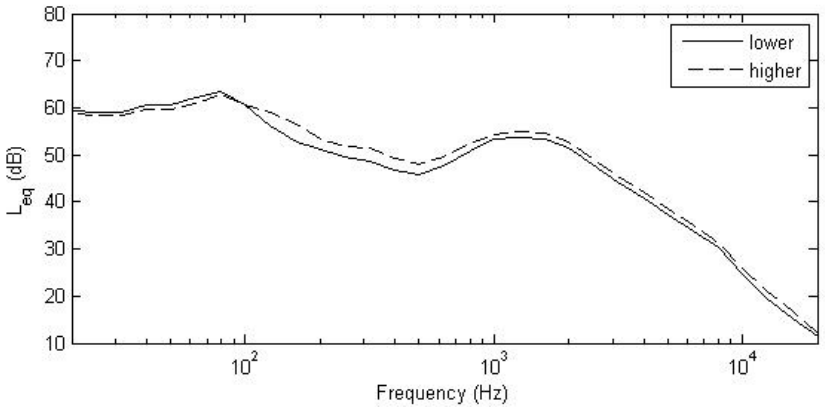

Figure 5.12: The L_{eq} in third-octave bands averaged over 30 minutes for two receiver heights at site V1: 2.55 m and 1.5 m from the top of the barrier.

5.5 Highway 17 and McKenzie Avenue

The effect of vines growing on a noise barrier was investigated along Highway 17 near McKenzie Avenue on Vancouver Island. Measurements were performed along a stretch of wall in two places shown in Figures 5.13(a) and 5.13(b): one where there were vines growing on it and one where there were no vines. There were trees to the sides of and behind the sites. Thus the microphones were placed 1 m from the barrier, and 1.5 m below the top. A microphone was also placed 1 m above the barrier.

Table 5.5 shows the un- and A-weighted L_{eq}'s from the vine and no-vine locations. The A-weighted L_{eq} from above the wall was 14 dBA higher than from behind the barrier, suggesting the barrier attenuated levels by at least 14 dBA. Figure 5.14 shows the L_{eq} averaged from the six five-minute intervals for the two different locations, taken simultaneously. The L_{eq} at the vine site was lower than that at the no-vine site by up to 5 dB, showing back-scattering and absorption, except between 500 and 1500 Hz. There, the vine site's L_{eq} was 1-1.5 dB higher. This indicated a small amount of sound scattering from the vines into the shadow zone.

(a) Vines (b) No Vines

Figure 5.13: The barrier on Highway 17.

Table 5.5: The un- and A-weighted L_{eq}'s from the two sites along McKenzie Avenue, vines and no vines, and from the microphone above the wall.

	Above wall	No vines	Vines
L_{eq} (dB)	-	70.4	69.4
L_{eq} (dBA)	73.3	58.6	58.7

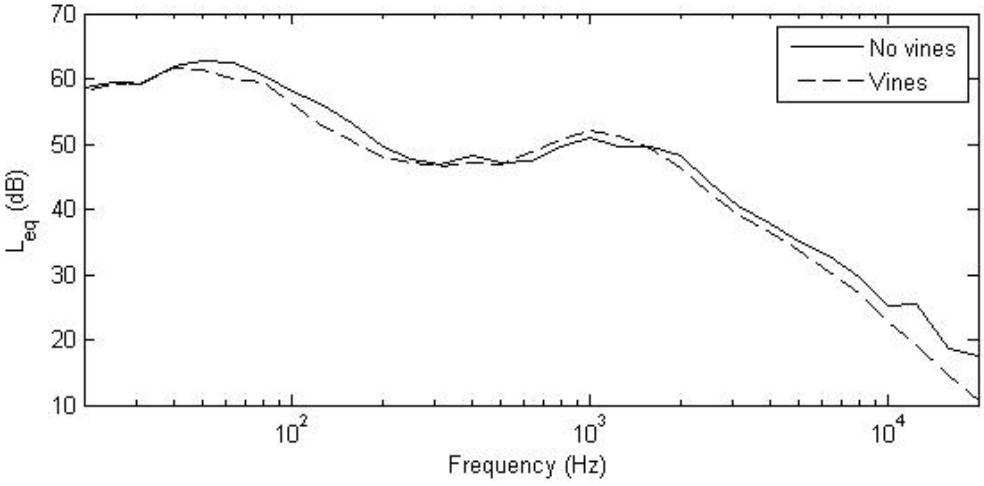

Figure 5.14: The L_{eq} in third-octave bands averaged over 30 minutes from the vine and no vine locations at the McKenzie Avenue site, measured simultaneously.

5.6 Summary

Several test sites were identified to test the effects of foliage near barriers: one site in Ladner, B.C. and several sites on Vancouver Island. Sound levels were measured for 30 minutes in five minute intervals behind barriers both with and without foliage nearby. The 30 minute levels for the foliage and non-foliage cases were compared to isolate the effects of the foliage. Sound levels were also taken above the barriers, giving an unshielded sound level. From this, the approximate barrier attenuation could be determined; attenuations of 12-15 dBA were seen. It was found that finding ideal test sites was difficult; in several cases there were other effects influencing the foliage and the no-foliage cases, making isolating effects from foliage difficult. In the cases where conclusions could be drawn, it appeared that both back-scattering and absorption, which decreased noise levels, and scattering into the shadow zone, which increased noise levels, occurred. The foliage size, height and density as well as the frequency affected the impact of the foliage on the performance of the barrier. In the case of tall, broad leafed trees, scattering of up to 8 dB of sound into the shadow zone occurred above 1000 Hz. Dense evergreen hedges appeared to back-scatter and absorb up to 5 dB of sound, while less dense evergreen hedges appeared to have effects below 2 dB. Vines growing on a barrier also appeared to back-scatter and absorb sound at most frequencies, with effects up to 5 dB. Effects of changing the position behind the barrier were also examined; it was found that noise levels decreased when the distance from the diffracting edge increased.

Chapter 6

Scale-Model Testing

In this chapter, a 1:31.5 scale model, originally developed by Busch [5] was redeveloped and used to examine the factors under investigation: absorptive barriers and foliage near barriers. Scale-model materials were selected using excess attenuation measurements and scale-model trees were compared with full-scale foliage. Results of the measurements were then analyzed. Before discussing this work, previous work and theory behind scale-modelling is discussed.

6.1 Previous Work

The first examination of acoustical scale modelling was in 1934 by Spandock [35]. Early models used fairly low scale factors, such as 8 or 10; however as transducer and recording device technology improved, higher frequencies were able to be studied, and therefore higher scale factors could be used. Scale modelling has been used to study many different acoustical environments, including auditoriums, offices, factories and outdoors. Much focus has been on material selection, which depends on the scale factor as well as the desired full-scale surface.

Many studies have been on the effects of ground surfaces, both with and without noise barriers. These effects are governed by the impedance of the ground, and therefore it is very important to select a material which accurately models the ground surface of interest. Delany et al. [36] tested various materials as candidates for a scale model at a 1:30 scale. They found that 11 mm thick Insulite softboard covered with a sheet of rough nylon cloth

gave the best excess attenuation associated with grassland. They used sheets of aluminum to model pavement. Hutchins et al. [37] did work on the selection process for scale model materials for a 1:80 scale. They used the same method of determining scale model materials as will be used here (see Section 6.2). Sanded sheets of expanded polystyrene covered with tissue were used for grass, with an effective flow resistivity of approximately 300 c.g.s. Rayls/cm.

Hutchins et al. used these materials to specifically study barriers over ground surfaces [38] at a scale of 1:80. The sound source was a set of ultrasonic whistles, which cover the 10- to 100-kHz range with high amplitude. They used a 1/8 inch Bruel and Kjaer microphone as their receiver. The reflective barriers were made from 1 mm thick aluminum sheets, giving a full-scale thickness of 8 cm. Aluminum sheets were also used to model asphalt and the grass surface developed in [37] was used. The scale model results agreed well with prediction and field tests.

Horoshenkov et al. [39] explored properties of porous materials to be used for scale modelling at a scale of 1:20. They used the Attenborough impedance model, which uses four independent variables to characterize the materials: porosity, tortuosity, flow resistivity and layer depth. They mainly examined the frequency dependence of the impedance, but also looked at the angular dependence. They found that rubber-backed carpet best modelled asphalt and a fiberglass surface best modelled dry sand.

Hutchins et al., using the setup described previously, also studied parallel barriers [40]. A four lane highway with a central grass section was created and several source and receiver positions were studied. The barriers were 4.9 m tall and placed 35 m away from each other. They found that reflections from the face of the second barrier were only significant when the source was placed near that second barrier.

Pirinchieva [41] used a 1:20 scale model to study sound propagation behind barriers of finite length. He used a point source for a frequency range of 5-20 kHz, and used a 1/4 inch

B&K microphone as a receiver. The ground was modelled using painted plywood and the barriers were made of 5 mm thick polystirol plates stuck on 4 mm glass and then painted.

Some work has already been done to study absorptive noise barriers using scale modelling. Osman [42] developed a 1:16 scale-model facility, later used to study different shapes of noise barriers, both reflective and absorptive [9]. Menge [43] studied the effects of using sloped barriers instead of absorption to reduce amplification between parallel barriers using a 1:30 scale model. Trucks were the dominant source of noise in the specific case he was working on, therefore the 250, 500 and 1000 Hz octave bands were studied. He used 16 mm medium-density overlay plywood with smooth, dense paper glued to both sides to model concrete, asphalt, brick and steel, as well as the reflective sloped barriers. He used fiberglass for the absorptive barriers. He used an electric spark discharge as an impulsive sound source and a 1/4 inch microphone as the receiver. Hothersall et al. [44] used a scale model at a scale of 1:20 to test reflective and absorptive railway noise barriers. They used a polished aluminum surface to simulate rigid ground and used specially manufactured, 8 mm thick porous plastic plates to simulate grass. The barriers were modelled using plastic or steel and were made absorptive by adding a layer of felt.

Busch [5] created a scale model to investigate noise walls, earth berms, and a combination of the two. He used an air-jet noise source and performed excess attenuation experiments to determine both the optimal scale factor and the materials to be used. He chose a scale-factor of 31.5 and created the model in an anechoic chamber. He tested the anechoic chamber thoroughly and determined it was an appropriate testing environment for the scale model. He used varnished particle board to model roadways, dense polystyrene to simulate noise walls, and expanded polystyrene to model soft ground and earth berms. He used felt and expanded polystyrene to make the earth berms softer and harder, respectively.

6.2 Theoretical Considerations

When building an accurate scale model, there are many factors that must be taken into consideration. For a scale factor n, all dimensions and distances are scaled by $1/n$. The speed of sound remains the same in the scale model, so to ensure that the relation between distances and the acoustical wavelengths remain constant the wavelength λ must become λ/n; therefore the frequency f must be scaled up to nf. Issues occur at these higher frequencies, such as air absorption becoming very significant (See Section 6.2.1 for the calculations). Another issue which needs to be taken into account is finding an approximately omni-directional sound source which has a fairly constant power output up to 100 kHz. The directionality of the microphones is also a problem, as one wants the microphone to be as omni-directional as possible, and therefore the smallest microphones available must be used. Furthermore, because the wavelengths of the frequencies of interest are so small, the protection grid on the microphone must be accounted for, as it is no longer a negligible size at these frequencies and may affect the frequency response. It is assumed here that effects such as diffraction and interference are consistent under scaling.

Selecting appropriate scale-model materials is crucial to the accuracy of a scale model. The method of selection here was used by Hutchins et al. [37]. Materials to be used in an acoustical scale model must be found which have the same acoustical impedance at scaled up test frequencies as real-world materials do at full-scale frequencies. The impedance of a fibrous material is given using the Delany-Bazley model [45]:

$$Z = 1 + 9.08\left(\frac{f}{\sigma}\right)^{-0.75} + i11.9\left(\frac{f}{\sigma}\right)^{-0.73}, \tag{6.1}$$

where σ is the flow resistivity in c.g.s. Rayls/cm. Since the frequency is scaled by the scale factor n in the model measurements, the flow resistivity must also be scaled by n to keep Z constant. It is the flow resistivity divided by the scale factor n, called the effective flow

resistivity, which is compared to real-world values. To calculate the surface impedance, and therefore the flow resistivity, of a material, the excess attenuation (EA) must be measured.

Excess attenuation measurements involve a source and receiver in a known configuration above a material of interest and measuring the sound pressure level. From this, the EA is calculated by:

$$EA = L_{p,surface} - L_{p,ff}, \tag{6.2}$$

where $L_{p,ff}$ is the free-field pressure level, with the scaled source-receiver distance taken into account when correcting for air absorption and divergence.

Once the measurements are taken, a least-squares fit is performed to fit the average measured EA to the EA predicted for the different flow resistivity values (for the predicted EA calculation, see Section 6.2.2). By this method, the effective flow resistivities of materials are determined and then compared to values for full-scale materials and chosen accordingly.

6.2.1 Air Absorption

In this section, the calculation of the air absorption coefficient α_A is shown, as done by Bass et al. [46]. The ANSI standard on the measurement of air absorption [47] gives the air absorption coefficient for still air in nepers per meter as:

$$\begin{aligned}\alpha_A = f^2\Bigg[1.84\times10^{-11}\left(\frac{p_{s0}}{p_s}\right)\left(\frac{T}{T_0}\right)^{1/2} &+ \left(\frac{T}{T_0}\right)^{-5/2}\frac{1.278\times10^{-2}\,e^{-2239.1/T}}{f_{r,O}+(f^2/f_{r,O})}\\ &+ \frac{1.068\times10^{-1}\,e^{-3352/T}}{f_{r,N}+(f^2/f_{r,N})}\Bigg],\end{aligned} \tag{6.3}$$

where p_{s0} is the reference atmospheric pressure (1 atm), p_s is the atmospheric pressure, T is the atmospheric temperature in K and T_0 is the reference atmospheric temperature (293.15 K). $f_{r,O}$ and $f_{r,N}$ are the relaxation frequencies of molecular oxygen and nitrogen

respectively, given as:

$$f_{r,O} = \left(\frac{p_s}{p_{s0}}\right)\left[24 + 4.04 \times 10^4 h \frac{0.02 + h}{0.391 + h}\right] \tag{6.4}$$

$$f_{r,N} = \left(\frac{p_s}{p_{s0}}\right)\left(\frac{T_0}{T}\right)^{1/2}\left(9 + 280he^{-4.17\left[\left(\frac{T_0}{T}\right)^{1/3}-1\right]}\right), \tag{6.5}$$

where h is the molar concentration of water vapour in percent. This is calculated from the relative humidity h_r, by:

$$h = h_r\left(\frac{p_{sat}}{p_{s0}}\right)\left(\frac{p_{s0}}{p_s}\right). \tag{6.6}$$

The fraction of the saturated vapour pressure p_{sat} over the ambient pressure p_{s0}, as done by Bass et al. in a later paper [48], is:

$$\log_{10}\left(\frac{p_{sat}}{p_{s0}}\right) = -6.8346\left(\frac{T_0}{T}\right)^{1.261} + 4.6151. \tag{6.7}$$

The conversion 1 Np $\approx$ 8.686 dB is used to obtain the air absorption coefficient in decibels per meter.

6.2.2 Excess Attenuation Prediction

In this section, a model to predict the excess attenuation of a ground surface will be developed. The velocity potential above a surface is calculated given a specific source and receiver geometry. Scale model materials will be chosen based on their excess attenuations compared to those of the full scale materials they are modelling.

The excess attenuation can be predicted from the velocity potential Φ and the free-field velocity potential Φ_0 using:

$$EA = 20\log\left(\frac{\Phi}{\Phi_0}\right). \tag{6.8}$$

The derivation of the velocity potential assumes a time dependence of $e^{-i\omega t}$. The math

behind this derivation is presented in [49]. The derivation has been done in detail in [50], [51], [52] and [53]. The source and receivers are assumed to be dimensionless points. The ground surface is assumed to be locally-reacting with a normalized admittance of $\beta = \rho c/Z$. The geometry is defined by the source height, h_1, the receiver height, h_2, and the source-receiver distance, d. The direct and reflected source-receiver distances are denoted r_1 and r_2 respectively, and are calculated by:

$$r_1 = \sqrt{d^2 + (h_2 - h_1)^2} \tag{6.9}$$

$$r_2 = \sqrt{d^2 + (h_2 + h_1)^2}. \tag{6.10}$$

The grazing angle ψ, the angle the reflected path makes with the impedance plane, is calculated by:

$$\psi = \arctan\left(\frac{h_1 + h_2}{d}\right). \tag{6.11}$$

The complex plane-wave reflection coefficient R_p, assuming locally-reacting ground, is given by:

$$R_p = \frac{\sin\psi - \beta}{\sin\psi + \beta}. \tag{6.12}$$

The spherical-wave reflection coefficient is defined as:

$$Q = R_p + (1 - R_p)F(w), \tag{6.13}$$

where $F(w)$ is called the spherical-loss factor and is given by:

$$F(w) = 1 + i\sqrt{\pi}w\, e^{-w^2}\mathrm{erfc}(-iw), \tag{6.14}$$

and w is the numerical distance, calculated by:

$$w = \left(\frac{1+i}{2}\right)\sqrt{r_2 k}\,(\sin\psi + \beta), \tag{6.15}$$

where k is the wavenumber in air. The importance of choosing the correct square root of i in the equation for w, here presented in the proper form $\frac{1+i}{2}$, is discussed by Stinson [54]. By defining $f(w)$ as a modified form of the complementary-error function:

$$f(w) = e^{-w^2}\mathrm{erfc}(-iw), \tag{6.16}$$

Equation 6.14 can be rewritten as:

$$F(w) = 1 + i\sqrt{\pi}w\, f(w). \tag{6.17}$$

The velocity potential is then defined to be:

$$\Phi = \frac{e^{ikr_1}}{4\pi r_1} + Q\,\frac{e^{ikr_2}}{4\pi r_2}. \tag{6.18}$$

The free-field velocity potential Φ_0 is defined for when there is no reflected component, so when $Q = 0$. The final step is the calculation of the modified complementary-error function:

$$f(w) = H(y,x) + iK(y,x), \tag{6.19}$$

where x and y are the real and imaginary parts of the numerical distance w respectively. A new constant h is introduced, related to the error bound E_h on calculating $f(w)$, defined to be:

$$E_h = 2\sqrt{\pi}\frac{e^{-\pi^2/h^2}}{1 - e^{-\pi^2/h^2}}. \tag{6.20}$$

Smaller values of h reduce the value of the error bounds, leading to more accurate calcu-

lations; $h = 1$ is sufficient for the calculations here. Four new variables are defined for the derivation of the terms in Equation 6.19:

$$A_1 = \cos(2xy) \tag{6.21}$$

$$B_1 = \sin(2xy) \tag{6.22}$$

$$C_1 = e^{-2\pi y/h} - \cos(2\pi x/h) \tag{6.23}$$

$$D_1 = \sin(2\pi x/h). \tag{6.24}$$

Using these variables, two new terms are calculated:

$$P_2 = 2e^{-(x^2+(2\pi y/h)-y^2)}\frac{A_1C_1 - B_1D_1}{C_1^2 + D_1^2} \tag{6.25}$$

$$Q_2 = 2e^{-(x^2+(2\pi y/h)-y^2)}\frac{A_1D_1 + B_1C_1}{C_1^2 + D_1^2}. \tag{6.26}$$

The real and imaginary parts of the error function in Equation 6.19 are defined by the following equations:

$$H(y,x) = \frac{hy}{\pi(y^2+x^2)} + \frac{2yh}{\pi}\sum_{n=1}^{\infty}\frac{e^{-n^2h^2}(y^2+x^2+n^2h^2)}{(y^2-x^2+n^2h^2)^2+4y^2x^2} - \frac{yE_h}{pi} + P_{2,final} \tag{6.27}$$

$$K(y,x) = \frac{hx}{\pi(y^2+x^2)} + \frac{2xh}{\pi}\sum_{n=1}^{\infty}\frac{e^{-n^2h^2}(y^2+x^2-n^2h^2)}{(y^2-x^2+n^2h^2)^2+4y^2x^2} + \frac{xE_h}{pi} - Q_{2,final}, \tag{6.28}$$

where $P_{2,final}$ and $Q_{2,final}$ are defined by comparing y to π/h. If $y < \pi/h$ then $P_{2,final} = P_2$ and $Q_{2,final} = Q_2$; if $y = \pi/h$ then $P_{2,final} = P_2/2$ and $Q_{2,final} = Q_2/2$; otherwise $P_{2,final} = 0$ and $Q_{2,final} = 0$.

6.3 Experimentation

A 1:31.5 scale model, developed by Busch as part of his Masters research [5], was redeveloped here. The scale-model measurements were performed in an anechoic chamber with dimensions 4.1 m x 4.7 m x 2.6 m. A 1/4" Bruel & Kjaer type 4135 free-field microphone was used as the receiver, with a Bruel & Kjaer type 2669 pre-amplifier and an adaptor for a 1/2" pre-amplifier to a 1/4" microphone. A B&K Nexus Conditioning Amplifier was used mainly for cable-adapting, and was set as a high-pass filter with a cut-off frequency of 20 Hz. The output sensitivity of the amplifier was set to 31.6 mV/Pa. A Stanford Research Systems SR-770 FFT Network Analyzer was used to average and record the acoustic signal in 400 spectral bins, 250 Hz wide, from 0-250 Hz up to 99,750-100,000 Hz. Each measurement took 2000 spectral averages. The results were stored on 3.5" floppy disks and analyzed in MATLAB. In order to calculate the air absorption, the temperature and humidity were measured with a Psychro-Dyne psychrometer.

6.3.1 Air-Jet Source

The sound source used here was the air-jet source used and tested in Busch's thesis [5], who provided a detailed description and the results of in-depth tests of the source in the anechoic chamber. Presented here is a brief description and an examination of several of the source's properties.

The air-jet source was developed from the description by Novak [55], designed specifically for scale-model traffic noise. An ideal source must have sufficient power output for a broadband spectrum up to 100 kHz. The source was made of six co-planar jets, each with a diameter of 0.3 mm, spaced at 60^o intervals around a cylinder with a diameter of 6.5 mm. The outer housing and the core piece, shown in Figure 6.1, were both made of brass. The core piece had resonant cavities which amplified the source power at lower frequencies.

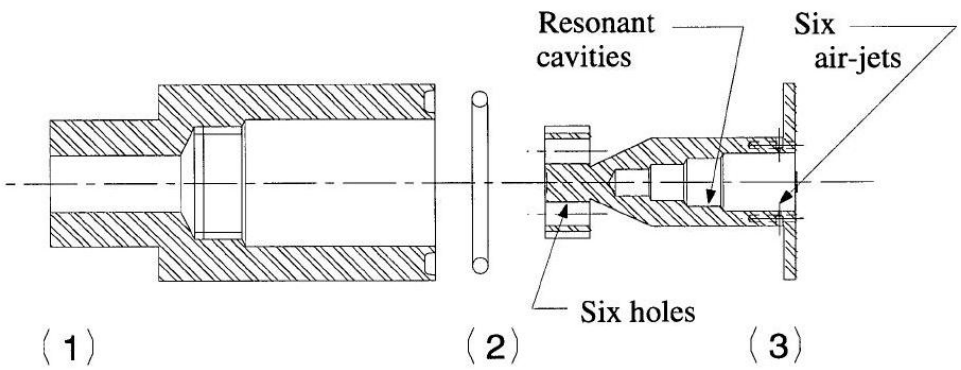

Figure 6.1: The air-jet source. (1) The outer housing. (2) O-ring, size no. 15. (3) The core piece. [5]

Protection Grid

At very high frequencies, the microphone protection grid is no longer a negligible size in comparison to the wavelength. Therefore, the effects must be taken into account when calculating the sound pressure level. The correction on the sound levels due to the protection grid was determined by measuring the sound pressure level 1 m from the source, both with and without the protection grid (PG). The correction was then calculated by:

$$\Delta L_{microphone} = L_{PG\,off} - L_{PG\,on}. \tag{6.29}$$

$L_{PG\,off}$ and $L_{PG\,on}$ are shown in Figure 6.2. All measurements were subsequently taken with the protection grid on and corrected, in order to protect the microphone.

Source Power Output

To determine the sound power level of the source, the sound pressure level was measured at eight different distances from the source, from 0.4 m to 2 m. The sound source was oriented vertically and the microphone was oriented horizontally, pointing towards the source. From

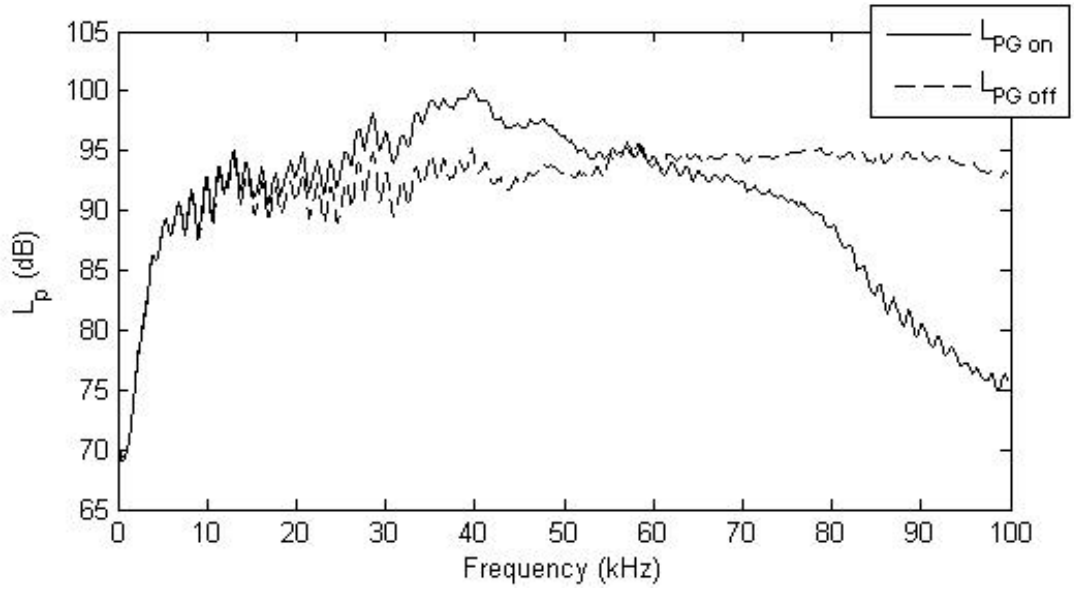

Figure 6.2: The sound pressure level measured at 1 m from the source, with and without the protection grid.

the sound pressure level L_p, the sound power level L_w was determined by:

$$L_w = L_p + 20\log(r) + 10\log(4\pi) + \Delta L_{air} + \Delta L_{microphone}, \tag{6.30}$$

where r is the source-receiver distance, ΔL_{air} is the air absorption correction, and $\Delta L_{microphone}$ is the microphone response correction due to the protection grid. The average L_w, shown in Figure 6.3, was calculated from the eight measurements at different source-receiver positions.

Source Inclination Angle

The effect of varying the inclination angle of the sound source was measured, by varying the angle while measuring the sound pressure level 1 m away from the source. 0° was defined to be the air-jet stream pointing directly towards the microphone, while 90° was defined to be when the air-jet stream was perpendicular to the microphone. The sound

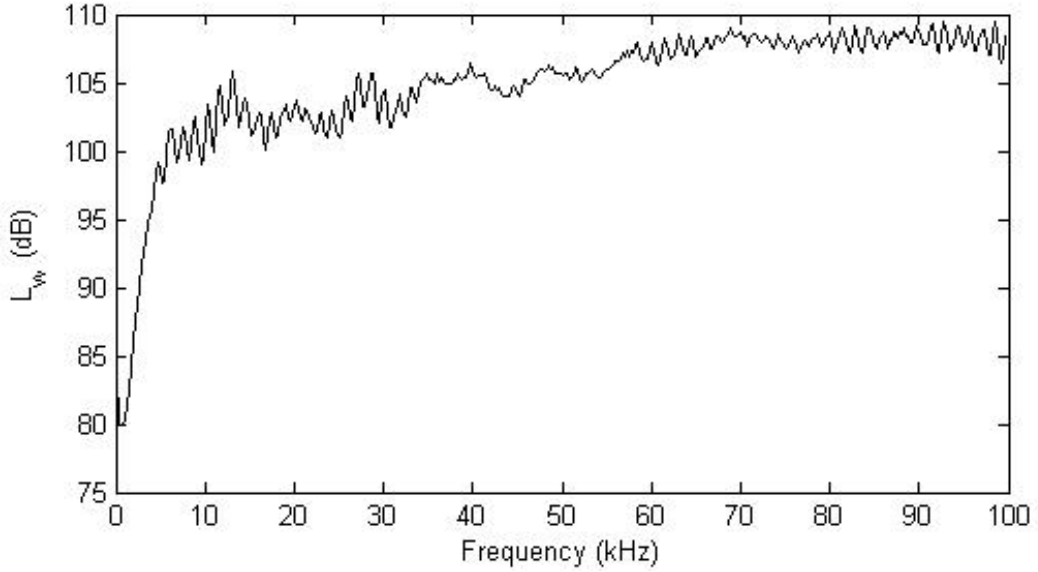

Figure 6.3: The sound power level of the air-jet source.

pressure level was then corrected for air absorption and protection grid response.

Figure 6.4 shows the sound pressure level as a function of source inclination angle and frequency. As the angle approached 90°, the high frequency power dropped off considerably, and the low frequency power increased sharply. This sharp increase was due to the air-jet stream directly hitting the microphone. From 0° up to 50° the spectrum was quite flat, and therefore the scale model measurements were limited to these angles.

6.3.2 Frequency Range

All subsequent measurements were performed using scaled frequencies, then the frequencies were scaled down over the full-scale range. Using a scale factor of 31.5 meant the frequency range over which measurements were performed was 1390 to 89100 Hz, corresponding to the range of the full-scale 63 Hz to 2000 Hz octave bands. Octave band results were calculated

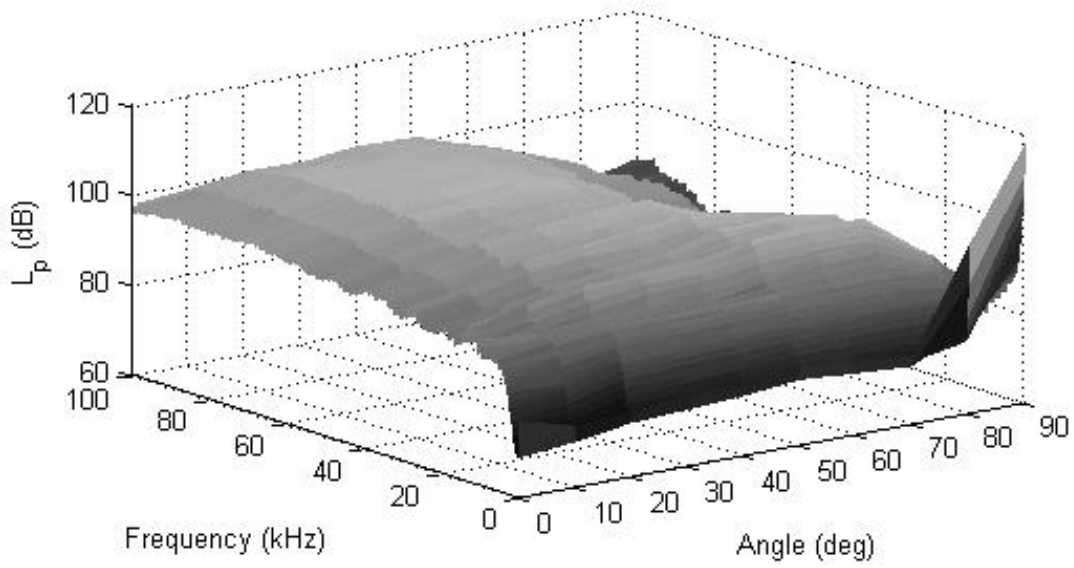

Figure 6.4: The sound pressure level varying with both source inclination angle and frequency.

from the 400 frequency bins, using:

$$L_{p,\text{band}} = 10\log_{10}\left(\sum_{i=m_1}^{m_2} 10^{L_{p,i}/10}\right) - 10\log_{10}(m_2 - m_1 + 1), \tag{6.31}$$

where m_1 and m_2 are the first and last bin numbers included in the band.

6.3.3 Excess Attenuation Measurements

Excess attenuation measurements were performed in Busch's thesis [5] to determine the flow resistivity of candidate scale-model materials. An error found in the thesis, dividing the effective flow resistivity by the scale factor to obtain an incorrect effective flow resistivity (corrected in a later paper [56]), led to the scale-model selection process being repeated here.

EA measurements were performed, as described in Section 6.2. The full scale configuration used for these measurements was as follows: source height of 0.5 m, receiver height

Table 6.1: Effective flow resistivities σ_{eff} for full-scale materials.

Ground	σ_{eff} (c.g.s. Rayls/cm)
Absorptive barrier	30-60
Grass	150-300
Loose-packed dirt	300-800
Asphalt roads	30,000
Concrete barrier	30,000-100,000

of 1.8 m and a source-receiver distance of 30 m; the source was pointing straight down in order for it to be as omni-directional as possible. The source and receiver heights were those used later in the insertion loss tests. Three measurements were taken for each surface, to average out any irregularities in the material.

Several full-scale materials were to be modelled: asphalt roadways, loose-packed dirt (highway shoulders), concrete (reflective) noise barriers and absorptive noise barriers. Table 6.1 gives the effective flow resistivities of these surfaces, all but the absorptive barrier given by Embleton et al. [57]. The absorptive barrier flow resistivity was determined by comparing the full-scale commercial barrier absorption coefficients with the calculated absorption coefficient using the Delany-Bazley model.

Several materials were tested to model these surfaces: a fuzzy blanket, felt, green fabric, one and two layers of linen, 3/4" plywood, varnished particle board, and 3 mm thick dense plastic. The results of the EA measurements, and the best-fit EA prediction curves for each material, are shown in Figures 6.5(a)-6.6(d). The effective flow resistivities are listed in Table 6.2.

The EA curves for materials with very high flow resistivities did not appear to have a distinct minimum. The minima for these surfaces could be above the frequency range and

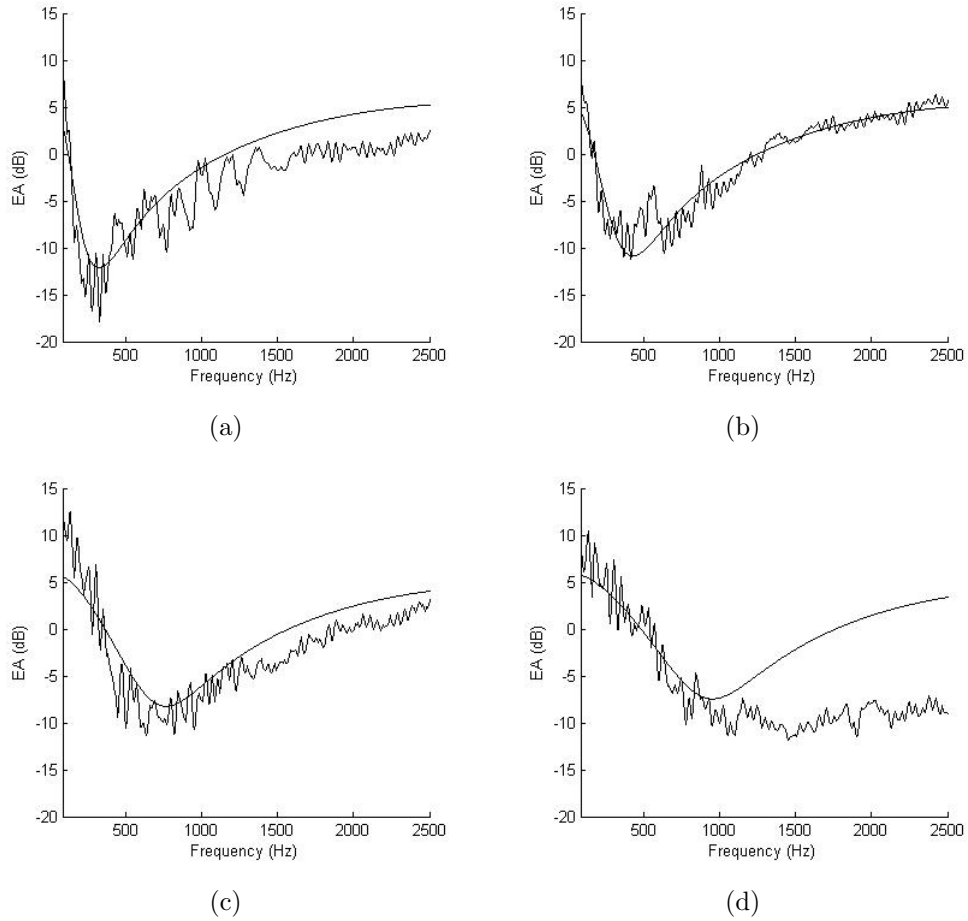

Figure 6.5: The excess attenuation measurements and best-fit predictions for a) the fuzzy blanket ($\sigma_{eff} = 33$ c.g.s. Rayls/cm), b) felt ($\sigma_{eff} = 64$ c.g.s. Rayls/cm), c) the green fabric ($\sigma_{eff} = 253$ c.g.s. Rayls/cm), and d) two layers of linen ($\sigma_{eff} = 430$ c.g.s. Rayls/cm)

therefore were not measured. The EA curves for one and two layers of linen had minima, but then at high frequencies did not rise as much as the predicted curves. The Delany-Bazley model is valid only for fibrous, absorptive material, and therefore the prediction model breaks down for higher flow resistivities and non-fibrous material. Due to the lack of distinct minima and the deviation from the model, especially at high frequencies, only full-scale frequencies up to 1500 Hz were considered when performing the least-squares fit.

By comparing the flow resistivity values, scale model materials were chosen. Asphalt was modelled by plywood, the roadside was modelled by two layers of linen, the green fabric

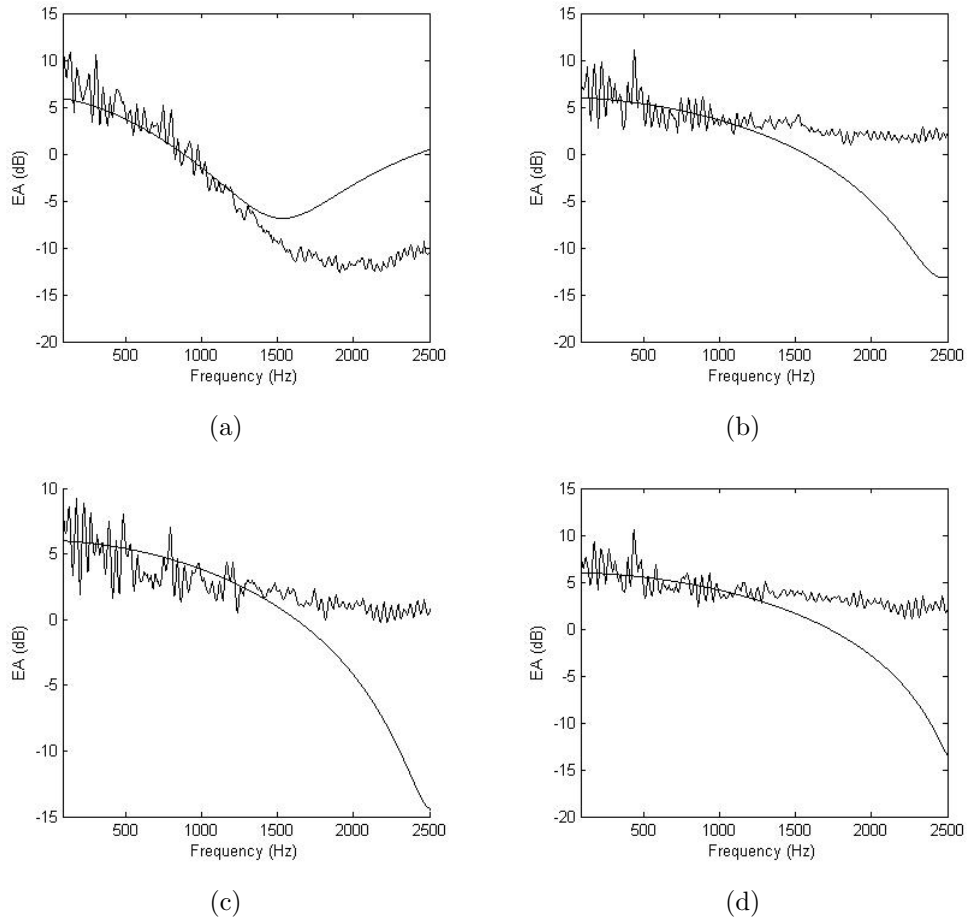

Figure 6.6: The excess attenuation measurements and best-fit predictions for a) linen ($\sigma_{eff} = 1,550$ c.g.s. Rayls/cm), b) plywood ($\sigma_{eff} = 14,600$ c.g.s. Rayls/cm), c) dense plastic ($\sigma_{eff} = 20,000$ c.g.s. Rayls/cm), and d) varnished particle board ($\sigma_{eff} = 40,000$ c.g.s. Rayls/cm).

modelled grass, the dense plastic modelled the reflective barriers and the fuzzy blanket was added to the source side of reflective barriers to make them absorptive.

Using the effective flow resistivity of the fuzzy blanket, the effective absorption coefficient was calculated with the Delany and Bazley model. The effective absorption coefficient at full scale frequencies is shown in Figure 6.7. This was similar to the results of the spherical decoupling and impedance tube tests performed on the full scale absorptive material.

Table 6.2: Effective flow resistivities σ_{eff} for scale model materials.

Material	σ_{eff} (c.g.s. Rayls/cm)
Fuzzy blanket	33
Felt	64
Green fabric	253
Two layers of linen	430
One layer of linen	1,546
Dense plastic	20,000
Plywood	35,500
Varnished particle board	370,000

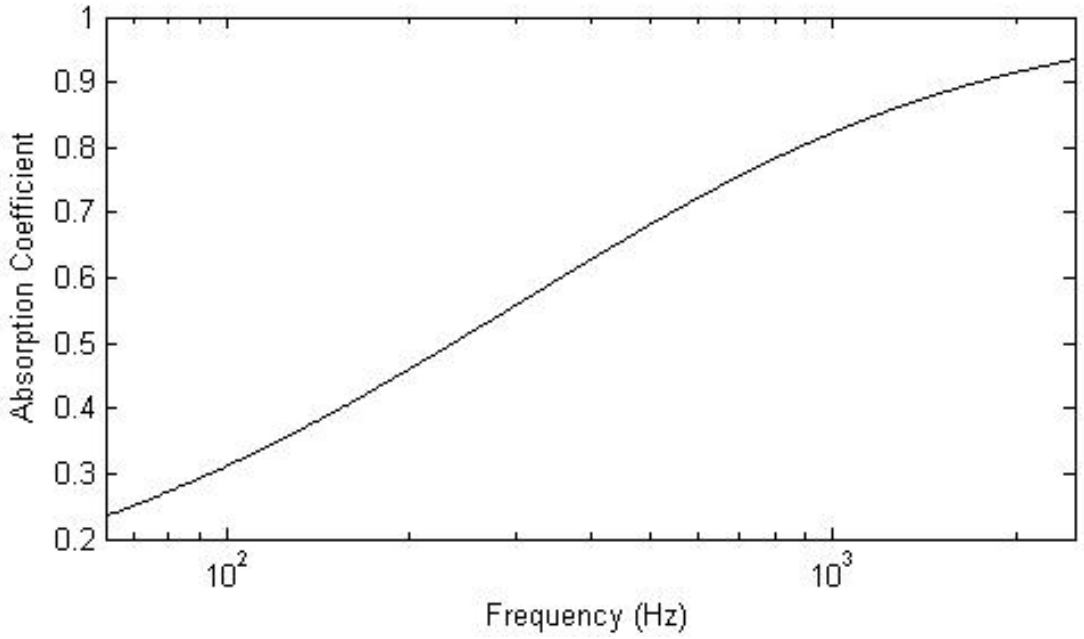

Figure 6.7: The effective absorption coefficient at full scale frequencies of the fuzzy blanket, calculated using the Delany and Bazley model.

Figure 6.8: The scale-model tree.

6.3.4 Scale-Model Trees

Scale-model trees, shown in Figure 6.8, were used to model tree foliage. The trees were 17.5 cm tall, corresponding to a full-scale height of 5.5 m. To characterize the foliage, scattering and absorption by the trees were measured. The sound source, at a full-scale height of 1 m, was located over grass, modelled by the green fabric, 10 m away from a line of trees. Receivers were placed 5 m in front of and 5 m behind the row of trees, at a height of 1 m. The sound pressure level (SPL) was measured at both receiver positions, with and without the row of trees present. From this, the tree insertion loss could be calculated, by subtracting the SPL with the trees from that without the trees.

This measurement was repeated at full-scale, on a hedge along the length of Wolfson Field, a rugby field on the UBC campus. Figure 6.9 shows a picture of the hedge. The insertion losses from both the scale-model measurements and the full-scale measurements are presented in octave bands in Figure 6.10.

There were some similarities and some large differences between the scale-model and

Figure 6.9: The evergreen hedge along Wolfson Field.

the full-scale field results. Attenuation through the foliage was seen in both cases: the trees attenuated sound by up to 3 dB in the scale-model tests and 5 dB in the full-scale tests, due to scattering or absorption. The IL in the field test was up to 2 dB smaller than the scale-model results below 600 Hz and higher by up to 2 dB above 600 Hz.

In the scale-model results, the trees had very little effect on the receiver in front of the trees. In the field tests, however, sound levels actually decreased in front of the barrier when the trees were present. One reason for this was the change of ground surface between measurements. The tests in the no trees case were done in the middle of a grass field, while the ground beneath the hedge contained roots which added porosity, increasing the ground absorption. This could also increase the appearance of attenuation due to foliage in the results taken behind the trees. In the scale-model measurements, the ground remained the same, as the removal of the trees did not affect the ground.

Another reason for the differing results is the leaf size; the leaves in the full-scale hedge were much smaller than those in the scale-model trees. The full-scale tests were done on an evergreen hedge, and therefore the leaves were very small. In contrast, the leaves

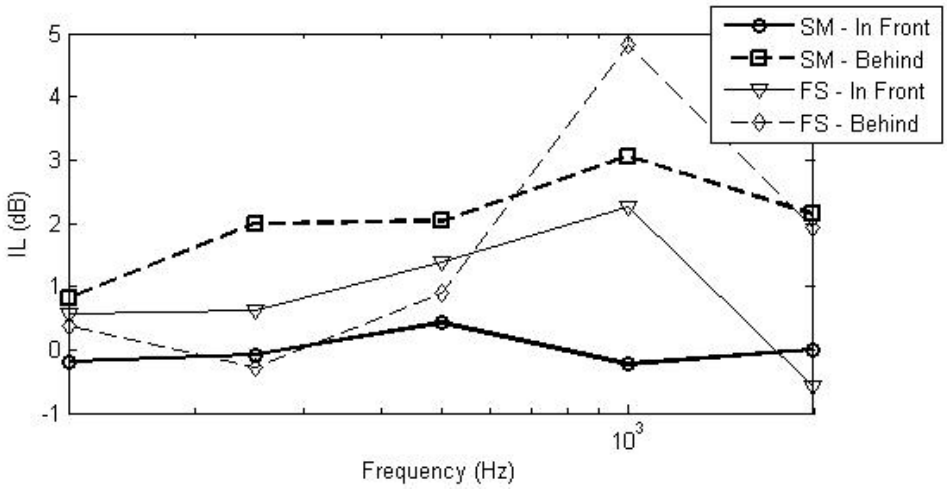

Figure 6.10: The measured IL in octave bands of a row of trees, measured 5 m in front of and 5 m behind the foliage. Full-scale field measurements (FS) are compared with scale-model measurements (SM).

on the scale-model trees were quite large compared with the wavelength; the leaves were approximately 2 mm wide, corresponding to a full scale size of 6 cm. This would be a closer model to a broad-leafed tree or hedge. It was attempted to locate such a hedge for testing; however an appropriate one could not be found.

The small change due to foliage seen in front of the hedge, in the scale-model measurements where the ground was consistent, and the much greater decrease in sound which reached the back suggested that energy was being scattered or absorbed by the foliage, while little was being back-scattered. The foliage absorbed energy by transferring the sound energy into vibrational energy of the leaves and branches. Sound that was scattered was sent in many directions, as opposed to transmitting through to the receiver on the other side of the foliage.

6.3.5 Insertion Loss Tests

The effects on barrier performance of two factors were examined using the acoustical scale model: barrier absorption and tree foliage. Both single and parallel barriers were used to

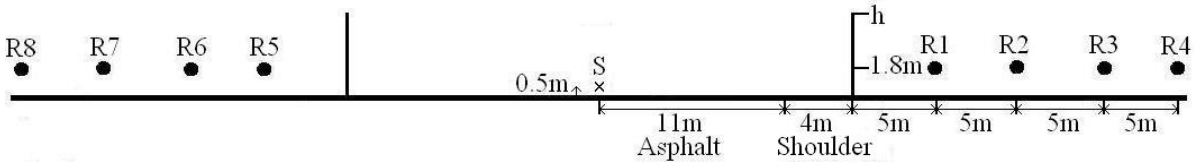

Figure 6.11: The parallel-barrier configuration. The barrier height varied, with h having values of 3, 4 and 5 m. Dimensions are shown using full-scale equivalent distances.

investigate these effects. In both configurations, described here using the corresponding full-scale dimensions, a 22 m wide, four-lane highway was modelled. The shoulder, the space between the asphalt and the barrier, was 4 m wide. A distance of 30 m between the parallel barriers was chosen due to the facts that a smaller distance is rarely found in the field and that the amplification effects are reduced at larger distances. The sound source was placed 0.5 m high, in the center of the highway, 11 m from the shoulder. Receivers were placed 5, 10, 15 and 20 m behind the barrier(s) at a height of 1.8 m. Barrier heights of 3, 4 and 5 m were tested. Figure 6.11 shows the full-scale test configuration with parallel barriers, and Figure 6.12(a) is a photo of the setup with reflective parallel barriers.

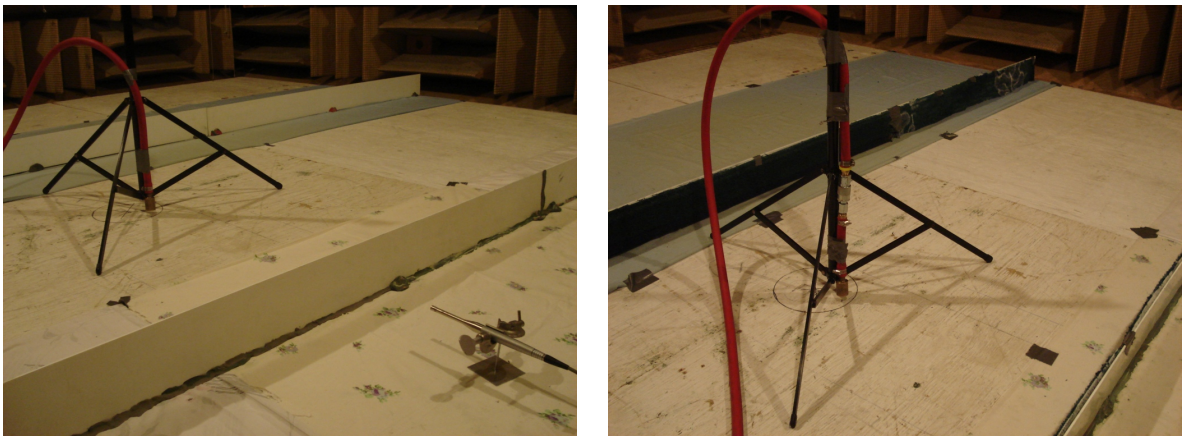

(a) (b)

Figure 6.12: The experimental setup of the scale model in the anechoic chamber with parallel barriers on either side of the air-jet source. a) Reflective Barriers. b) Absorptive Barriers.

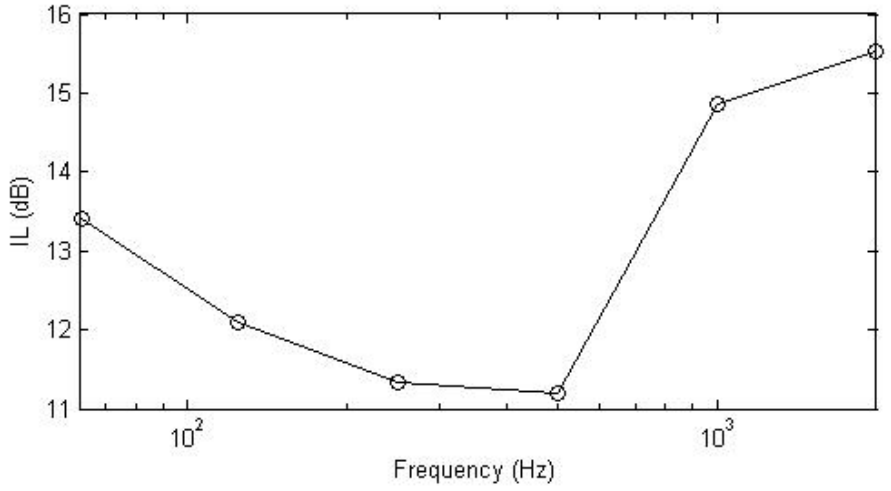

Figure 6.13: The measured IL in octave bands at receiver position R2 for the 5 m high reflective parallel barriers.

Absorption

The effects of barrier absorption on the source side of the barrier were examined for three different barrier heights: 3, 4 and 5 m. Several configurations were measured: reflective and absorptive single barriers, reflective and absorptive parallel barriers, and parallel barriers with one reflective and one absorptive. In the last of these configurations, the reflective barrier was the one between the source and receiver positions R1-R4, while the one between the source and positions R5-R8 was absorptive. Figure 6.12(b) shows a picture of the absorptive parallel barriers. When testing one barrier, the barrier between the source and receivers R5-R8 was removed; the IL's for those tests at those receivers were close to zero and are not shown.

Figure 6.13 shows the octave band IL at receiver position R2 for the 5 m high reflective parallel barriers. IL varies with frequency from 11-16 dB, due to complex ground interactions. Figure 6.14 shows the IL differences between the reflective parallel barriers and the other barrier and absorption configurations. The IL shown in Figure 6.13 has been subtracted from the IL's for the other configurations; therefore a positive change in IL is

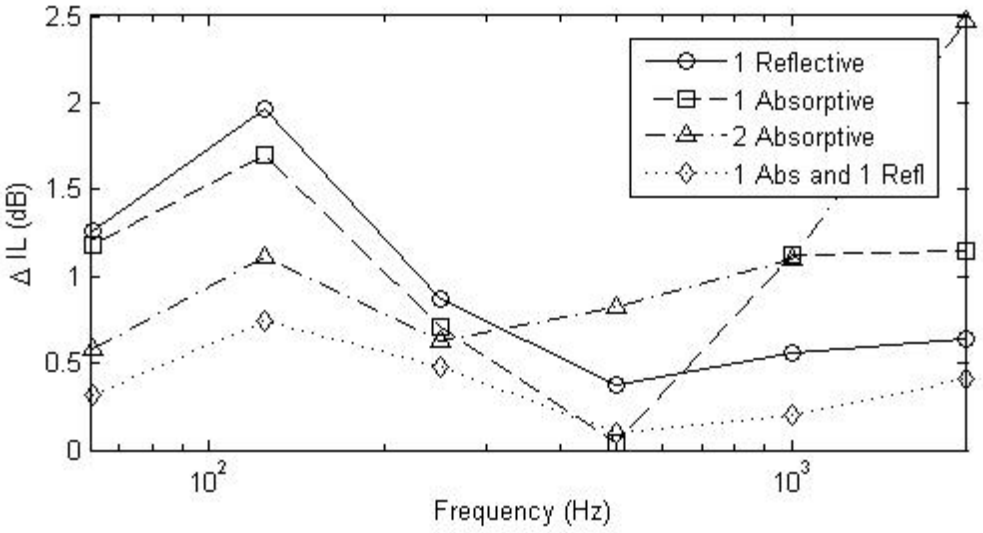

Figure 6.14: The measured difference in IL between reflective parallel barriers and the other configurations. Shown in octave bands and measured at receiver position R2 for the 5 m high barriers.

a decrease in noise levels and an improvement in barrier performance. At low frequencies, the effect of adding a second barrier is apparent; the IL was up to 2 dB higher for a single barrier than for parallel barriers. Here, absorption increased IL by 1 dB for the parallel barriers. At high frequencies, adding absorption to a single barrier increased IL by 0.5 dB. For parallel barriers, making them absorptive increased IL by up to 2.5 dB. Adding absorption to one of the parallel barriers improved IL slightly; however the IL was still slightly lower than a single reflective barrier.

The A-weighted IL's for the different configurations at each receiver position, and for a barrier height of 5 m, are shown in Figure 6.15. Changing from a single 5 m reflective barrier to 5 m parallel reflective barriers decreased the IL by approximately 1 dBA. This demonstrates the amplification that occurs between parallel barriers. When using absorptive barriers, the parallel barriers gave IL's which were very similar to those of a single barrier. Absorption added to the reflective walls increased the IL very slightly (< 0.2 dBA), but reduced reflections from the wall by up to 1 dBA.

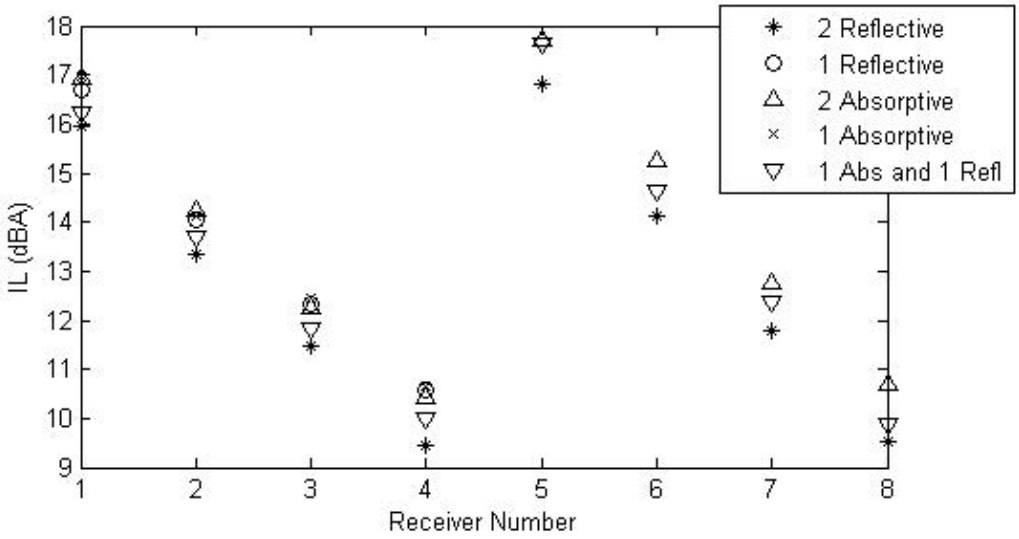

Figure 6.15: The measured A-weighted IL's for the 5 m tall barriers at the eight receiver positions.

Figure 6.16 shows the A-weighted IL's for parallel barriers at receiver position R2 for the three barrier heights. Based on these results, increasing the height of a barrier by 1 m increased the IL by more than adding absorption to a smaller noise barrier. By fitting a line through the data points, it was determined that adding absorption had the same effect on IL as increasing the barrier height by 0.33 m.

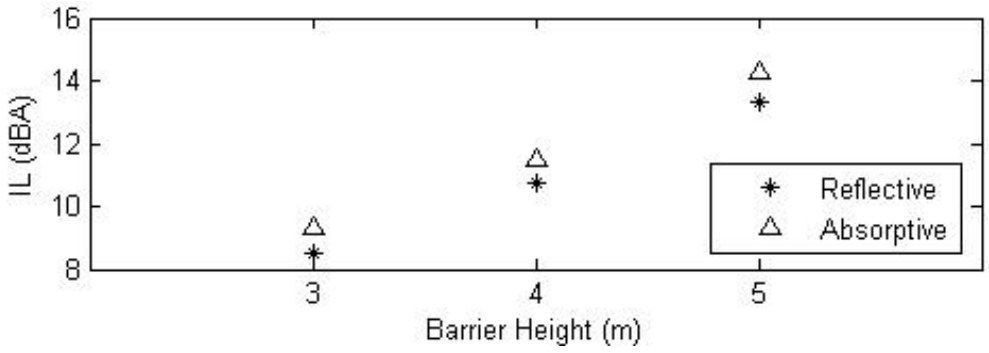

Figure 6.16: The measured A-weighted IL's for absorptive and reflective parallel barriers at R2 for the three different receiver heights.

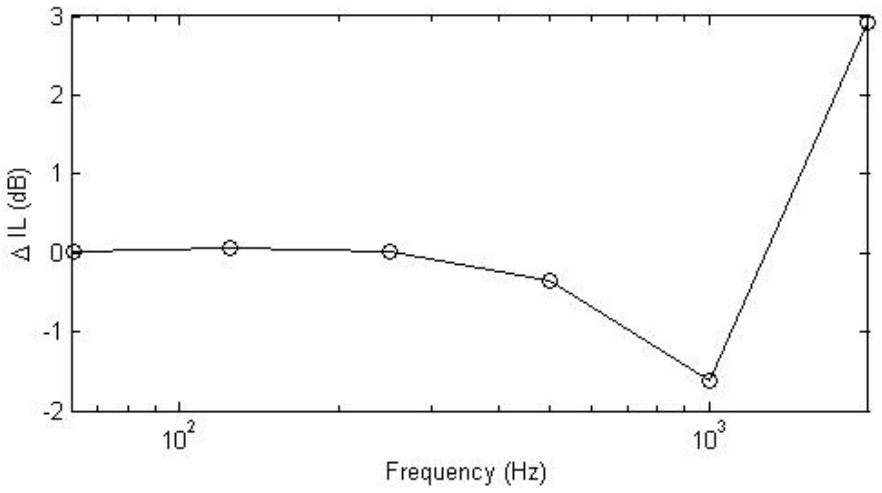

Figure 6.17: The measured change in IL in the case of parallel barriers with and without a line of trees along the source sides of the barriers. Shown in octave bands and measured at receiver R2 for 5 m high parallel barriers.

Foliage: Parallel Barriers

Figure 6.17 shows the effect of adding a row of trees along the source sides of 5 m high parallel barriers. The trees were approximately 5.5 m high, so they overtopped the wall slightly. The measured change in IL in the case of reflective barriers with and without the rows of trees is shown in octave bands, measured at position R2. The foliage had negligible effect up to 500 Hz, then decreased the IL at frequencies up to 1250 Hz. Above this the foliage increased IL, acting as a scatterer; sound that would normally reflect from one barrier and diffract around the other is scattered in other directions. Below 1250 Hz, the foliage which overtopped the barrier scattered sound into the shadow zone, causing the decrease in IL.

Figure 6.18 shows the total A-weighted IL of reflective and tree-lined parallel barriers at all receiver positions. The trees on the source sides of the barriers decreased the total IL by up to 1 dBA. The increase observed at high frequencies is not enough to balance the decrease below 1250 Hz.

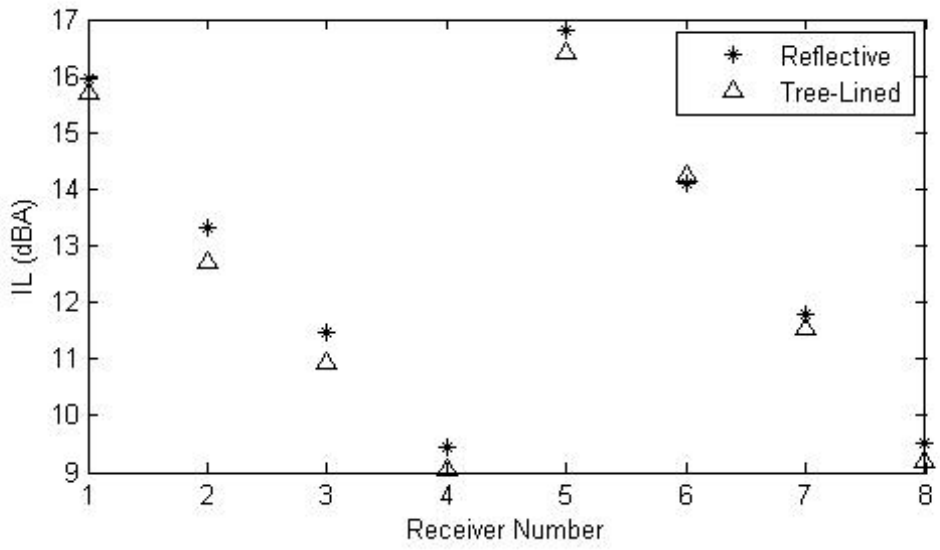

Figure 6.18: The measured A-weighted IL's for the 5 m tall barriers at the eight receiver positions, with and without a line of trees along the source sides of the barriers.

Foliage: Single Barrier

The effects of foliage at different positions around the barrier were examined using a single, 3 m high barrier. Only four receiver positions, R1-R4, were behind the single barrier, therefore measurements were taken only at those four positions. The trees were placed at different positions around the barrier: directly behind the barrier, directly in front of the barrier, and 10 m behind the barrier such that receiver position R1 is between the trees and the barrier. Two different foliage heights were used: 5.5 m and 7.2 m. For the taller trees, both the regular density of trees, where the tree bases were placed approximately 1.5 m apart, and a thicker row of trees, where tree bases were placed 0.9 m apart, were tested. Figure 6.19 shows the taller, denser foliage placed behind the barrier.

The differences in IL between a reflective wall and the different foliage configurations are shown in Figures 6.20 and 6.21 for the shorter and taller trees, respectively. Placing the foliage directly next to the barrier, either in front or behind, had little effect at low

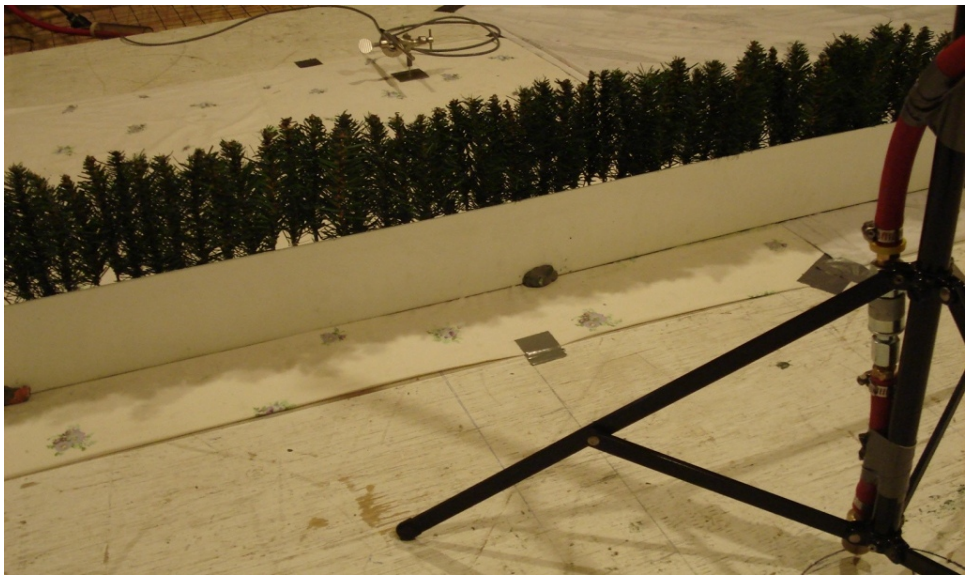

Figure 6.19: Taller, denser foliage behind the barrier.

frequency and caused an increase in IL at mid-frequencies. Here the sound was absorbed and back-scattered by the foliage. At high frequencies, the IL decreased by up to 4 dB. At these frequencies, sound was scattered by the foliage into the shadow zone. For taller trees, the attenuation at lower frequencies was greater, and scattering into the shadow zone began to occur at a lower frequency. At low frequencies, the taller trees provided more opportunity for sound absorption and back-scattering, much like increasing the height of a noise barrier. At higher frequencies, there was more effective foliage surface area to scatter the noise. The foliage had very little effects on the total A-weighted IL values; the low frequency increase and high frequency decrease in general averaged out.

Placing the trees behind the receiver position had very little effect on the IL, in agreement with earlier tests that found little sound is back-scattered from a row of trees. Using denser foliage also had a small effect on the IL. In general, IL increased very slightly, meaning that the denser foliage attenuated more sound, which was to be expected.

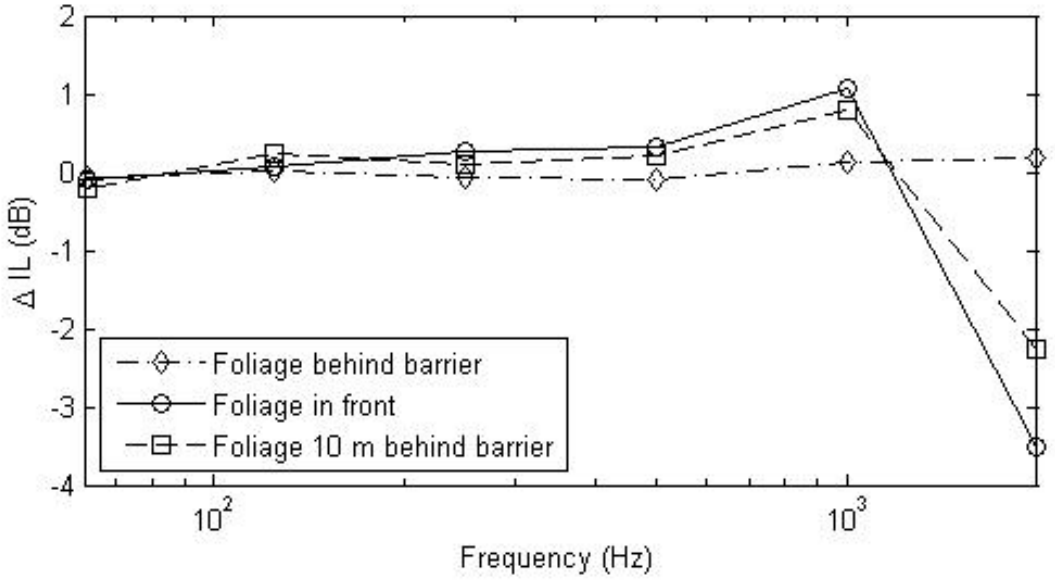

Figure 6.20: The measured change in IL between a reflective barrier and the different foliage configurations. Shown in octave bands at receiver R1 for a 3 m high barrier, with 5.5 m tall trees.

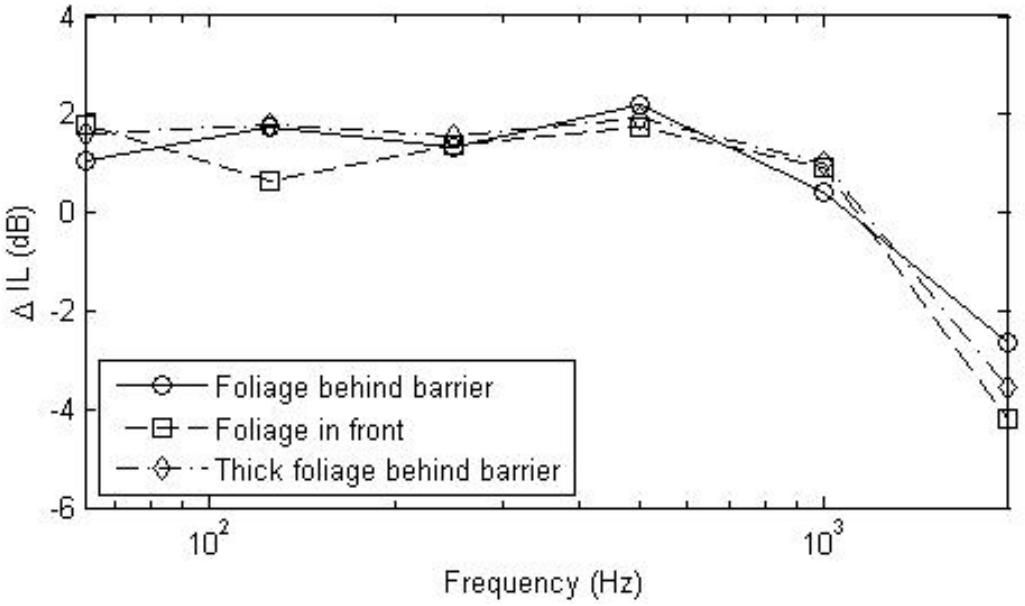

Figure 6.21: The measured change in IL between a reflective barrier and the different foliage configurations. Shown in octave bands at receiver R1 for a 3 m high barrier, with 7.2 m tall trees.

6.4 Summary

A scale model was developed to test factors which affect highway noise barriers. Excess attenuation measurements were performed to select appropriate model materials. The parameter flow resistivity was used and the Delany-Bazley model was assumed, which is not valid for acoustically hard materials. A four-lane highway configuration was then set up, with the option of having a single barrier or parallel barriers. Absorptive barriers were investigated using barriers of varying height. It was shown that adding absorption to the source side of parallel barriers increased the total IL by 1 dBA, which was found to be equivalent to increasing the height of the barrier by 0.33 m. It was also seen that using absorptive barriers prevented the 1 dBA decrease in IL when adding a second barrier that occurred with reflective barriers.

The effects of tree foliage near barriers were also examined using the scale model. Measurements done on the scale-model trees were compared with the same measurements done at full scale on an evergreen hedge, where the results varied by up to 2 dB. This could indicate that there is another material which would better model an evergreen hedge and that the model trees used model a different type of foliage more accurately, such as a broad-leafed tree. These trees were placed in different positions near the barrier, as seen in the field. It was seen that foliage directly in front of or behind the barrier scattered up to 4 dB of sound into the shadow zone above 1000 Hz, causing the barrier to be less effective at these frequencies. It was also seen that foliage attenuated up to 2 dB of sound at mid-frequencies, increasing the effectiveness of the barrier.

Chapter 7

Prediction

This chapter discusses the prediction of the effects of absorption and vegetation on barrier performance. Three prediction methods were used: ray tracing, finite elements and the method of images. Two different diffraction algorithms were used: the Uniform Theory of Diffraction and Svensson's model. The results from the full-scale anechoic chamber testing (Chapter 4) were predicted using all three prediction methods in hopes of validating the prediction models. The foliage characterization tests done for the scale-model trees (Section 6.3.4) were then predicted using ray tracing. The following sections will go into the details of both diffraction models as well as each prediction method, and then the results will be shown and discussed.

7.1 Edge Diffraction

Diffraction is the bending of sound waves around an edge. It is the mechanism that allows sound to reach the shadow zone behind a barrier; therefore the accuracy of the diffraction model is crucial when modelling outdoor noise barriers, where the diffraction paths contribute all of the sound at a receiver position. Two theories of diffraction were used here: the Uniform Theory of Diffraction and Svensson's model.

Keller [58] developed the Geometric Theory of Diffraction (GTD), a frequency-domain model which calculates a complex diffraction coefficient for electromagnetic waves travelling over an infinitely long, perfectly conducting wedge. The diffraction coefficient depends on the geometry of the wedge and the source and receiver positions. His work was an extension

of geometrical optics, where the wavelength of interest is very small; therefore the theory is only valid at high frequencies.

Kouyoumjian and Pathak [59] modified the GTD to create the Uniform Theory of Diffraction (UTD). This method is valid for the shadow and reflection boundaries, where Keller's theory had singularities. Further prediction work has been done using the UTD by Kawai [60], who extended the UTD to study many sided barriers, and Tsingos et al. [61], who studied the modelling of virtual environments using beam-tracing.

Biot and Tolstoy [62] developed a time-domain model, studying the impulse response of a diffracted spherical sound wave by a rigid wedge. Medwin [63] went on to study the Biot-Tolstoy model when applied to noise-barriers and found good agreement in the case of infinite edges. He extended the model to account for finite-length wedges and used the concept of a secondary edge source.

Svensson et al. [64] further extended Medwin's work to form a new impulse-response model. They used line-integrals to model the edge, which removed a singularity found in the Biot-Tolstoy model. In a later paper [65], Svensson et al. went on to remove a different type of singularity from the Biot-Tolstoy model, along the specular-zone and shadow-zone boundaries. More work was then done [66] to transform the model to the frequency domain.

The theory of both the UTD and Svensson's model are presented in Appendix A.

7.2 Ray Tracing

The ray tracing program used, PRAY, was developed by Hodgson et al. [67], originally based on the energy algorithm developed by Ondet and Barbry [68]. A source emits a number of rays in random directions, each with an equal amount of initial sound pressure (using the phase model) or pressure squared (using the energy model). Each ray's trajectory is followed as it travels in a straight line until it encounters an obstacle, where it is reflected, either specularly or diffusely. An obstacle may be a wall or a scattering obstacle defined by

a volume of randomly distributed scatterers. Each obstacle has a defined complex reflection coefficient, which reduces the amount of energy the ray contains, as well as the phase of the ray. A wall may also reflect diffusely, controlled by a user-defined diffusion coefficient. The ray's energy and pressure can also decrease due to propagation over a distance and air absorption. A plane of cubic receivers is defined, and the pressure and energy of all rays which pass through each receiver are accumulated to give the total sound pressure level.

Diffraction was included in PRAY by Chan in 2007 [69] using the UTD. Yousefzadeh [70] considered Svensson's model as an alternate method of diffraction using beam-tracing. However, this was never integrated into PRAY, but was implemented as part of an image method. His implementation was modified and integrated into PRAY here. Predictions were performed using both the UTD and Svensson's model.

Because each ray in infinitely thin, one will almost never hit the tip of an edge exactly. Therefore if a ray hits an obstacle within half of a wavelength to the edge, it will diffract. This value was decided on by Chan [69], who performed anechoic chamber measurements.

7.3 Method of Images

In the simplest case, where a source and receiver are placed above a reflecting surface, the method of images (MOI) reflects the source in the surface and treats it as a second (image) source. The sound level at the receiver is then the sum of the direct sound from two sources: the real source and the image source. When a barrier is inserted between the source and receiver, there are four paths to consider instead of two, reflecting both the source and the receiver in the ground, as shown in Figure 7.1. The image source accounts for the reflected path on the source side, while the image receiver accounts for the reflected path on the receiver side.

This method assumes that the surface is perfectly reflecting; however finite-impedance surfaces can be modelled approximately [71]. The pressure components from the image

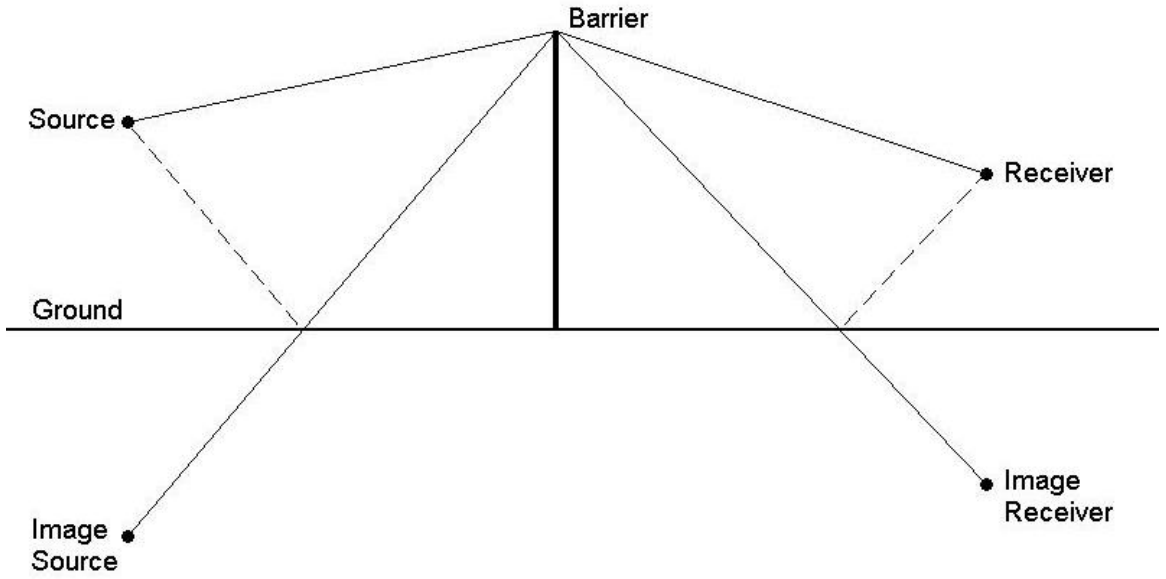

Figure 7.1: The four sound paths between a source and a receiver with a barrier in between. The method of images uses an image source and image receiver to model the reflected paths.

source or reaching the image receiver are multiplied by the reflection coefficient of the surface before the sound levels from the four paths are summed.

7.4 Finite Element Method

The finite element method (FEM) is a numerical method which solves differential equations, defined over a relatively simple domain with defined boundary conditions. It is useful for acoustics in a well-defined space, because the governing differential equation, the wave equation, is fairly straight forward. A mesh is created, where the domain is split up into a number of elements; the number of elements needed for an accurate solution is dependent on the wavelength of interest, and the accuracy will diminish if there are not a sufficient number of elements per wavelength. Run times and computer memory become problems for larger domains and higher wavelengths; therefore only the full-scale anechoic chamber results at 1000 Hz were predicted, in two dimensions. Here the domain is fairly small —

4.6 m wide by 2.6 m high — and the wavelength corresponding to 1000 Hz is 0.34 m. The finite element code used here was created in MATLAB by the author for a course project at the University of British Columbia.

The wave equation, defined over the two-dimensional domain Ω with appropriate boundary conditions defined on the boundary $\partial\Omega$, is given by:

$$\begin{aligned} \nabla^2 p + k^2 p &= f(x,y) \qquad \text{on } \Omega \\ \nabla p \cdot n &= \frac{ik}{Z} p \qquad \text{on } \partial\Omega, \end{aligned} \tag{7.1}$$

where p is the pressure, k is the wavenumber, Z is the impedance and ∇^2 is the two-dimensional Laplacian operator using Cartesian coordinates. $f(x,y)$ is the source function, given by:

$$f(x,y) = C\,\delta(x - x_0, y - y_0) \tag{7.2}$$

where C is a constant which depends on the source strength and (x_0, y_0) are the source's coordinates. To model an outdoor environment, the sides and top of the domain were given a reflection coefficient of zero and, since Z is given as:

$$Z = \frac{1+R}{1-R}, \tag{7.3}$$

the impedance has a value of one. The discretization of these equations, and the formulation of the matrix equation implemented in MATLAB, will not be presented here, however one can find it in [72]. Piecewise linear shape functions were used. For a full description of the creation of the mesh and the MATLAB code, see Appendix B.

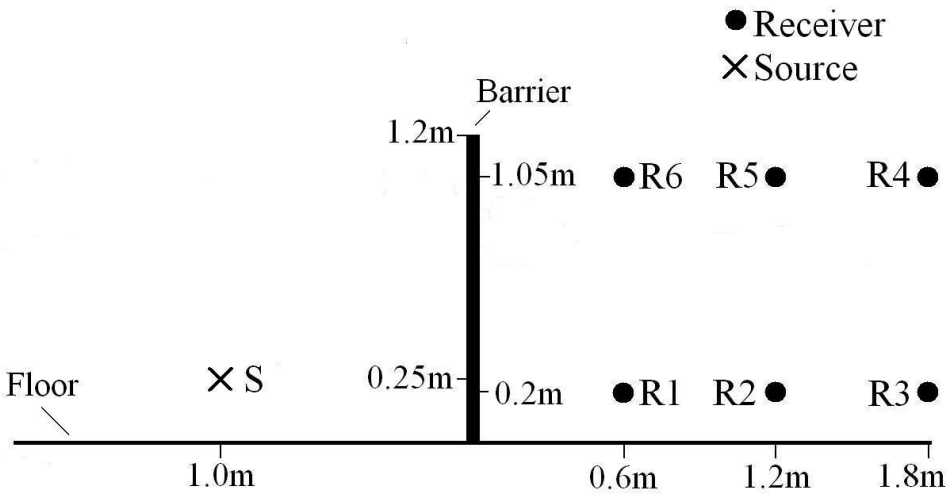

Figure 7.2: The anechoic chamber test configuration with the locations of receiver positions R1-R6.

7.5 Results

7.5.1 Full-Scale Laboratory Testing

The results from the full-scale barrier testing in the anechoic chamber (Chapter 4) were predicted using all three prediction methods. The results in the 1000 Hz third-octave band, for the low source position at the six receiver positions shown in Figure 7.2, were predicted. Predictions were done for the no barrier case, for a reflective barrier and for an absorptive barrier.

In the methods which required a diffraction coefficient to be calculated — ray tracing and method of images — both the UTD and Svensson's model were used. In FEM, diffraction is an inherent part of the solution to the wave equation, and therefore a diffraction theory is not needed.

In FEM and ray tracing, in which the boundaries of the chamber can be defined, the walls and ceiling of the anechoic chamber were modelled as completely absorptive, with a reflection coefficient of zero or an impedance of one. In all three prediction models,

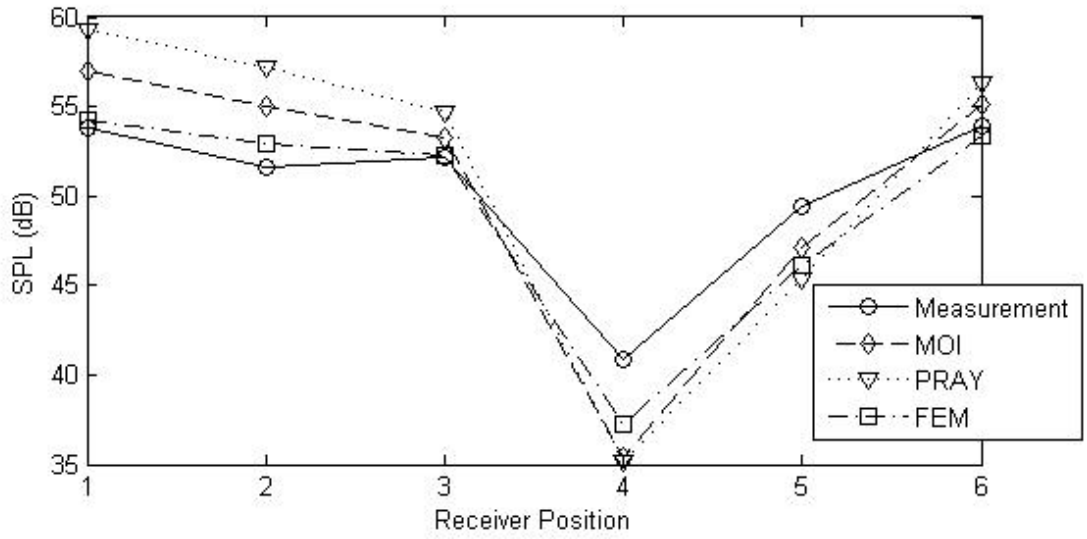

Figure 7.3: Measured and predicted 1000 Hz sound pressure levels with no barrier at the six receiver positions in the anechoic chamber.

the painted plywood floor was assigned a reflection coefficient of 0.9, based on spherical decoupling measurements done previously [73].

All three methods of prediction — FEM, ray tracing (PRAY) and MOI — predicted the results of the no-barrier case within 5 dB of the measured results, as shown in Figure 7.3. All accurately showed the minimum SPL at receiver position R4, however all methods underestimated the SPL at this position, with MOI and PRAY being under by 5 dB and FEM by 2 dB. All methods also overestimated the SPL at the low receiver positions, R1-R3, with FEM again giving results 2 dB from measurement and PRAY giving results 5 dB too high.

Figure 7.4 shows the predicted IL's of the barrier found using the three prediction models as well as the measured values. All prediction results had very similar overall trends to the measurement results, when comparing the variations with receiver position; however, the magnitudes of the IL's were very different. FEM gave results within 2 dB to measurement at several receiver positions, however at other receiver positions results were

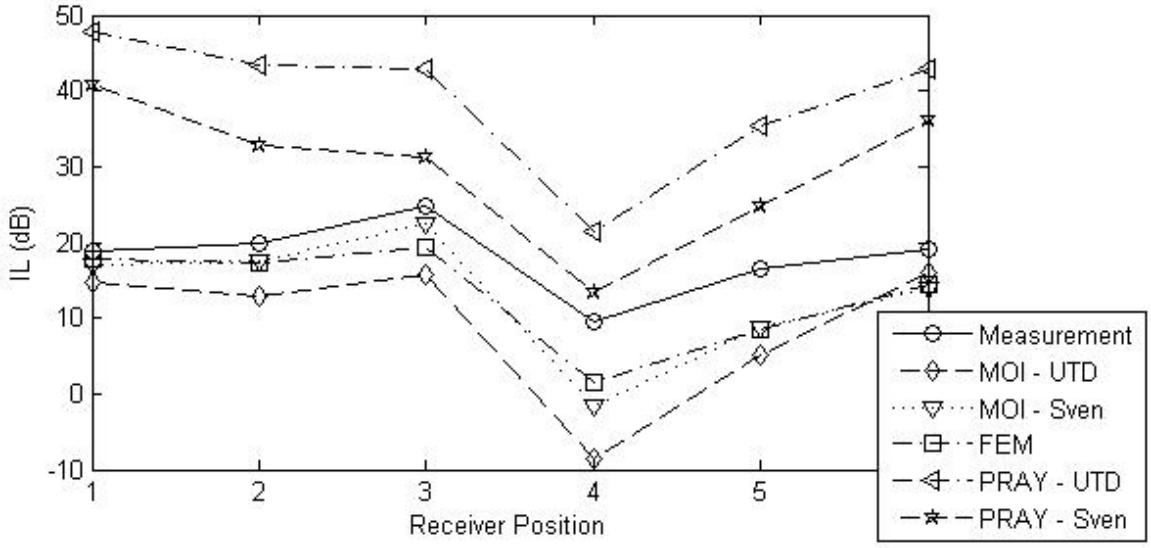

Figure 7.4: Measured and predicted 1000 Hz IL of the wall built in the anechoic chamber at receiver positions 1-6.

up to 8 dB too low. The predicted IL's using ray tracing with the UTD were up to 30 dB higher than measurement, while using Svensson's model were up to 20 dB too high. Both diffraction models performed better when implemented using the MOI, with Svensson's model performing more accurately, giving results 2-10 dB from measurement. From these results, it was known that it was not the diffraction coefficient calculations which caused the inaccurate results in ray tracing.

The discrepancies between MOI and measurements may come from several things. MOI assumes that the barrier is infinitely thin, while in reality the barrier was 12 cm wide. Diffraction around the edges of the barrier and second order diffraction may have occurred and were not accounted for in this model. Svensson's model proved to be more accurate in these predictions; the UTD assumes an infinitely long barrier while Svensson's model accounts for finite length barriers. The FEM model is a two-dimensional model and therefore does not account for any diffracted sound which was not perpendicular to the barrier; this could account for the discrepancies seen between the FEM predictions and

measurements.

Using PRAY, the high IL's indicated a low sound level behind the barrier. This occurred because not enough rays were being diffracted to reach the receivers placed behind the barrier. In ray tracing, rays are emitted in every direction; in the case of barriers outdoors there are in fact only four sound paths between a source and receiver, as discussed in regards to the MOI. Therefore, the vast majority of the rays which are emitted are unnecessary, leading to a very inefficient model. A very large amount of rays are required, leading to very long run times, and even then there are an insufficient number of rays which are diffracted. In room acoustics, where ray tracing has been the most successful, there are many sound paths which allow for rays to reach a defined receiver and each ray may have many reflections. In the case of outdoor barriers there is at most two reflections, off the ground on either side of the barrier, while most rays will not reflect at all before being absorbed by the perfectly absorbing walls and ceiling. Due to these reasons, it is hypothesized that ray tracing is not a valid method for the prediction of outdoor noise barrier performance.

The MOI does not allow the barrier to be absorptive, as it is inherent in the code that the diffracting edge is reflective. Therefore it was determined that FEM was the best option to perform absorption measurements.

The change in IL due to absorption placed on the source side of the barrier in the anechoic chamber was investigated using FEM. Figure 7.5 shows the results, where FEM gave values within 2 dB of measurement. These discrepancies can be due to several things. The first is that again the predictions are done in two dimensions, ignoring all sound not perpendicular to the barrier. Another is that in the anechoic chamber, adding absorption to the front of the barrier also added 50 mm, the thickness of the baffles, to the thickness of the barrier. In the predictions, there was no increase in barrier thickness when the barrier's source side became absorptive.

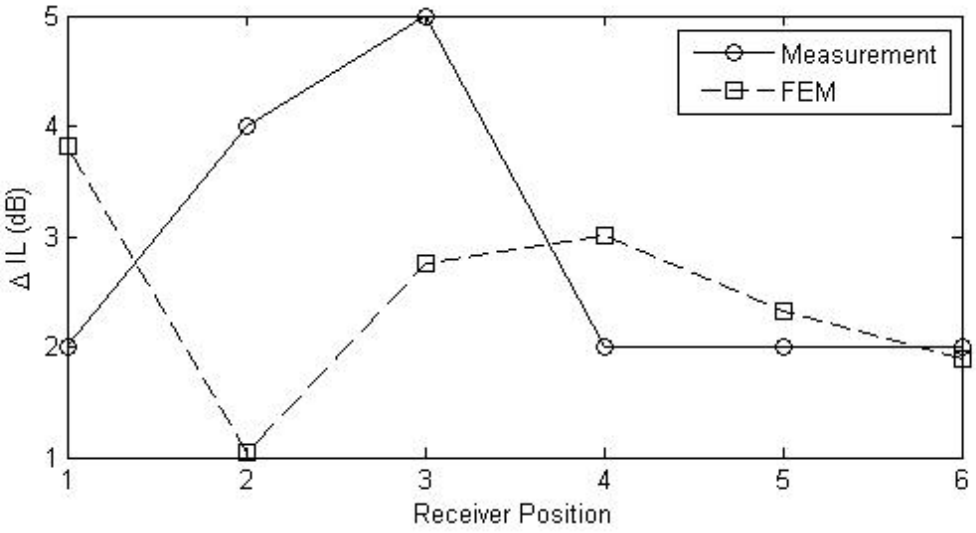

Figure 7.5: Measured and predicted change in IL due to absorption on the source side of the barrier, at 1000 Hz.

7.5.2 Foliage

The results from Section 6.3.4, where the model foliage was characterized by comparing scale-model measurements to full-scale field tests, were modelled using PRAY. Receivers were placed 5 m in front of and 5 m behind the row of trees placed on grass, and the source was placed 10 m from the trees. Both the source and the receivers were 1 m above the ground, as in the measurements. A room 25 m long by 20 m wide by 6 m high was created, with perfectly absorbing ceiling and walls. Results were predicted at 125, 250, 500, 1000 and 2000 Hz. The ground reflection coefficient was determined by using the no-foliage case from the scale-model measurements and performing a best-fit using the method of images. Figure 7.6 shows the measured and best-fit sound pressure levels at the receiver position 5 m from the source and Table 7.1 gives the results of this fit. The foliage was modelled as a 1 m thick, 6 m high zone of volume scatterers, with a fitting density of 0.3 m^{-1}. This value was found by comparing results with a variety of fitting densities and selecting the one which agreed best with measurement.

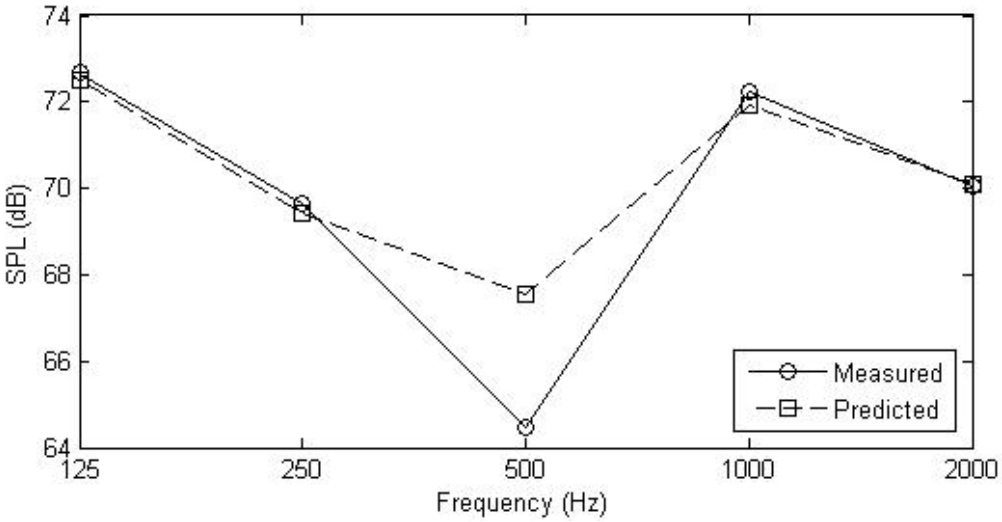

Figure 7.6: The measured and best-fit predicted SPL at the receiver position 5 m from the source with no trees present, used to determine the ground reflection coefficient.

Table 7.1: Grass reflection coefficients as determined by a best-fit using MOI.

Frequency (Hz)	125	250	500	1000	2000
Reflection Coefficient	.5-.4i	.4-.2i	.6-.2i	.3-.3i	.2-.3i

Figure 7.7 shows the IL due to the row of trees, both from PRAY predictions and scale-model measurements. Predictions demonstrated very similar trends to measurements. Ray tracing showed sound amplification of up to 1 dB in front of the barrier at several frequencies and the magnitude of the IL stayed below 1 dB, as in the measurements, until the 2000 Hz band. Using ray tracing, the IL of the foliage behind the barrier was greater in magnitude than in front, again agreeing with measurements; however the peak IL was found to be 4 dB and occurred at 500 Hz using ray tracing, as opposed to 3 dB at 1000 Hz in the measurements. These discrepancies may come from the fact that the foliage was being modelled as volume scatterers, which assumed random scattering. In reality, foliage

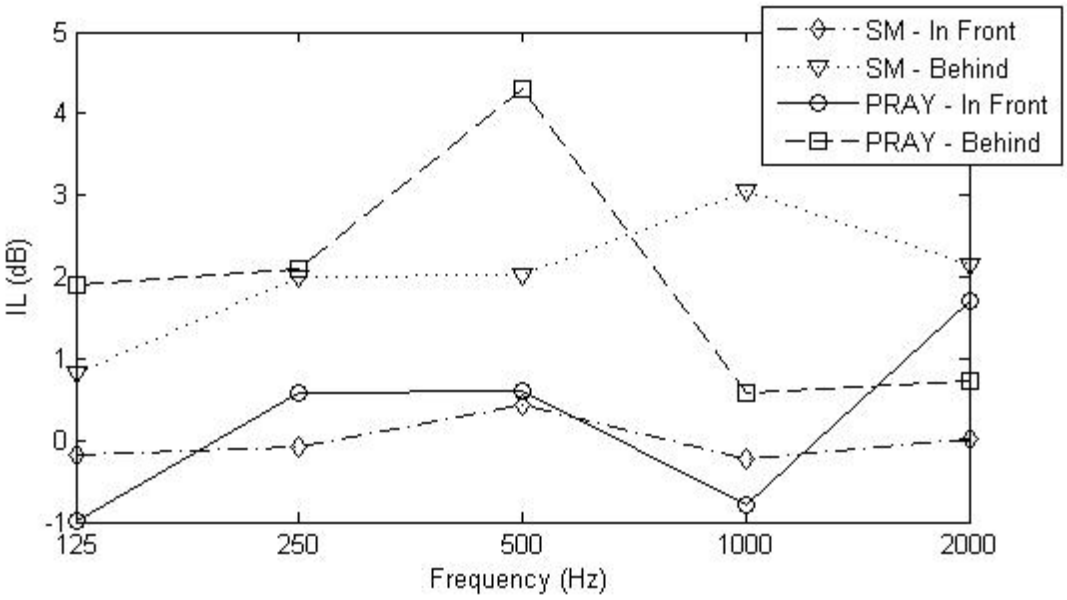

Figure 7.7: IL of a row of trees, 5 m in front and 5 m behind the foliage. Ray tracing results (PRAY) are compared with scale-model measurements (SM).

has complex absorption characteristics and do not scatter omni-directionally.

Because the anechoic chamber barrier predictions showed that PRAY was an unfit prediction model to use for outdoor barrier predictions, no further predictions were made on the effects of foliage on barrier performance. FEM may be used, however tests must first be performed to determine how to model the foliage using finite elements.

7.6 Summary

Three prediction methods — ray tracing, finite elements, and the method of images — were studied in hopes to show them to be useful tools in the prediction of the performance of noise barriers and the factors studied in this work. Two diffraction methods were used for ray tracing and the method of images: the Uniform Theory of Diffraction and Svensson's model. Results from the full-scale anechoic chamber testing were also predicted; finite elements and the method of images using Svensson's model gave results closest to measurement,

varying by 2-10 dB from the measured values. Some discrepancies of the MOI could be due to the assumptions of an infinitely thin barrier and no diffraction around the ends of the barrier. The fact that the FEM was a two-dimensional model could account for the differences between FEM predictions and measurements. Ray tracing using both methods of diffraction gave IL results up to 30 dB higher than measurement and showed to be an inadequate modelling technique to be used for outdoor noise barriers. Since MOI does not allow for the barriers to be absorptive, the effects of making the source side of the barrier in the anechoic chamber absorptive were predicted using the FEM. The prediction results differed from measurement by up to 2 dB, which could be due to the fact that the thickness increase which occurred in the anechoic chamber did not occur in the model.

Ray tracing was used to predict the experiments which measured the amount of sound back-scattered from and transmitted through foliage. The magnitudes of the changes in IL due to foliage were within 2 dB of measurement, with discrepancies due to the fact that the foliage was being modelled as random volume scatters. The foliage effects on barriers were not predicted, as PRAY showed to be unfit to model outdoor barrier performance.

Chapter 8

Conclusion

In this work, several factors which affect the performance of highway noise barriers comprising thin vertical walls were investigated with the aim of improving the practice of noise mitigation. One of these factors was making the barrier surfaces sound absorbing, which could reduce the sound amplification that occurs between two reflective parallel barriers. The other factor was foliage growing near a barrier; this could have both a positive or negative effect, depending on whether the foliage absorbs and back-scatters sound (decreasing noise levels) or scatters sound into the shadow zone (increasing noise levels). The main objective of this thesis was to explore these factors and determine how they affect the performance of roadside noise barriers. This was done using four methods of investigation: full-scale barrier testing, field testing, scale-model testing and prediction.

The first detailed objective was to determine the optimal amount and placement of absorption on a barrier and the effects it has on the barrier's performance. This was achieved by constructing a 1.2 m high barrier on a plywood floor in an anechoic chamber. By covering the wall with different configurations of absorptive material, it was determined that covering all of both sides of the wall would prevent amplification and give the greatest IL. The reflective wall's IL was improved by 2-3 dBA using this configuration when the source and receiver positions were within 1.8 m of the wall and the NRC value of the absorptive material was 0.71. The distance was closer than what is typically seen in the field and therefore slightly lower IL improvements should be expected in practice. However the NRC value was lower than 0.8, the value recommended by the Ministry. It was seen in

the results that an absorptive material with the highest NRC value gave the greatest IL, with an NRC improvement of 0.15 giving an IL improvement of 1-2 dBA.

Prediction was to be used to achieve this objective; once the available models were validated, it was hoped that further predictions could be made of barriers with varying absorption configurations. In order to validate three prediction models, the full-scale anechoic chamber measurements were predicted at 1000 Hz. It was found that ray tracing gave IL results of the reflective wall which were up to 30 dB higher than measurements. From this, it was hypothesized that ray tracing is not a valid prediction method for outdoor noise barriers, due to the large amount of rays which are absorbed by the ceiling and walls without ever being diffracted. To ensure that the errors were not due to the implementation of the diffraction models, UTD and Svensson's model were implemented into the method of images. The MOI approach was much more accurate, with Svensson's model giving IL's 2-10 dB from measurement and the UTD giving results 5 dB further. Svensson's model does not assume an infinite length barrier as the UTD does, and therefore this could account for the more accurate results. When using MOI one cannot make the barrier sound absorptive, as a reflective barrier is assumed. Therefore in regards to absorptive barrier predictions, this method is not relevant. FEM gave results for the reflective barrier similar to MOI using Svensson's model, varying from measurement by 2-8 dB. This discrepancy can be due to the fact that the FEM was performed in two dimensions, and therefore sound that was not perpendicular to the barrier was ignored. However, this method appeared to be the best option in performing absorptive barrier measurements. Making the source side of the barrier sound absorptive was predicted using FEM; results were found to be within 2 dB of measurements. Discrepancies could be due to the fact that in the anechoic chamber, the effective barrier width increased by 50 mm, the width of the baffles, while in prediction no change in width was accounted for.

The second objective was to study the effects of absorption on the performance of

parallel barriers. A scale model was created to achieve this objective. Excess attenuation measurements, which use the flow resistivity as a single parameter and assume the Delany-Bazley model to be valid, were performed to select the scale-model materials to model a four-lane highway. The Delany-Bazley model is valid for porous material only and was therefore not valid for hard surfaces. This could have a large impact on the performance of the scale model, and other methods of selection should be investigated.

Using the scale model, more realistic source and receiver distances could be used. The source was placed in the center of the highway, 15 m from the barrier, at a height of 0.5 m. Receivers were placed 5 to 20 m behind the barriers at a height of 1.8 m. Three different heights of parallel barriers were used to study absorption; it was found that for parallel barriers in this configuration, adding absorption to the source side of the barriers was equivalent to increasing the reflective barriers' height by 0.33 m. The effects of adding either a reflective or absorptive barrier across a highway parallel to another barrier was examined. Adding a 5 m high barrier decreased the total IL of the original barrier by 1 dBA, making it less effective. When the parallel barriers were absorptive, the IL was very similar to that of a single absorptive barrier and no amplification occurred.

Parallel barrier predictions were not performed in this work. FEM was found to be a valid model for these predictions; however a very large mesh would be required for predictions up to 2500 Hz for barriers 30 m apart and a computer with the necessary memory was not available.

The third objective was to determine the frequency-dependent effects of nearby foliage on the performance of noise barriers. Field testing was performed at several sites to test these effects. Time-averaged equivalent sound levels of traffic noise were taken simultaneously behind nearby sections of barrier, one with some configuration of foliage around it and one bare. Microphones were placed 1 to 3 m behind the wall and 1.5 to 2.5 m below the top of the wall. It was found that isolating foliage effects were difficult, as other factors

such as the distance between the traffic and the barrier were difficult to keep constant.

In the cases where conclusions could be drawn, it was seen that the height, size and density of the foliage behind the barrier had a large role. In the case of 10 m high, broad-leafed trees directly behind the barrier, a 5 dB increase in noise level was seen at frequencies above 1000 Hz, indicating scattering into the shadow zone. Below 1000 Hz the sound level decreased by up to 4 dB, indicating sound was being back-scattered or absorbed. In the case of vines growing on a barrier, which only grew 0.5 m above the barrier, up to 5 dB of sound was back-scattered and absorbed at most frequencies, and no high frequency scattering into the shadow zone was seen. Dense evergreen hedges showed a decrease in sound level by up to 5 dB at frequencies above 500 Hz, again showing that sound was back-scattered and absorbed, while less dense hedges showed effects of less than 2 dB.

The scale model was used here to test the effects of foliage. Scale-model trees were characterized by measuring the amount of sound which propagated through them and back-scattered from them. These results were compared with field tests performed on an evergreen hedge. It was seen that the scale-model trees likely modelled a different type of foliage, as they back-scattered more and transmitted less sound than the measured hedge.

It was found that foliage directly in front of or behind a barrier scattered up to 4 dB of sound into the shadow zone at high frequencies. At mid-frequencies, the foliage decreased levels behind the barrier by up to 2 dB, indicating that sound was being back-scattered or absorbed. Foliage placed 10 m behind a barrier had very little effect on the sound level at a receiver placed directly between the barrier and the foliage. By comparing these results with the field tests, it was concluded that the scale-model trees more closely resembled broad-leafed trees.

Predictions were also made of the scale-model foliage test which measured the amount of sound that propagated through and back-scattered from a row of trees. These predictions were done using ray tracing, where the foliage was modelled using volume scatterers.

The predictions showed similar trends to measurements and were accurate within 2 dB. Discrepancies could be due to the fact that the foliage was being modelled as random volume scatterers, where as in reality they do not scatter omni-directionally and have complex absorption characteristics. The effects of foliage near barriers were not predicted, as PRAY was seen to be unfit to model the performance of an outdoor barrier.

The final objective was to determine the practical implications of this research. It was seen that a fully absorptive barrier can give an IL improvement of up to 2-3 dBA when the source and receivers are quite close to a single barrier. In the case of parallel barriers 30 m away from each other, an IL improvement due to absorption was found to be 1 dBA, which was equivalent to a reflective barrier height increase of 0.33 m. The cost benefit of this would depend on the reflective and absorptive barrier costs. However, in many cases a height increase is not possible, and if an improvement in barrier performance is necessary then making the barriers sound absorptive is a valid method, especially if the receiver is close to the traffic.

It was seen that the effects of foliage were frequency-dependent and complicated, and varied depending on the type of foliage. If a barrier is to be built near a tall, broad-leafed tree, scattering into the shadow zone should be expected above 1000 Hz, with effects less than 8 dB. While this does not have a large impact on the total A-weighted sound level, residents may find high frequency noise to be more annoying. High frequency scattering was not seen with evergreen hedges; if a barrier is to be built near a dense hedge, the hedge may increase the effectiveness of the barrier by back-scattering and absorbing sound and preventing it from reaching the shadow zone. If the hedge is not dense and the leaves are small, the effects of the foliage should be less than 2 dB.

8.1 Future Work

Now that this research has been performed, the practical implications can be applied in the field. If absorptive barriers or barriers near foliage are constructed, sound level measurements before and after construction should be studied.

The selection process of scale-model materials is an area which requires further investigation. Using excess attenuation measurements for model selection uses one parameter — the flow resistivity — to choose an appropriate material. It does not account for the frequency-varying behaviour of the material. The Delany-Bazley model is assumed, which does not hold for non-porous materials. Different selection processes should be investigated and compared with excess attenuation measurements.

There is opportunity for more work to be done when examining different types of foliage and their interactions with sound. There are many classifications of foliage and an examination of the physical properties of their leaves and branches and how they interact with sound would be an interesting follow up to this work. In this work there was evidence that absorption of the leaves and branches is an important mechanism which requires further understanding.

In this work, prediction was not used to study the effects of absorption or foliage beyond predicting measurements done here. Further FEM tests can be done with a capable computer to study the effects of different configurations of absorption on both single and parallel barriers at all frequencies of interest. While PRAY can be used to study the effects of foliage alone, it is not a valid method to predict the effects of foliage with barriers. A further study on how to model different types of foliage using FEM is needed before the effects of foliage on barrier performance can be predicted.

Bibliography

[1] British Columbia Ministry of Transportation and Highways. *Revised policy for mitigating the effects of traffic noise from freeways and expressways.* Victoria, British Columbia, November 1993.

[2] K.B. Rasmussen. Outdoor sound propagation under the influence of wind and temperature gradients. *Journal of Sound and Vibration*, 104(2):321–335, 1986.

[3] V.I. Tatarskii. *The Effects of the Turbulent Atmosphere on Wave Propagation.* Israel Program for Scientific Translation, Jerusalem, 1971.

[4] Z. Maekawa. Noise reduction by screens. *Applied Acoustics*, 1:157–173, 1968.

[5] T. Busch. Scale-model investigation of highway traffic noise barriers. Master's thesis, Department of Mechanical Engineering, University of British Columbia, 1997.

[6] A.D. Rawlins. Diffraction of sound by a rigid screen with an absorbent edge. *Journal of Sound and Vibration*, 47:523–541, 1976.

[7] K. Fujiwara, Y. Ando, and Z. Maekawa. Noise control by barriers - Part 2: Noise reduction by an absorptive barrier. *Applied Acoustics*, 10(3):167–179, 1977.

[8] T. Isei. Absorptive noise barriers on finite impedance ground. *J. Acoust. Soc. Jpn.*, 1:3–10, 1980.

[9] D.N. May and M.M. Osman. Highway noise barriers: New shapes. *Journal of Sound and Vibration*, 71(1):73–101, 1980.

[10] W. Bowlby, L.F. Cohn, and R.A. Harris. A review of studies of insertion loss degradation for parallel highway noise barriers. *Noise Control Engineering Journal*, 28(2):40–54, 1987.

[11] D.C. Tobutt and P.M. Nelson. A model to calculate traffic noise levels from complex highway cross-sections. Transport Research Laboratory Report RR 245, Crowthorne, UK, 1990.

[12] K. Fujiwara, D.C. Hothersall, and C. Kim. Noise barriers with reactive surfaces. *Applied Acoustics*, 53:255–272, 1998.

[13] P.A. Morgan, D.C. Hothersall, and S.N. Chandler-Wilde. Influence of shape and absorbing surface - A numerical study of railway noise barriers. *Journal of Sound and Vibration*, 217(3):405–417, 1998.

[14] G.R. Watts and N.S. Godfrey. Effects on roadside noise levels of sound absorptive materials in noise barriers. *Applied Acoustics*, 58:385–402, 1999.

[15] A. L'Esperance, J. Nicolas, and G.A. Daigle. Insertion loss of absorbent barriers on ground. *J. Acoust. Soc. Am.*, 86:1060–1064, 1989.

[16] N. Ilgurel and M.S. Sozen. Comparison of the plain-shape noise barrier's effectiveness with and without absorptive layer by means of measurements in the semi-anechoic chamber. *Euronoise*, 2009.

[17] C.F. Eyring. Jungle acoustics. *J. Acoust. Soc. Am.*, 18(2):257–270, 1946.

[18] F.M. Wiener and D.N. Keast. Experimental study of the propagation of sound over ground. *J. Acoust. Soc. Am.*, 31(6):724–733, 1959.

[19] T.F.W. Embleton. Sound propagation in homogeneous deciduous and evergreen woods. *J. Acoust. Soc. Am.*, 35(8):1119–1125, 1963.

[20] D. Aylor. Noise reduction by vegetation and ground. *J. Acoust. Soc. Am.*, 51(1B):197–205, 1972.

[21] E.S. Morton. Ecological sources of selection on avian sounds. *The American Naturalist*, 109:17–34, 1975.

[22] D.I. Cook and D.F. Van Haverbeke. *Trees and shrubs for noise abatement.* University of Nebraska College of Agricultural Experimental Station Bulletin, RB246, 1993.

[23] J. Kragh. Pilot study on railway noise attenuation by belts of trees. *Journal of Sound and Vibration*, 66(3):407–415, 1979.

[24] D. Aylor. Sound transmission through vegetation in relation to leaf width. *J. Acoust. Soc. Am.*, 51(1B):411–414, 1972.

[25] M.A. Price, K. Attenborough, and N.W. Heap. Sound attenuation through trees: Measurements and models. *J. Acoust. Soc. Am.*, 84(5):1836–1844, 1988.

[26] M.J.M. Martens. Foliage as a low-pass filter: Experiments with model forests in an anechoic chamber. *J. Acoust. Soc. Am.*, 67(1):66–72, 1980.

[27] R.M. Hoover. Tree zones as barriers for the control of noise due to aircraft operations. *Bolt, Beranek and Newman Inc.*, Report 844, 1961.

[28] D.I. Cook and D.F. Van Haverbeke. Suburban noise control with plant materials and solid barriers. *In: Heisler, Gordon M.; Herrington, Lee P., eds. Proceedings of the conference on metropolitan physical environment; Gen. Tech. Rep. NE-25. Upper Darby, PA: U.S. Department of Agriculture, Forest Service, Northeastern Forest Experiment Station*, pages 234–241, 1977.

[29] T. Van Renterghem, D. Botteldooren, W.M. Cornelis, and D. Gabriels. Reducing

screen-induced refraction of noise barriers in wind by vegetative screens. *Acta Acustica united with Acustica*, 88:231–238, 2002.

[30] T. Van Renterghem and D. Botteldooren. Effect of a row of trees behind noise barriers in wind. *Acta Acustica united with Acustica*, 88:869–878, 2002.

[31] L. De Geetere. *Analysis and improvement of the experimental techniques to assess the acoustical reflection properties of boundary surfaces.* PhD thesis, Katholieke Universiteit Leuven, 2004.

[32] ISO/CD 10534-2. Determination of sound absorption coefficient and impedance in impedance tubes - Part 2: Transfer-function method. 2004.

[33] H. Boden and M. Abom. Influence of errors on the two-microphone method for measuring acoustic properties in ducts. *J. Acoust. Soc. Am.*, 79:541–549, 1986.

[34] C. Bibby. Point-source design and performance. Technical report, University of British Columbia, 2009.

[35] V.F. Spandock. Akustische modellversuche. *Annalen der Physik*, 20:345–360, 1934.

[36] M.E. Delany, A.J. Rennie, and K.M. Collins. Scale model investigations of traffic noise propagation. *National Physics Laboratory*, Report Ac 58, Sept. 1972.

[37] D.A. Hutchins, H.W. Jones, and L.T. Russell. Model studies of acoustic propagation over finite impedance ground. *Acustica*, 52(3):169–178, 1983.

[38] D.A. Hutchins, H.W. Jones, and L.T. Russell. Model studies of barrier performance in the presence of ground surfaces. Part I - Thin, perfectly reflecting barriers. *J. Acoust. Soc. Am.*, 75(6):1807–1816, 1984.

[39] K.V. Horoshenkov, D.C. Hothersall, and K. Attenborough. Porous materials for scale model experiments in outdoor sound propagation. *Journal of Sound and Vibration*, 194(5):685–708, 1996.

[40] D.A. Hutchins, H.W. Jones, B. Paterson, and L.T. Russell. Studies of parallel barrier performance by acoustical modelling. *J. Acoust. Soc. Am.*, 77(2):536–546, 1985.

[41] R. Pirinchieva. Model study of the sound propagation behind barriers of finite length. *J. Acoust. Soc. Am.*, 87(5):2109–2113, 1990.

[42] M.M. Osman. MTC Scale model facility for transportation noise problems: Materials choice and validation for scale modelling. Technical report 77-AC-4, Ontario Ministry of Transportation and Communications, June 1977.

[43] C.W. Menge. Highway noise: Sloped barriers as an alternative to absorptive barriers. *Noise Control Engineering*, 14(2):74–78, 1980.

[44] D.C. Hothersall, D.B. Horoshenkov, P.A. Morgan, and M.J. Swift. Scale modelling of railway noise barriers. *Journal of Sound and Vibration*, 243(2):207–223, 2000.

[45] M.E. Delany and E.N. Bazley. Acoustical properties of fibrous absorbent materials. *Applied Acoustics*, 25(114):339–344, 1971.

[46] H.E. Bass, L.C. Sutherland, and A.J. Zuckerwar. Atmospheric absorption of sound: Update. *J. Acoust. Soc. Am.*, 88(4):2019–2021, 1990.

[47] ANSI S1.26-1978. American national standard method for the calculation of the absorption of sound by the atmosphere. *American National Standards Institute*, 1978.

[48] H.E. Bass, L.C. Sutherland, A.J. Zuckerwar, D.T. Blackstock, and D.M. Hester. Atmospheric absorption of sound: further developments. *J. Acoust. Soc. Am.*, 97(1):680–683, 1995.

[49] F. Matta and A. Reichel. Uniform computation of the error function and other related functions. *Mathematics of Computation*, 25(114):339–344, 1971.

[50] C.F. Chien and W.W. Soroka. Sound propagation along an impedance plane. *Journal of Sound and Vibration*, 43(1):9–20, 1975.

[51] C.F. Chien and W.W. Soroka. A note on the calculation of sound propagation along an impedance surface. *Journal of Sound and Vibration*, 69(2):340–343, 1980.

[52] R.K. Pirinchieva. Model study of sound propagation over ground of finite impedance. *J. Acoust. Soc. Am.*, 90(5):2678–2682, 1991.

[53] R.K. Pirinchieva. Erratum: Model study of sound propagation over ground of finite impedance [J. Acoust. Soc. Am. 90, 2678-2682 (1991)]. *J. Acoust. Soc. Am.*, 94(3):1722, 1993.

[54] M.R. Stinson. A note on the use of an approximate formula to predict sound fields above an impedance plane due to a point source. *J. Acoust. Soc. Am.*, 98(3):1810–1812, 1995.

[55] J. Novak. Technical note: Sound source for scale model measurements of traffic noise. *Applied Acoustics*, 24(1):63–70, 1988.

[56] T.A. Busch and M.R. Hodgson. Improved method for selecting scale factors and model materials for scale modelling of outdoor sound propagation. *Journal of Sound and Vibration*, 243(1):173–181, 2001.

[57] T.F.W. Embleton, J.E. Piercy, and G.A. Daigle. Effective flow resistivity of ground surfaces determined by acoustical measurements. *J. Acoust. Soc. Am.*, 74(4):1239–1244, 1983.

[58] J.B. Keller. Geometrical theory of diffraction. *Journal of the Optical Society of America*, 52(2):116–130, 1962.

[59] R.G. Kouyoumjian and P.H. Pathak. A uniform geometrical theory of diffraction for an edge in a perfectly conducting surface. *Proceedings of the IEEE*, 62(11):1448–1461, 1974.

[60] T. Kawai. Sound diffraction by a many-sided barrier or pillar. *Journal of Sound and Vibration*, 79(2):229–242, 1981.

[61] N. Tsingos, T. Funkhouser, A. Ngan, and I. Carlbom. Modeling acoustics in virtual environments using the uniform theory of diffraction. *Proceedings of the 28th Annual Conference on Computer Graphics and Interactive Techniques*, pages 545–552, 2001.

[62] M.A. Biot and I. Tolstoy. Formulation of wave propagation in infinite media by normal coordinates with an application to diffraction. *J. Acoust. Soc. Am.*, 29(3):381–391, 1957.

[63] H. Medwin. Shadowing by finite noise barriers. *J. Acoust. Soc. Am.*, 64(4):1060–1064, 1981.

[64] U.P. Svensson, R.I. Fred, and J. Vanderkooy. An analytic secondary source model of edge diffraction impulse responses. *J. Acoust. Soc. Am.*, 106(5):2331–2344, 1999.

[65] U.P. Svensson and P.T. Calamia. Edge-diffraction impulse responses near specular-zone and shadow-zone boundaries. *Acta Acustica united with Acustica*, 92:501–512, 2006.

[66] U.P. Svensson, P.T. Calamia, and S. Nakanishi. Frequency-domain edge diffraction for finite and infinite edges. *Acta Acustica united with Acustica*, 95:568–572, 2009.

[67] M. Hodgson, O. Cousins, G. Chan, and V. Valeau. Ray-tracing prediction of sound-pressure and sound-intensity fields in empty and fitted rooms. *J. Acoust. Soc. Am.*, 123(5):3760, 2008.

[68] A.M. Ondet and J.L. Barbry. Modeling of sound propagation in fitted workshops using ray tracing. *J. Acoust. Soc. Am.*, 85(2):787–796, 1989.

[69] G. Chan. Prediction of low-frequency sound-pressure fields in fitted rooms for active noise control. Master's thesis, Department of Mechanical Engineering, University of British Columbia, 2005.

[70] B. Yousefzadeh. Acoustical modeling of the transient response of rooms using a beam-tracing model. Master's thesis, Department of Mechanical Engineering, University of British Columbia, 2010.

[71] J.B. Allen and D.A. Berkley. Image method of efficiently simulating small-room acoustics. *J. Acoust. Soc. Am.*, 65(4):943–950, 1979.

[72] S.C. Brenner and L.R. Scott. *The Mathematical Theory of Finite Element Methods*. Springer, 2008.

[73] S. Daltrop. Measurement of the acoustical characteristics of surfaces using the spherical decoupling method. Technical report, University of British Columbia, 2010.

Appendix A

Diffraction Theory

A.1 Uniform Theory of Diffraction

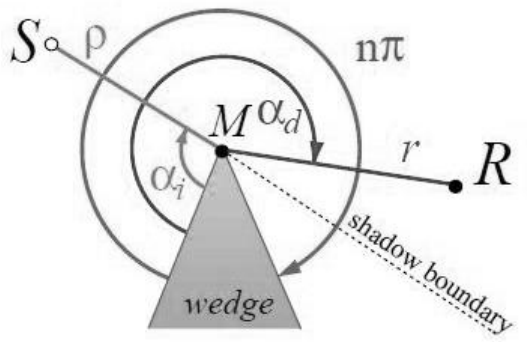

Figure A.1: A diffracting edge, with definitions of the parameters used in the UTD formulation. [61]

The UTD assumes an infinitely long, perfectly reflecting wedge. The sound diffracted by an edge P_d can be defined in terms of parameters defined in Figure A.1 and the incident sound P_i as:

$$P_d = P_i \, D(n, k, \rho, r, \theta_i, \alpha_i, \alpha_d) \, A(r, \rho) \, e^{-ikr}. \tag{A.1}$$

θ_i is the angle between the incident direction and the vector lying along the edge. A is an attenuation term dependent on the distances from the edge to the source and receiver:

$$A(r, \rho) = \sqrt{\frac{r\rho}{r + \rho}}. \tag{A.2}$$

D is the diffraction coefficient which accounts for the amplitude and phase change due to the diffracting edge:

$$\begin{aligned} D(n,k,\rho,r,\theta_i,\alpha_i,\alpha_d) =& \frac{-e^{-i\pi/4}}{2n\sqrt{2k\pi}\sin\theta_i} \\ & \Bigg[\cot\left(\frac{\pi+(\alpha_d-\alpha_i)}{2n}\right) F\left(kLa^+(\alpha_d-\alpha_i)\right) \\ & + \cot\left(\frac{\pi-(\alpha_d-\alpha_i)}{2n}\right) F\left(kLa^-(\alpha_d-\alpha_i)\right) \\ & + \cot\left(\frac{\pi+(\alpha_d+\alpha_i)}{2n}\right) F\left(kLa^+(\alpha_d+\alpha_i)\right) \\ & + \cot\left(\frac{\pi-(\alpha_d+\alpha_i)}{2n}\right) F\left(kLa^-(\alpha_d+\alpha_i)\right) \Bigg], \end{aligned} \tag{A.3}$$

where $F(x)$ is a Fresnel integral, given by:

$$F(X) = 2i\sqrt{X}e^{iX}\int_{\sqrt{X}}^{\infty} e^{-i\tau^2}\mathrm{d}\tau. \tag{A.4}$$

L is a distance parameter, given as:

$$L = \frac{r\rho}{r+\rho}\sin^2\theta_i \tag{A.5}$$

and $a^{\pm}$ is defined as:

$$a^{\pm}(\beta) = 2\cos^2\left(\frac{2\pi N^{\pm}n-\beta}{2}\right), \tag{A.6}$$

where $N^{\pm}$ are the integers that satisfy the following relations the closest:

$$2\pi N^{\pm}n - \beta = \pm\pi. \tag{A.7}$$

Kawai [60] gives a rational approximation for $F(X)$:

$$F(X) = \begin{cases} \sqrt{\pi X}\left(1 - \frac{\sqrt{X}}{0.7\sqrt{X}+1.2}\right) e^{i\frac{\pi}{4}\sqrt{\frac{X}{X+1.4}}} & \text{for X} < 0.8 \\ \left(1 - \frac{0.8}{(X+1.25)^2}\right) e^{i\frac{\pi}{4}\sqrt{\frac{X}{X+1.4}}} & \text{for X} \geq 0.8 \end{cases} \tag{A.8}$$

Approximations are also used for $N^{\pm}$:

$$N^+ = \begin{cases} 0 & \text{for } \beta \leq \pi(n-1) \\ 1 & \text{for } \beta > \pi(n-1) \end{cases} \quad ; \quad N^- = \begin{cases} -1 & \text{for } \beta < \pi(1-n) \\ 0 & \text{for } \pi(1-n) \leq \beta \leq \pi(1+n) \\ 1 & \text{for } \beta > \pi(1+n) \end{cases} \tag{A.9}$$

A.2 Svensson's Model

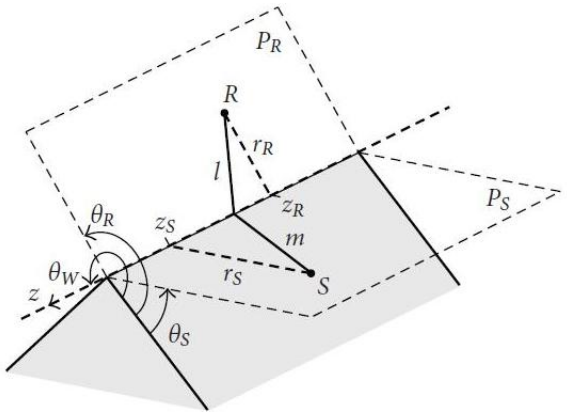

Figure A.2: The diffracting edge, with definitions of the parameters used in the Svensson model. [65]

The Svensson model uses a line integral formulation along a finite-length diffracting edge to model the edge as a secondary source when hit by a sound wave. Much of this derivation is taken from references [65] and [66], and a cylindrical coordinate system

with the axis along the diffracting edge is used. Assuming an $e^{i\omega t}$ time dependence, the frequency-domain edge-diffraction transfer function is given by:

$$H_{diffr}(\omega) = -\frac{\nu}{4\pi}\sum_{j=1}^{4}\int_{z_1}^{z_2} e^{-ik(m+l)}\frac{\beta_j}{ml}\mathrm{d}z \tag{A.10}$$

where $\nu = \pi/\theta_W$ is the wedge index and z_1 and z_2 are the two ends of the edge. m and l are the distances between the edge and the source S and receiver R, respectively, given by:

$$m = \sqrt{r_S^2 + (z - z_S)^2}, \quad l = \sqrt{r_R^2 + (z - z_R)^2}. \tag{A.11}$$

The β_j's are edge-source directivity functions, given by:

$$\beta_j = \frac{\sin(\nu\phi_j)}{\cosh(\nu\eta) - \cos(\nu\phi_j)} \tag{A.12}$$

where the angles ϕ_j are:

$$\begin{aligned} \phi_1 &= \pi + \theta_S + \theta_R, \quad \phi_2 = \pi + \theta_S - \theta_R \\ \phi_3 &= \pi - \theta_S + \theta_R, \quad \phi_4 = \pi - \theta_S - \theta_R. \end{aligned} \tag{A.13}$$

The auxiliary function η is:

$$\eta = \cosh^{-1}\left(\frac{ml + (z - z_S)(z - z_R)}{r_S r_R}\right). \tag{A.14}$$

Figure A.3 shows the three different zones around an edge for a given source position. Neglecting diffraction, a receiver in Zone 1, say R1, will receive direct and specularly reflected sound. A receiver in Zone 2, such as R3, will receive only direct sound. A receiver in Zone 3, say R5, will receive neither, and is therefore called the shadow zone. When diffraction occurs, diffracted sound reaches all three zones. For receivers lying on

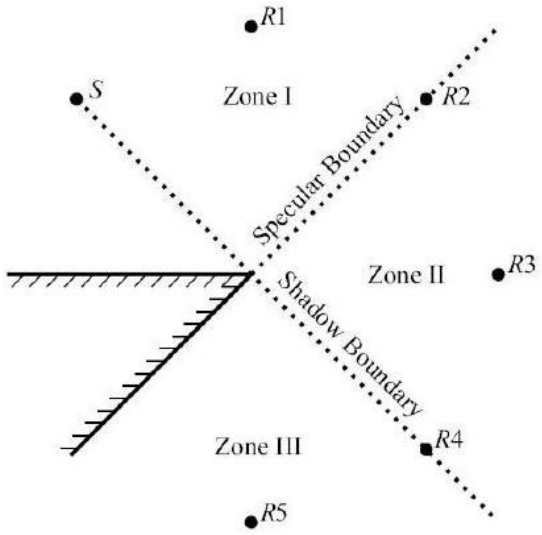

Figure A.3: The zones around a diffracting edge. [65]

the boundaries, say R2 and R4, $\theta_R = \pi \pm \theta_S$ and a singularity occurs for a certain value of z in Equation A.10. This value is called the apex point, the point which gives the shortest source-edge-receiver path length and is denoted z_a, given by:

$$z_a = \frac{z_R r_S + z_S r_R}{r_S + r_R}. \tag{A.15}$$

If z_a is not contained within the limits of integration z_1 and z_2, the singularity has no effect and regular numerical-integration techniques can be used. For ease of notation, the parameter $z_{rel} = z - z_a$ is used, and therefore the bounds of integration are $z_1' = z_1 - z_a$ and $z_2' = z_2 - z_a$. In order to integrate efficiently, the integration range is split up into three parts: a small region around the apex point where $z_{rel} = 0$, which contains the singularity, and from each limit of integration to that region. Using z_{split} to denote a point on the diffraction edge very close to the apex point, Equation A.10 can be rewritten as the sum

of three different terms:

$$\begin{aligned} H_{diffr}(\omega) =& I_1 + I_2 + I_3 = \\ & - 2\frac{\nu}{4\pi}\sum_{j=1}^{4}\int_{0}^{z_{split}} e^{-ik(m+l)}\frac{\beta_j}{ml}\mathrm{d}z_{rel} \\ & - \frac{\nu}{4\pi}\sum_{j=1}^{4}\int_{z_1'}^{-z_{split}} e^{-ik(m+l)}\frac{\beta_j}{ml}\mathrm{d}z_{rel} \\ & - \frac{\nu}{4\pi}\sum_{j=1}^{4}\int_{z_{split}}^{z_2'} e^{-ik(m+l)}\frac{\beta_j}{ml}\mathrm{d}z_{rel}. \end{aligned} \tag{A.16}$$

I_2 and I_3 have no singularities and can be solved using ordinary numerical-integration; in this work the MATLAB function *quadgk* was used with a relative tolerance of 10^{-6}, as suggested by Svensson et al. [66]. The first term includes a singularity, and an approximation of the integrand must be used. Since the range of integration is very close to the apex point, the first term can be rewritten as:

$$I_1 = -2\frac{\nu}{4\pi}e^{-ik(m_0+l_0)}\sum_{j=1}^{4}\int_{0}^{z_{split}}\frac{\beta_j}{ml}\mathrm{d}z_{rel} \tag{A.17}$$

where m_0 and l_0 are the distances from the apex point to the source and receiver, respectively. For this to be valid, it is necessary for z_{split} to satisfy the following conditions:

$$\begin{aligned} & z_{split} << \sqrt{\frac{2m_0l_0(m_0+l_0)}{k(r_S+r_R)^2}} \\ & z_{split} << m_0, \quad z_{split} << l_0. \end{aligned} \tag{A.18}$$

The following approximations were used for the integrand:

$$\cosh(\nu\eta) \approx 1 + \nu^2\frac{(1+\rho)^4}{2\rho^2R_0^2}z_{rel}^2 \tag{A.19}$$

$$ml \approx \frac{R_0^2\rho}{(1+\rho)^2} + \frac{\cos\psi\, R_0(\rho-1)}{\rho+1} z_{rel} + \frac{\sin^2\psi(1+\rho^2)}{2\rho} z_{rel}^2 - \cos^2\psi\, z_{rel}^2 \tag{A.20}$$

where $R_0 = m_0 + l_0$ and ψ is the horizontal angle between the ray and the edge:

$$\psi = \sin^{-1}\left(\frac{r_S + r_R}{R_0}\right). \tag{A.21}$$

Appendix B

Creation of Finite Element Mesh

The finite element code was implemented in MATLAB. For the creation of the mesh, the PDE toolbox and the command *pdepoly* were used . The toolbox was opened and the boundary locations were defined by the command 'pdepoly([0 0 3.6 3.6],[0 2.6 2.6 0])', which labeled the domain as P1. The barrier was defined using the command 'pdepoly([1.74 1.74 1.86 1.86],[0 1.2 1.2 0])' and labeled P2. To create the mesh for the no barrier case, the mesh was initialized on P1 only. The mesh was then refined four times and the coordinate, boundary and element matrices were exported into MATLAB. To create a mesh for the barrier case, a mesh was initialized on the domain P1-P2, which left the barrier out of the domain. Again, this was refined four times before the matrices were exported to MATLAB.

Once the matrices p, e and t are defined, the following MATLAB script was run, using the function *assemble* as defined below.

```
f=900:50:1100;
k=2*pi*f/343;
P2L=zeros(length(f),6);
for mm=1:length(f)
[Ah,fh]=assemble(p,e,t,k(mm));
uh=Ah\fh;
R=zeros(1,6);cL=zeros(1,6);
for n=1:length(p)           % find elements within receiver radius
    if p(2,n)-.2 < .1
        if ((p(1,n)-2.4)^2+(p(2,n)-.2)^2)<1E-3
            R(1)=R(1)+uh(n);
            cL(1)=cL(1)+1;
        elseif ((p(1,n)-3)^2+(p(2,n)-.2)^2)<1E-3
            R(2)=R(2)+uh(n);
            cL(2)=cL(2)+1;
```

```
        elseif ((p(1,n)-3.6)^2+(p(2,n)-.2)^2)<1E-3
            R(3)=R(3)+uh(n);
            cL(3)=cL(3)+1;
        end
    end
end
for n=1:length(p)
    if p(2,n)-1.05 < .1
        if ((p(1,n)-3.6)^2+(p(2,n)-1.05)^2)<15E-3
            R(4)=R(4)+uh(n);
            cL(4)=cL(4)+1;
        elseif ((p(1,n)-3)^2+(p(2,n)-1.05)^2)<1E-3
            R(5)=R(5)+uh(n);
            cL(5)=cL(5)+1;
        elseif ((p(1,n)-2.4)^2+(p(2,n)-1.05)^2)<1E-3
            R(6)=R(6)+uh(n);
            cL(6)=cL(6)+1;
        end
    end
end
P2L(mm,:)=P2L(mm,:)+R./cL;
end
P_tot=20*log10(abs(P2L)/2E-5);
P=zeros(1,6);
for ii=1:length(f)
    P=P+10.^(P_tot(ii,:)/10);
end
SPL=10*log10(P)-10*log10(length(f));

%%%%%%%%%%%%%%%%%%%%%%%%%%%%%%%%%%%%%%%%%%%%%%%%%%%%%%%%%%%%%%%%%%%%%%%%%%%

function [Ah,fh]=assemble(coords,boundary,elems,k)
Nnod=length(coords);                    % number of nodes
Nedge=length(boundary);                 % number of boundary edges
Nel =length(elems);                     % number of elements
fh=zeros(Nnod,1);                       % allocate load vector
Ah=sparse(Nnod,Nnod);                   % allocate stiffness matrix
for n=1:Nel                             % loop over elements
  x0=coords(1,elems(1,n));              % coordinates of the vertices
  y0=coords(2,elems(1,n));              % of triangle n
  x1=coords(1,elems(2,n));
  y1=coords(2,elems(2,n));
  x2=coords(1,elems(3,n));
```

```
  y2=coords(2,elems(3,n));
  mx=1/3*(x0+x1+x2);                      % barycenter
  my=1/3*(y0+y1+y2);
  det=(x1-x0)*(y2-y0)-(x2-x0)*(y1-y0);      % determinant of mapping
  area=0.5*det;                             % area of triangle
  D=[y1-y2, y2-y0, y0-y1; x2-x1, x0-x2, x1-x0];
  AK=0.25/area*transpose(D)*D;              % element stiffness matrix
  MK=area/12*[2 1 1; 1 2 1; 1 1 2];         % element mass matrix
  if ((mx-0.8)^2+(my-0.25)^2)<0.01
      value=-50;                            % within source radius
  else
      value=0;                              % not within source radius
  end
  FK=area*value*[1/3;1/3;1/3];              % element load vector
  for kk=1:3                                % loop over shape functions
    iii=elems(kk,n);                        % global index of shape function iii
    for l=1:3                               % inner loop over shape functions
      j=elems(l,n);                         % global index of shape function l
      Ah(iii,j)=Ah(iii,j)+AK(kk,l)-k^2*MK(kk,l);      % update global matrix
    end
    fh(iii)=fh(iii)+FK(kk);                       % update load vector
  end
end

for ii=1:Nedge                              % loop over edges in boundary
  x1=coords(1,boundary(1,ii));              % coordinates of the vertices
  y1=coords(2,boundary(1,ii));
  x2=coords(1,boundary(2,ii));              % coordinates of the vertices
  y2=coords(2,boundary(2,ii));
  h=max(abs(x1-x2),abs(y1-y2));
  B=h/6*[2 1; 1 2];
  if (abs(x1)==0 && abs(x2)==0) || (abs(x1)==3.6 && abs(x2)==3.6) || (y1==2.6 && y2==2.
      B=i*k*B;                              % absorbing wall
  elseif y1==0 && y2==0
      B=i*k*B/19;                           % ground, z=19 (R=0.9)
  else
      B=i*k*B/9;                            % barrier, R=0.8
  end
  Ah(boundary(1,ii),boundary(1,ii))=Ah(boundary(1,ii),boundary(1,ii))+B(1,1);
  Ah(boundary(2,ii),boundary(2,ii))=Ah(boundary(2,ii),boundary(2,ii))+B(2,2);
  Ah(boundary(2,ii),boundary(1,ii))=Ah(boundary(2,ii),boundary(1,ii))+B(2,1);
  Ah(boundary(1,ii),boundary(2,ii))=Ah(boundary(1,ii),boundary(2,ii))+B(1,2);
end
```